

REGULATION
of
WATER FLOW
in the
SOIL-ROOT DOMAIN



New Tools and Methods

Guillaume Lobet

Monday 10th December, 2012

*Thèse présentée en vue de l'obtention du titre de
docteur en sciences agronomiques et ingénierie biologique*

EARTH AND LIFE INSTITUTE
UNIVERSITÉ CATHOLIQUE DE LOUVAIN

THESIS EXAMINING BOARD

SUPERVISOR: Prof. Xavier Draye

PRESIDENT OF THE JURY: Prof. Jacques Mahillon

MEMBERS OF THE JURY: Dr. Ian Dodd
Prof. Mathieu Javaux
Dr. Loïc Pagès
Dr. François Tardieu

CREDITS

The first four years of this thesis were funded by the belgian Fond National de la Recherche Scientifique (FNRS) under a grant from the Fond pour la formation à la Recherche dans l'Industrie et dans l'Agriculture (F.R.I.A.) (<http://www.frs-fnrs.be/>).

The last three months of the thesis were funded by the european project DROPS (<http://www.drops-project.eu>)

This work is dedicated to Capucine and Zoé,
my greatest accomplishments.



When the root is strong, the fruit is sweet.

BOB MARLEY

ACKNOWLEDGMENTS

WHEN BILBO LEFT THE SHIRE, he told Frodo these wise words:

*You step onto the road, and if you don't keep your feet,
there's no knowing where you might swept off to.*

Five years ago, when I first entered the ECAV lab as a master student, I had no idea how far it would lead me. Like Frodo bringing the Ring into the fire of Mount Doom, the road, thought to be a short walk into the woody hills of Hobbiton, turned out to be long journey paved with surprises. And like Frodo, I would never have gotten so far alone. This is the place to thanks all the wonderful people who helped me complete my journey.

Mes remerciements les plus chaleureux iront à mon promoteur, le professeur Xavier Draye. Xavier, tu as été pour moi le promoteur idéal. Tel Gandalf accompagnant Frodon lors de son épopée, durant ces cinq dernières tu as été une présence tantôt bienveillante, tantôt ingénieuse, tantôt discrète, toujours là en cas de besoin. Pour l'amour de la science que tu m'a transmise, encore merci.

I would also like to warmly thank all the members of my examining board and supervising comity. All of them gave me great advices and feedbacks, either during the thesis or concerning the final document. More specifically, Prof. Mathieu Javaux has been of great help and advise during the last four year for all my questions related to soil science. All the plant modelling work presented in this thesis has been heavily supported and inspired by Dr. Loïc Pagès. Dr. Ian Dodd welcomed me in his lab in Lancaster to learn everything there is to know about abscisic acid. Dr. François Tardieu welcomed me in Montpellier and the few talks we had together have been amongst the most inspirational. Finally, Prof. François Chaumont always kept is door open for any question about aquaporins.

Cette thèse n'aurait pas été la même, et certainement pas aussi agréable sans la chaleureuse équipe du labo ECAV. En vrac, merci à Pierre, Pierre, Pierre (et oui...), Anne-Michelle, Maxime, Gauthier, Adrien, Aurélie, Beata, Alek, René, Nathalie, Willy, Léopold, William, Igor, Han, John, Taha, Laure-Anne, Walid, Inès, Rémi, Dieudonné et Vivianne pour avoir fait de ces cinq années un plaisir et une stimulation scientifique permanente.

Un merci tout spécial à Piet, l'éternel copain sans qui ces années auraient paru bien ternes. Les aventures étranges vécues avec toi sont bien trop nombreuses pour être relatées ici, mais ça ne m'empêche pas de te remercier une fois de plus pour les avoir toujours déclenchées / suivies.

Il est une personne sans qui le labo ECAV serait comme un bateau sans capitaine, dérivant au gré des vents. Merci à toi Isabelle d'être toujours là pour le moindre conseil, besoin, ragot.

Plusieurs personnes m'ont accompagné lors de mes manip et mes longues heures de codes. Merci à Nicolas, Vincent, Maxime et Geoffrey pour l'aide apportée dans l'élaboration de cette thèse. Merci également aux GIPSies, Valentin, Laure, Mathieu, Xavier, Bertrand, Suman et Alek, pour les régulières discussions animées sur le système sol-plante.

Et parce que tout n'est pas toujours à propos de science, parce que mes longues heures de manips/traitement de données/code/rédaction furent rythmées de leurs magnifiques mélodies, merci, entre autres, à Sigur Ros, Yo-Yo Ma, Bon Iver, Harrison Stafford et Xavier Rudd.

En dehors des heures de boulot (et oui il y en avait), ils ont toujours été présents pour colorer mon quotidien. Merci Françoise pour ta sagesse, Flav pour avoir toujours été un modèle, Moust pour ton côté divin et ton charisme et Ben pour ta cuisine.

Je leur dois tout et bien plus encore, merci à vous Papa et Maman. Votre éternel support et vos encouragements ont rendu cette thèse possible. Merci également à Martine, Ghislain, Marie-Cécile et Jean-Luc pour avoir toujours été là en cas de besoin, spécialement pour garder une certaine petite Capucine.

Merci aussi à tous les membres de ma fratrie, toujours grandissante, pour leurs innombrables coups de mains et marques de soutiens. Merci à Sophie, Sylvain, Ben, Laura, Mai-Linh, Juan, Sophie, Corentin, Lucie, Greg, Anne-Lise et Alex.

Et enfin, pour terminer, il me faut remercier les personnes qui comptent le plus à mes yeux. Marie-Pierre, tu m'as récemment dit que je te servais parfois d'encrage dans la réalité, un peu comme les racines d'un arbre. Si je suis les racines de notre arbre familial, tu ne peux qu'en être les branches, me donnant accès à la grandeur et la beauté du ciel. Merci du fond du coeur pour avoir toujours été là durant ces quatre dernières années, me relevant des coups durs et m'accompagnant dans les moments de joies. Merci de m'avoir offert les plus beaux des cadeaux, nos deux petites filles.

Capucine et Zoé, mes puces, il faudra sans doute encore un paquet d'années avant que vous ne compreniez pourquoi votre papa a été un peu absent ces derniers temps mais, d'ici là, merci du fond du coeur pour tout ce que vous m'apportez. Ou comme Capucine le dirait si bien:

A'i Capucine, a'i Toé!

Guillaume,
Louvain-la-Neuve,
Monday 10th December, 2012

SHORT CONTENTS

INTRODUCTION AND OBJECTIVES	1
CONTEXT	15
QUANTIFICATION OF ROOT SYSTEMS	47
MONITORING SOIL WATER CONTENT	91
MODELING WATER FLOW	135
DISCUSSION AND PERSPECTIVES	179
ANNEXES	233

TABLE OF CONTENTS

INTRODUCTION AND OBJECTIVES

Introduction	8
Objectives	13

CONTEXT

1 Water flow in the soil-root domain	19
1.1 Water moves in a complex system	21
1.2 Control of water flow in the soil matrix	24
1.2.1 Soil hydraulic properties that affect water flow .	24
1.2.2 Soil water dynamics in the presence of roots . .	25
1.2.3 Hydraulic properties of the rhizosphere	26
1.2.4 The soil, constitutive part of the SPAC	27
1.3 Control of radial water flow	28
1.3.1 Radial water movement	28
1.3.2 Modification of anatomical structures	28
1.3.3 Regulation by water channels	29
1.3.4 Interplay between root anatomy and aquaporin .	32
1.4 Control of the axial water flow	33
1.4.1 Cavitation onset	33
1.4.2 Cavitation avoidance	33
1.4.3 Cavitation recovery	34
1.5 Root architecture	37
1.5.1 RSA and the potential for water uptake	37
1.5.2 Root placement and the availability of water . .	38

TABLE OF CONTENTS

1.6	Integration of water flow in the soil-plant domain . . .	39
1.6.1	Novel techniques supporting integration	41
1.6.2	The need for integration in plant physiology studies	42
1.6.3	Integration helps understand water uptake patterns	43
1.6.4	Integration to find where and when controls are effective	44
1.7	Future outlooks	44

QUANTIFICATION OF ROOT SYSTEMS

2	Preliminary concepts	51
3	A novel root image analysis toolbox	55
3.1	Results and discussions	56
3.1.1	Multi-dimensional representations of roots	56
3.1.2	Root tracing principle	56
3.1.3	Topology	60
3.1.4	Root annotations	64
3.1.5	Time series analysis	65
3.1.6	Data handling	65
3.1.7	Image requirements (type and quality)	67
3.1.8	Ex. 1: Architectural analysis of <i>Zea mays</i>	68
3.1.9	Ex. 2: Time-lapse analysis of cluster root formation	70
3.2	Conclusions	74
3.3	Material and methods	77
3.3.1	Experience 1	77
3.3.2	Experience 2	77
3.4	Supplemental data	77
4	Digitizing root systems	79
4.1	Results and discussions	80
4.1.1	Architectural analysis of complex root systems	82
4.1.2	Local analysis of root-soil interactions	85
4.2	Conclusions	86

4.3	Methods	87
4.3.1	Hybrid method	87
4.3.2	Local analysis of root-soil interactions	90

MONITORING SOIL WATER CONTENT

5	Preliminary concepts	95
5.1	Architectural traits	95
5.1.1	Root system size	95
5.1.2	Root system shape	95
5.1.3	Root distribution	96
5.2	Hydraulic properties	96
6	Light Transmission Imaging	99
6.1	Material and methods	100
6.1.1	Experimental procedure	100
6.1.2	Plant and soil parameters	103
6.1.3	Statistical analysis	104
6.2	Results and discussions	105
6.2.1	Plant architecture	105
6.2.2	General water content variations dynamics	107
6.2.3	Effect of architectural traits on the soil water content distribution	110
6.3	Conclusions	116
7	In vivo and in silico experiments	117
7.1	Methodology	118
7.1.1	General methodology	118
7.1.2	Experiments	118
7.1.3	R-SWMS input data	120
7.2	Results	121
7.2.1	Experimental results	121
7.2.2	Modeling results - WSE1	123
7.2.3	Modeling results - WSE2	126

TABLE OF CONTENTS

7.3	Discussion	132
7.3.1	R-SWMS is able to represent the majority of the water content variation observed experimentally . . .	132
7.3.2	Water content can not be used as a proxy of water uptake	132
7.3.3	Changes in root hydraulic properties may not have significant effects on the soil water content distribution	133
7.3.4	Experimental water content distribution is not sufficient for the model calibration	133
7.4	Conclusions	134

MODELING WATER FLOW

8	Preliminary concepts	139
9	Modeling water flow and its regulations.	141
9.1	Model description	142
9.1.1	General principles	142
9.1.2	Architecture module	144
9.1.3	Carbon module	145
9.1.4	Water fluxes module	147
9.1.5	Conditions for simulations	152
9.1.6	Model validation	153
9.2	Results and discussions	154
9.2.1	Root system size and hydraulic regulations . . .	154
9.2.2	Hydraulic signal alone is not sufficient to reproduce effect of different irrigation practices	155
9.2.3	Regulation sensibility	159
9.3	Conclusions and perspectives	164
9.3.1	Functional-structural modeling as a useful tool to decrypt plant water relations	164
9.3.2	Envisaged model development	165
9.3.3	Future experimental needs	165
10	Modeling ABA fluxes and their effects.	167

10.1	Model description	168
10.1.1	ABA production	168
10.1.2	ABA degradation	168
10.1.3	ABA transport	169
10.1.4	Stomatal conductance g_s	170
10.1.5	Conditions for simulations	171
10.2	Preliminary results	172
10.3	Discussions	175
10.4	Conclusions	177

DISCUSSION AND PERSPECTIVES

11	General discussion	183
11.1	Quantification of complex root architectures	184
11.2	Monitoring soil water content	188
11.3	Modeling water flow in the SPAC	192
11.4	Quantifying the influence of root architecture	195
11.5	Quantifying the influence of root hydraulic properties	197
11.6	Quantifying the influence of long distance signaling	199
12	Conclusions	201
	General bibliography	203

ANNEXES

A	Hoagland solution	235
B	Light transmission imaging	237

TABLE OF CONTENTS

B.1	Image acquisition	237
B.2	Image processing	238
B.2.1	Change image type	238
B.2.2	Geographic registration	238
B.2.3	Average of the image repetitions	238
B.2.4	Color registration	239
B.2.5	Geographic registration	239
B.2.6	SIR images creation	239
B.2.7	Humidity image creation	239

LIST OF FIGURES

0.1	Specific objectives of the thesis	9
0.2	Visual representation in PlaNet-Maize	11
1.1	Water flow in the soil-plant-atmosphere continuum	20
1.2	Typical soil water retention curves	24
1.3	Scenario for xylem refilling under tension.	36
1.4	Soil and plant conductivity ranges	40
1.5	Effect of soil type on ABA production by roots	42
1.6	Effect of cavitation on transpiration	45
3.1	Multilayer approach in SmartRoot	57
3.2	Effect of the distance between nodes	58
3.3	Diagram of SmartRoot tracing algorithm	59
3.4	Stepwise construction of the segmented line	61
3.5	Multipoint border search and centering algorithm.	62
3.6	Sub-pixel resolution vs diameter estimation	62
3.7	Detection of root junctions	63
3.8	Lateral root detection algorithm	64
3.9	Analysis of time-lapse image sequences	66
3.10	Analysis of 15-day old maize root systems	69
3.11	Histograms generated with SmartRoot	69
3.12	Analysis of a 16-day old lupin root system	71
3.13	Evolution of a single proteoid root	72
3.14	Relationship between growth rates and diameter	72
3.15	Histogram of the timing of lateral root formation	73
3.16	Sequence of cluster root formation	74
4.1	Procedure to digitize an entire root system	81
4.2	Example of digitized maize root system	82
4.3	Scanned vs traced root system area	83
4.4	Skeleton comparison between GiA Roots and SmartRoot	83
4.5	Architectural results	84
4.6	Evolution of the soil water content	86
4.7	Scanning procedure	88
4.8	Local uptake analysis	90
6.1	Time line of the LTI experiments	100

LIST OF FIGURES

6.2	Rhizotron storing device	101
6.3	Light transmission imaging calibration	102
6.4	Soil hydraulic properties	103
6.5	Soil and root system layers	104
6.6	Plant size comparison between genotype	106
6.7	Size parameters variability	107
6.8	Correlation matrix of architectural features	108
6.9	Soil water content evolution	109
6.10	Soil water content evolution - graph	109
6.11	Effect of transpiration on the soil water content decrease	110
6.12	Water depletion and architectural traits - I	112
6.13	Water depletion and architectural traits - II	113
6.14	Transpiration vs soil water extraction	115
6.15	Root length density in the different soil layers	115
7.1	Methodology used to decrypt water flow	119
7.2	Timeline for the LTI-RSWMS experiment	119
7.3	Parameters used for R-SWMS' simulations	120
7.4	Transpiration response	121
7.5	Water content profiles	122
7.6	Experimental decrease in water content	123
7.7	Visual comparison of simulation and experiment results	123
7.8	Experimental and simulated water content variations	124
7.9	Water content vs water uptake	125
7.10	Water uptake vs. decrease in soil water content	126
7.11	Parameter modifiers in R-SWMS	128
7.12	Visualisation of simulation results for WSE2	130
7.13	Collar water potential	131
7.14	Experimental and simulated water content variations	131
9.1	PlaNet-Maize UML scheme	143
9.2	PlaNet-Maize representations	144
9.3	PlaNet-Maize conductivity modifiers	151
9.4	Comparison between experimental and simulated data	153
9.5	Root-to-shoot surface ratio vs the collar water potential.	154
9.6	Effect of the irrigation technique on the shoot	156
9.7	Effect of the irrigation technique on the roots	157
9.8	Response of leaf water potential to soil drying	159
9.9	Regulation sensibility	160
9.10	Effect of regulation processes on the plant water status	162
9.11	Effect of regulation processes on the plant water status	163
9.12	Effect of the regulation processes on the water uptake	164

10.1	ABA production	169
10.2	Leaf conductivity modifier	170
10.3	Response of leaf water potential to soil drying	173
10.4	Water potential evolution vs soil drying	173
10.5	ABA concentration vs soil drying	174
10.6	Transpiration vs soil drying - 1	174
10.7	Evolution of ABA concentration	175
10.8	Evolution of g_s and transpiration	176
11.1	Specific objectives of the thesis	183
11.2	Weekly visits	185
11.3	Manual root drawing	190
B.1	Light transmission imaging setup	237
B.2	Light transmission imaging calibration.	240

LIST OF TABLES

2.1	Available root image analysis softwares	53
3.1	Export options in SmartRoot	67
3.2	Architectural data of maize	70
3.3	Strengths and weaknesses of SmartRoot.	75
6.1	LTI experiment details	101
6.2	Parameters for light transmission imaging analysis .	105
6.3	Correlation between plant parameters and SWC . .	111
7.1	LTI-RSWMS experiment details	120
7.2	R-SWMS simulations	127
9.1	PlaNet-Maize conditions for simulations	152
10.1	ABA production	168
10.2	Half lives of ABA in the different plant articles. . . .	169
10.3	Conditions for the ABA simulations	171
11.1	Projects using SmartRoot	184

LIST OF ABBREVIATIONS

ABA	abscisic acid
AQP	aquaporin
DAT	Day After Transplantations
FSPM	Functional-structural plant model
g_s	leaf radial conductivity
GUI	Graphical User Interface
K_x	root axial conductivity
K_r	root radial conductance
K_{sat}	soil saturated conductivity
L_p	plant conductivity
L_{pr}	root system conductivity
L_{pcell}	cell conductivity
LAUZ	Length of Apical Unbranched Zone
PIP	Plasma Membrane Intrinsic Protein
PRD	Partial Root-zone Drying
PWP	Permanent Wilting Point
Ψ_{soil}	soil water potential
Ψ_{atm}	air water potential
RSSR	Root-to-Shoot Surface Ratio
RW	Re-Watered
RSA	Root System Architecture
SPAC	Soil-Plant-Atmosphere Continuum
SWC	Soil Water Content
VPD	Vapor-Pressure Deficit

WD	Water Deficit
WSE	Water Shortage Episode
WW	Well-Watered

PART I

INTRODUCTION
AND OBJECTIVES

In this first section, we will shortly introduce the thesis and formulate its different objectives.



I know my corn plants intimately, and I find it a great pleasure to know them.

BARBARA MCCLINTOCK

INTRODUCTION

WATER IS BY FAR the resource that plants absorb in largest amounts from their environment. However, only a tiny fraction of the water taken up is used in the synthesis of new assimilates. The largest part is lost to the atmosphere as stomata open to allow the diffusion of carbon dioxide into leaves. For the maize crop, this expensive exploit represents annually ca. 3×10^{14} litres of water worldwide, enough to fill 250 million olympic swimming pools (London 2012 Olympic Games had two of them), about twice the volume of the Dead Sea. Although transpiration prevents excessive heating of sunlit leaves and ensures long-distance transport of nutrients from the bulk soil to the upper plant organs, the contrasting transpiration efficiencies of C3 and C4 species is an indication that actual crop water use often exceeds theoretical requirements. However, the fact that breeding for reduced crop water use has often led to negative results (Blum, 2005) stresses that a more detailed consideration of the dynamics of water fluxes in the soil-plant-atmosphere system is needed (Gregory et al., 2005).

The transport of water in the soil-plant-atmosphere is a passive process enabled by a handful a bio-physical features (Steudle, Peterson, 1998). When stomata are open, the large water potential difference between the atmosphere and the leaf substomatal chambers drives the outflow of water from the sub-stomatal space and the evaporation of water from the mesophyl cell walls. Since xylem vessels ensure the presence of a continuous water column between the leaves and the roots, this loss of water at the leaf level creates a tension that is quickly transmitted to the root surface, creating an inflow of water from the soil.

Although this flow is primarily defined by the regulation of the stomata aperture, different features at the root system level are thought to play an important role in regulating water uptake.

The water flow from the root surface to the xylem lumen is impeded by the radial morphology of the roots, the deposition of hydrophobic substances in specific cell layers and the activity of water channels

known as aquaporins. The integration of these different features defines the root radial conductance, usually thought to be an important limitation to the water inflow.

Inside the xylem, the flow of water is essentially influenced by the root axial conductivity, determined by the maturation of the vessels and, in situation of increasing tension in the water column, the progressive embolisation of the vessels network. Although in normal conditions, the axial conductivity is larger than the root radial conductance by several order of magnitude, its integration over the length of the root system and the onset of cavitation are thought to play a significant influence on the uptake.

Moving to different dimensions, the root system architecture in itself defines the volume of soil explored by the plant and the spatial distribution of water uptake sites. Ultimately, the integration of root architecture and root hydraulic properties, referred as the *hydraulic architecture* (Doussan et al., 1998), defines where the water is most likely to be taken up in the soil domain.

On the soil side, the flow of water from the bulk soil to the root surface is defined by the soil conductivity, itself depending on the soil type and its water content. As the soil is drying, the conductivity of the soil decreases and the refilling of water depleted area slows down. In parallel, as water is extracted from the soil pores, the soil water potential decreases and renders the removal of additional water more and more difficult.

In order to decrypt the water dynamics of the soil-plant-atmosphere continuum and more precisely of the soil-root domain, the different plant and soil features described above must be considered simultaneously. Unfortunately, the multi-scale nature of the system makes it difficult to observe each component at the same time.

Following the development of digital photography, the analysis of root system images has seen an increasing interest throughout the scientific community. As a direct consequence, recent years have seen the development of a number of root image analysis software. Unfortunately, none of those software allows the architectural analysis of complex root systems.

Despite the development of new technologies enabling the observation of water flow in the soil-root system, the concurrent observation of root system architecture and soil water content is often restrained to a small number of plants.

In parallel to the development of new experimental tools and techniques, the introduction of mathematical modeling provides new investigation tools to decrypt water flows in the soil-root domain. However, at present time, none of the existing models takes into account the whole soil-plant-atmosphere continuum with a resolution that allows to account for the spatio-temporal heterogeneity of the plant and soil hydraulic properties.

Note about the thesis structure

This thesis is a compilation of published and unpublished work. The different sections were partially rewritten from their original parts to improve the coherence of the document. However, as some repetitions might still occur from one part to the other, I would like to apologize to the persons reading the entire document.

Why maize was the obvious choice

The work presented in this thesis has been carried out with maize (*Zea mays*), though it might have been done with any plant species. The choice of maize followed several reasons:

- Several research groups in the direct lab neighbourhood were already working on maize when the project started.
- Maize is a major crop production worldwide. It is used as human staple food, livestock feed and in bio-ethanol production.
- Maize plants have been extensively studied and the scientific literature covers almost every aspect of the maize physiology, morphology, genetics, etc.
- Large genetic stocks have been identified and created (mutants, GMO's) and are available.
- Maize plants quickly develop a large leaf area and display, therefore, an important transpiration.
- Maize roots are thicker than those of most cereals which makes them easy to observe and quantify.

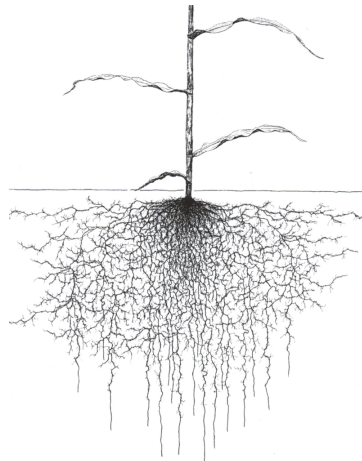


Illustration from Kutschera et al. (1997)

OBJECTIVES

General objective

THE OBJECTIVE OF THIS THESIS was to develop new tools and methods (1) to analyse the water flows in the soil-root domain and (2) quantify the contribution of plant regulatory processes. Since the latter span molecular (abscissic acid), tissue (root hydraulic properties) and organ scales (root system architecture), different strategies have been considered to develop a global and precise view of the whole system.

To address this general objective, three methodological objectives were defined, related to the development of new tools and methods (fig. 0.1., grey boxes). Three «proof-of-concept» objectives were also defined to show the utility of these new tools to help understanding the role of plant regulatory processes in the water dynamics of the soil-root domain (fig. 0.1., white boxes).

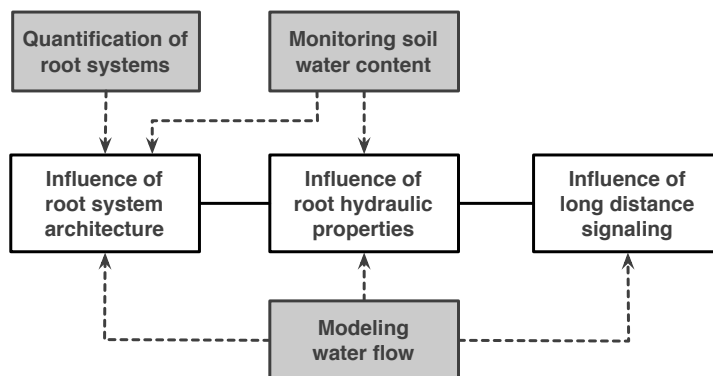


Figure 0.1: Specific objectives of the thesis. Grey boxes represent methodological objectives. White boxes represent research objectives.

Specific methodological objectives

Quantification of complex root architectures

Plant root architecture is a central actor in the water uptake process (Lynch, 1995; Tuberosa, 2012). A precise description of architecture is necessary to address the spatial dynamics (patterns) of water uptake. Such descriptions are mostly obtained with imaging techniques, however no root image analysis tools enable the characterization of complex root systems. In general, a trade off is observed between the level of precision/detail of the analysis and the time required to process the images. Few root parameters can be estimated en masse using fully automated software (e.g. WinRhizo, Arsenault et al. (1995)) while the detailed tracing of complex root system requires fully manual software and is highly time consuming (e.g. DART, Le Bot et al. (2010)).

The first objective of the thesis was to implement an interactive root image analysis tool that allows a fast tracing of complex root systems at a reasonable throughput without significant loss of architectural information. The tool, SmartRoot, initially created by Xavier Draye, was strongly improved in the framework of this thesis.

➔ CHAPTER 2 | CHAPTER 3 | CHAPTER 4

Monitoring soil water content in the soil-plant domain

Several techniques have been developed to observe water flow in the soil-plant system. However, these techniques often rely on expensive equipment, require extensive technical knowledge and are usually restricted to the analysis of a small number of plants (Carminati et al., 2010). Moreover, depending on the technique, a precise quantification of the root system architecture is not always possible.

The second methodological objective of the thesis was to develop an experimental platform enabling the simultaneous observation of soil water content and root system architecture for a larger number of plants. Our experimental setup relies on the light transmission imaging technique (Garrigues et al., 2006) and enables the observation of 20 plants during 4 days.

➔ CHAPTER 5 | CHAPTER 6 | CHAPTER 7

Modeling water flow in the soil-plant-atmosphere continuum

Over the last decades, scientists have been developing models to simulate the growth and development of plants in their environment (Tardieu, 2010), moving from purely architectural models (Diggle, 1988; Lynch et al., 1997) to functional-structural models (Bidel et al., 2000; Drouet, Pagès, 2003; Godin, Sinoquet, 2005). These models have proved to be useful to address the complexity of biological systems and support our understanding of plant-environment interactions (Ge et al., 2000; Postma, Lynch, 2011b).

The third objective of the thesis was to develop a functional-structural plant model that simulates the growth and development of a maize plant, alongside with an explicit resolution of water flow in the soil-plant domain. The model, PlaNet-Maize (fig. 0.2), was based on the meta-model PlaNet created by Loïc Pagès.

➔ CHAPTER 8 | CHAPTER 9 | CHAPTER 10

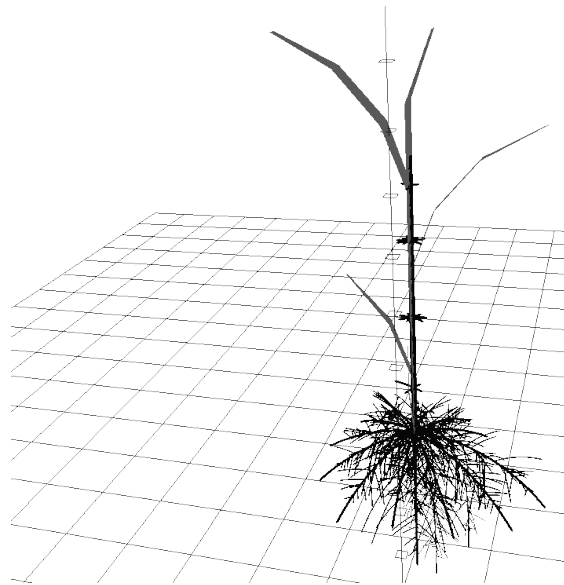


Figure 0.2: Visual representation of a whole maize plant in PlaNet-Maize.

Specific research objectives

Quantification of the influence of root architecture

At many occasions, root architectural traits have been linked to different water uptake strategies in agricultural plants (Hammer et al., 2009; Tuberosa, 2012; Wasson et al., 2012). However, for practical reasons, most of these studies focused on global dynamics rather than local phenomena.

The first specific research objective was to link explicitly root architectural parameters to local soil water content. This objective was pursued to demonstrate the utility of experimental (light transmission imaging, Garrigues et al. (2006)) and modeling tools (PlaNet-Maize, Lobet et al. (2012)).

→ CHAPTER 5 | CHAPTER 6 | CHAPTER 9

Quantification of the influence of root hydraulic properties

Root hydraulic properties (axial and radial) are thought to influence the water uptake dynamics at the plant level (Draye et al., 2010). However, their contribution have always been assessed separately and either at the local level (individual root, Frensch, Steudle (2007)) or averaged at the plant level (Li et al., 2009).

The second specific research objective was to explicitly investigate the quantitative contribution of root axial and radial properties in the water uptake process. The precise observation and manipulation of the plant hydraulic properties were performed to establish the utility of modeling tools in the framework of soil-root interaction research (R-SWMS (Javaux et al., 2008) and PlaNet-Maize (Lobet et al., 2012)).

→ CHAPTER 7 | CHAPTER 8 | CHAPTER 9

Quantification of the influence of long distance signaling

The transmission of a stress signal from the root to the shoot (long-distance signaling) is essential for the regulation of the plant water consumption in situations of soil water deficit (Tardieu, Davies, 1993). While different signals have been identified, abscissic acid (ABA), a plant hormone involved in stress responses, is thought to play a central role in the signaling process (Dodd, 2005).

The last specific objective of this thesis was to use the model PlaNet-Maize to investigate how long distance ABA signaling might interfere with the water flow in the SPAC.

➤ CHAPTER 8 | CHAPTER 10

PART II

CONTEXT

This section will present in details the current knowledge about water uptake and water flow in the soil-root domain.



I believe that scientific knowledge has fractal properties; that no matter how much we learn, whatever is left, however small it may seem, is just as infinitely complex as the whole was to start with. That, I think, is the secret of the Universe.

ISAAC ASIMOV

ROOT WATER UPTAKE AND WATER FLOW IN THE SOIL-ROOT DOMAIN



This chapter is a modified version of a book chapter entitled:

Lobet, G., Hachez, C., Chaumont, F., Javaux, M. & Draye, X.
2013. Root water uptake and water flow in the soil-root domain.
In A. Eshel & T. Beekman, eds. *Plant Roots: The Hidden Half*.
Taylor and Francis.

IN A TRANSPIRING PLANT, the diffusion of vapor to the atmosphere through stomata leads to the evaporation of water from the mesophyll cell walls and the displacement of the water-air interface to narrower interstitial spaces between wall fibrils. This increases capillary forces at the wall surface and the tension at the leaf-side of the soil-plant hydraulic continuum. In the absence of any resistance to water flow along the continuum, this tension would lead to an immediate displacement of water from the soil and maintain the system in a steady state. However, water movement is impeded by several features of both the soil matrix and plant structures, which complicate water entry into the plant and decrease the water potential in the whole continuum (fig. 1.1.A). The master control, played by the stomata, which operates where the water potential gradient is the largest, is therefore subordinate to the ability of the upstream continuum to cope with the transpirational demand. If the impedence between the bulk soil and the stomata gets so large that the plant water potential decreases to damaging levels, the plant will wilt and die unless it closes its stomata.

In the absence of transpiration, the xylem tension disappears and the residual water potential gradient between the soil and the root is dominated by the osmotic component (Javot, Maurel, 2002). In such conditions, the driving force to water flow relies on the difference in solute concentration between the xylem and the soil solution, resulting from the active pumping of solutes from the soil to the root results. The resulting water flow can generate a small positive pressure in the xylem, which can assist the refilling of embolized vessels (see below) but does not contribute to the massive absorption of water. For this

1. WATER FLOW IN THE SOIL-ROOT DOMAIN

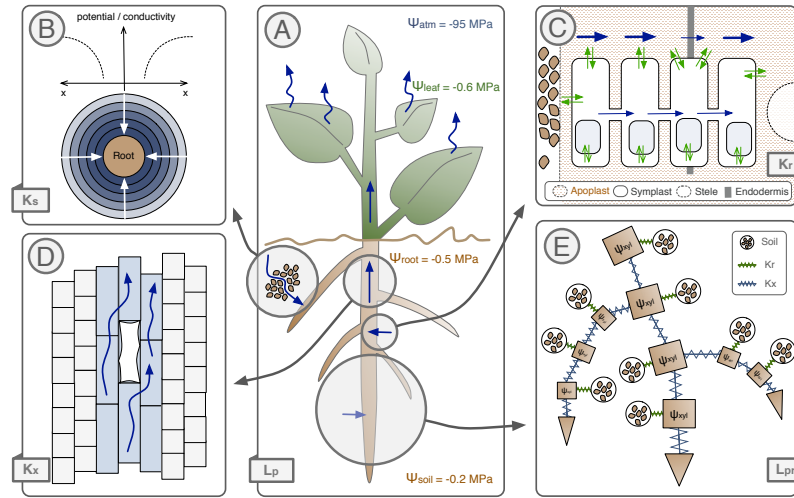


Figure 1.1: Water flow in the soil-plant-atmosphere continuum (SPAC). **A.** Cohesion tension mechanism. The water flows along the SPAC following the gradient of water potential between the different compartments. **B.** Water movement in the soil. The water flows in the soil following local gradient of matrix forces. Close to the root surface, the radial nature of the water flow induces a strong water potential gradient. **C.** Radial movement of water in the root. Water entering the roots has to traverse several cell layers using a combination of symplastic, cell to cell and apoplastic pathway. Blue arrows represent pressure-driven convection while green arrows represent osmotically-driven flow. **D.** Axial movement of water in the root. Water moves in xylem vessels following water potential gradients between roots and leaves. The path can be interrupted locally at embolized vessels (cavitation). **E.** Importance of the root system architecture as an integrative element. The analogy between the root system hydraulic architecture and an electric network makes it possible to predict the sites of water uptake within the root system.

reason, the scenario of root pressure-driven flow is only briefly mentioned in the section dealing with xylem refilling.

Biologists often use the analogy with the Ohm's law to express the dependency between water potential, water flux and hydraulic resistance (van den Honert, 1948). At the whole plant scale, the electrical analogy is expressed as

$$E = (\Psi_{atm} - \Psi_{soil}) * L_p \quad (1.1)$$

where E is the total water flow, Ψ_{atm} is the water potential of the atmosphere and L_p and Ψ_{soil} are aggregated values of the plant hydraulic conductivity and soil water potential. As will be explained throughout this chapter, the complex hydraulic architecture of the soil-plant system and the values of all resistances impeding water movement determine the water potential, hydraulic conductivity, and water flow at every location in the system, at any given transpiration rate. It is their integration at a higher scale which sets the spatial distribution and amount of water E flowing through the plant, referred to as *uptake*. Excellent reviews of root water uptake have been published already (Aroca et al., 2011; Draye et al., 2010; Jackson et al., 2000; Javot, Maurel, 2002; Maurel et al., 2010). This chapter focuses on the mechanisms or principles which impede (and, thereby, control) water flow on its way from the bulk soil to the shoot of transpiring plants, and on novel ways of analyzing how water uptake patterns emerge from the integration of several hydraulic controls in the soil-plant system.

1.1 Water moves in a complex system

Despite a general agreement on the driving forces of water flow in the soil-plant-atmosphere continuum, on the possible routes taken by water and on the local mechanisms which control its flow, it remains difficult to predict quantitatively the contribution of specific mechanisms to the overall regulation of root water uptake. This is largely due to the composite pathway and the spatially distributed and temporally variable nature of the hydraulic controls.

1. WATER FLOW IN THE SOIL-ROOT DOMAIN

Before entering the root, water flows in the bulk soil towards the soil-root interface. Its movement follows Ψ_{soil} gradient and is impeded by friction against the solid phase. Because soils are comprised of an ensemble of pores of different sizes, their hydraulic conductivity decreases non-linearly with water content (fig. 1.1.B), viz. with water getting restricted to narrower pores. As mentioned above, transpiration decreases the amount of water, and thus the water potential in the immediate vicinity around the roots. In a homogeneous domain, this is likely to cause a drop of the soil conductivity, leading to a redistribution of the sites of water uptake. In the corresponding electrical analogy, the soil domain is represented by spatially distributed capacitance and resistance elements that are physically linked to the soil water potential.

When entering the root, water flows into a structure comprised of several layers of differentiated cells. As stated in the composite transport model (Steudle, Peterson, 1998), water crosses the successive layers using pressure-driven apoplastic (cell wall and intercellular spaces) and symplastic (plasmodesmata) pathways or osmotically-driven transcellular pathways (water channels). As water flows preferably in routes of low resistance, the contribution of the three pathways is ultimately controlled by the geometry, cell wall properties and membrane permeability of each layer (Steudle, 2000; Steudle, Peterson, 1998) (fig. 1.1.C). The most obvious controlling features are the number of cell layers laid down by the meristem (organ level), the irreversible deposition of hydrophobic barriers in the apoplast (tissue level, Enstone et al. (2003); Ranathunge et al. (2011)) and the dynamically regulated activity of water channels (cell level, Chaumont, Moshelion (2005); Javot, Maurel (2002); Maurel et al. (1993)). The electrical analogy could be used to integrate cell, tissue and organ level effects on the control of the radial flow. It would comprise resistances to flow between the different compartments (cell walls, intercellular space and cytoplasm), connected in agreement with the radial anatomy and subjected to a difference of water potential between the root surface and the xylem lumen.

Once in the xylem, water flows over long distances through the network of vessels (fig. 1.1.D). Because xylem conductivity is by several order of magnitude higher than that of tissues along the radial path, it is often assumed that the xylem route imposes a negligible impedance to water flow in the soil-plant-atmosphere continuum (Steudle, Peterson, 1998). However, this route is by large the longest one taken

by water within the plant. In a maize plant, for example, water runs for several meters in the xylem, but only a few millimeters from the root surface to the xylem and from the xylem to the mesophyll cells, viz. a difference of three orders of magnitude. There is also abundant evidence that the xylem route can be the limiting route in the system as the likelihood of cavitation increases with path length (Peirce, 1936; Sperry et al., 2002; Tyree, Sperry, 1989). Frictional drag and cavitation, the major limitations to water flow in the xylem, obey two very different laws, with friction being predicted by Poiseuille's law while cavitation is, at best, only predicted by probability models. As previously mentioned, an electrical analogy could be used to work out the detailed flow of water through the network of xylem conduits. Here, however, in addition to using resistances where friction is operating, on/off switches with partially stochastic behaviors would be needed at the level of each xylem vessel.

The obvious need to integrate different types and scales of control at the sub-organ level also applies at the whole plant level. Indeed, water flows simultaneously from many different places in the bulk soil and enters the plant through many different roots, following trajectories which are not hydraulically equivalent. Even for plants growing in uniform hydroponic systems, water uptake is unlikely to be uniform over the root surface. The structure and geometry of the soil/root system place therefore additional constraints on water flow and uptake. It is certainly at this level that the electrical analogy has been most used (Doussan et al., 1998), probably due to the simplicity of the circuit, comprising a simple tree of nodes connected by axial resistances and linked to their local environment by radial resistances (fig. 1.1.E).

Looking at the whole array of conductivities of the media or structures in which water is flowing, some appear to be variable on long time scales while others are highly dynamic. Some appear to vary following simple physical laws, while others follow intrinsic or responsive regulatory pathways. In the next section, we review our understanding of the phenomena responsible for the variation of these conductivities, considering successively those which operate in the soil, in the radial path, in the xylem network and at the system level.

1.2 Control of water flow in the soil matrix

1.2.1 Soil hydraulic properties that affect water flow to the roots

In soils, water follows passively the water potential gradient to move from the bulk soil to the root surface. Accordingly, the soil water potential gradients and the soil hydraulic conductivity will, at any given time, control the supply of water to the plant. As discussed below, these hydraulic properties of the soil compartment display highly dynamic behavior, which is most likely to determine the patterns of water availability and uptake. A crucial feature of soils is their ability to store water, which is due to their porous structure. However, the amount of energy needed to extract water from the soil increases as the soil water content decreases, because capillary and surface-binding forces reduce the free energy of water retained in pores (matric potential). At equilibrium, the matric potential is related to the volumetric soil water content by a water retention (or release) curve, which is principally determined by the pore size distribution and the wetting properties of the pores surface (fig. 1.2). Water retention curves also display hysteresis according to the wetting or drying cycle of the soil.

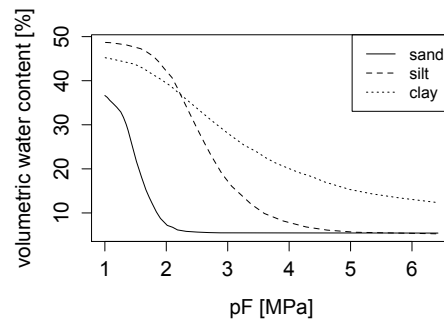


Figure 1.2: Typical soil water retention curves. Plain line: sand. Dashed line: silt. Dotted line: clay. $pF = -\log(hPa)$.

A second crucial feature of soils is their ability to conduct water when subjected to a gradient of water potential. The soil hydraulic conductivity is inversely related to friction and is therefore affected

by fluid properties (viscosity and density) and soil structure, i.e., the size, shape, tortuosity and connectivity of the pore network filled with water. Even in fully saturated conditions, the conductivity value (K_{sat}) may vary by several orders of magnitude between fine- and coarse-textured soils. At the field scale, values of the saturated conductivity in certain horizons exhibit a coefficient of variation up to 900%, mainly determined by structural features like macropores (Mallants et al., 1997). When the soil desaturates, the hydraulic conductivity decreases dramatically because flow paths become increasingly tortuous and drag forces between the fluid and the solid phases increase. This steep curve induces ratios between saturated and unsaturated conductivity values at 1.5 MPa ranging between 10^6 (for a clay) and 10^{21} (for a sand). The hydraulic conductivity curve characterizes this dependence of the hydraulic conductivity on soil moisture.

1.2.2 Soil water dynamics in the presence of roots

The Richards equation (Richards, 1931) is usually used to model soil water flow, taking into account the non-linear water release and hydraulic conductivity behaviors of soils. At the root scale, considering a radial geometry, the solution of this equation close to the root surface indicates that, under constant uptake, the soil matrix potential decreases non-linearly towards the root surface (fig. 1.1.B), which results in a higher resistance to water flow compared to the bulk soil (Gardner, 1965). In conditions of high transpiration rate and medium to dry soil moisture, the decreased soil conductivity near the root surface may limit root water uptake, despite the presence of sufficient water in the bulk soil (Schröder et al., 2009).

The redistribution of soil water can also affect root water uptake. At night, as long as the plant hydraulic conductivity is large enough and no capillary or hydrophobic barrier develop during the previous day, soil hydraulic potential tends to even out, restoring the water content around roots and in the water-depleted zones. The intensity of this lateral and vertical redistribution depends on soil hydraulic properties and on the soil and plant hydraulic status. At the field scale, it also depends on soil hydraulic properties that are shaped by natural (e.g. soil horizons due to pedogenesis) and entropic processes (e.g. soil tillage), but also by soil topography (through runoff) and row / inter-row patterns

1.2.3 *Hydraulic properties of the rhizosphere*

The rhizosphere is the soil zone that surrounds, and is affected by the presence and activity of roots. Its boundaries are diffuse and its spatial extent ranges from sub- μm to supra-cm scales, depending on the process of interest (Darrah, 1993; Hinsinger et al., 2005). In the rhizosphere, soil hydraulic properties can be profoundly modified by the presence and activity of roots and microorganisms (Pierret et al., 2007). The combination of structural, chemical and biological effects is relatively complex and not well understood. In addition, the hydraulic properties of the rhizosphere are difficult to measure with conventional techniques. It follows that different and sometimes contradicting results were obtained with respect to the impact of rhizosphere processes on soil hydraulic properties (Moradi et al., 2012).

Root growth causes compaction of the surrounding soil in front of the root apex (Dexter, 1987). This increases the bulk density (Guidi et al., 1985) and reorganizes the soil pore distribution and continuity. While Whalley et al. (2004) suggest that this would generate a decrease of the infiltration, Aravena et al. (2011) show with modeling that this could increase the soil conductivity by raising soil water connectivity modelled instead that this could causing an increase in the soil conductivity by raising soil water connectivity.

Exudates from roots and microbial and fungal communities also affect the hydraulic properties of the rhizosphere. Mucilage principally contains polysaccharides that retain high water content at low water potentials (McCully, Boyer, 1997; Read et al., 1999; Watt et al., 1994). Exsudates contain also surfactants that reduce the surface tension of soil solution (Read et al., 2003) and other hydrophobic compounds that increase the soil water repellency as compared to bulk soil (Hallett et al., 2003), potentially generating a slower rate of infiltration in drier soils (Czarnes et al., 2000). Carminati et al. (2011) combined the observations of higher water holding capacity and unsaturated conductivity into a simple model and proposed that water availability to plants would increase under unsaturated conditions.

The geometry of the root-soil contact in itself can also influence the conductivity of the rhizosphere. In young root segments, this is commonly modified by the production of hairs that extend into the rhizosphere, arising from selected cells of the root epidermis (or rhizodermis (Esau, 1965)). Root hairs increase the apparent conductivity

of the soil-root contact by increasing the surface through which water flows into the root (Bibikova, Gilroy, 2003; Gilroy, Jones, 2000; Segal et al., 2008). Root hair formation and length are tightly controlled in response to local environmental conditions.

Another modification of the root-soil geometry consists in the shrinkage of roots (and soil), which generates air gaps at the soil-root interface (Carminati et al., 2009; Veen et al., 1992). This phenomenon, which occurs typically under very dry conditions, can be seen as a safety mechanism leading to a dramatic reduction of the transfer of water between the soil and the root.

1.2.4 The soil, constitutive part of the soil-plant-atmosphere continuum

Because the water supply from the bulk soil to the root surface depends on soil properties that are shaped by prior water uptake, the non-linear water retention and hydraulic conductivity behaviors of the soil, combined with the array of rhizosphere processes are likely to generate complex patterns of water uptake at the whole plant scale. As the soil has long been considered a continuous medium, the analogy with the electrical circuit has never been used in soil physics. Unlike plants, the whole soil domain can be approached with a unique equation, such as Richard's equation, that can be solved numerically.

The complexity of the soil compartment has been largely neglected in the past and water uptake has been assumed to be mostly determined by root length density. This simplified view is supported by several reports showing, by experiments or calculations, that under wet conditions, the soil conductivity is much higher than the root radial conductivity (Arya et al., 1975; Gardner, Ehlig, 1962; Newman, 1969a; Passioura, 1980). However, under low moisture conditions that are often encountered, the soil conductivity may become limiting for water uptake (Draye et al., 2010). Interestingly, this suggests that our current understanding of water capture largely ignores many aspects of its dynamics.

1.3 Control of radial water flow

1.3.1 Radial water movement

In response to the hydraulic gradients, water molecules that enter the root have to flow through the complex anatomical structure of roots, as described by the composite transport model (Steudle, Peterson, 1998). Depending on the tissue anatomy, developmental stages and environmental conditions, water will flow through a combination of paths that offers the lowest hydraulic resistance to its passage. It was generally assumed that under transpiring conditions, when hydrostatic water gradients are dominant, the apoplastic path would be dominant (Steudle et al. 1998). This simplified view has been recently challenged by reports that water flowing via the cell-to-cell path could account for almost the whole radial root water transport, even while the plant is transpiring (Bramley et al., 2009; Knipfer, Fricke, 2010; Knipfer et al., 2011). In addition, the relative contribution of cell-to-cell and apoplastic paths to the total hydraulic conductivity depends on the species and even on the ecotype (Bramley et al., 2009; Sutka et al., 2011). Nowadays, the common view is that there is neither a purely apoplastic nor a pure cell-to-cell root water movement but rather a combination of both, due to the local variations of water potentials, cell wall and cell membrane hydraulic resistances (fig. 1.1.C).

1.3.2 Modification of anatomical structures

The conductivity of the root apoplasm is primarily determined by the overall structure of the cortex viz. the number of cell layers, wall thickness and cell size. This basic organization can be further modified by highly selective cell death and dissolution in the cortex leading to the formation of large air cavities (aerenchyma) within the root cortical cylinder. This results in a reduction of root conductivity (L_{pr}) which is at least partly due to a drastic reduction of the cumulated membrane surface and of the aquaporin-mediated radial transport of water (Fan et al., 2007; Yang et al., 2012).

The hydraulic conductivity of the apoplasm is locally disrupted by the deposition of lignin and suberin compounds within the cell wall matrix, which occlude wall pores otherwise filled with water (reviewed by Schreiber et al. (1999)). The endodermis is a major apoplastic barrier which develops with a very regular maturation pattern in most angiosperm species (Perumalla, Peterson, 1986). It, contributes to the

prevention of water loss (cutting-off apoplastic by-passes), the maintenance of root pressure (Peterson et al., 1993) and the protection against pathogen and detrimental environmental conditions (Enstone et al., 2003; Hose et al., 2001; Thomas et al., 2007).

The exodermis (defined as an hypodermis with Casparian bands) fulfils similar functions (with the exception of root pressure maintenance). However, the extent, composition and rate at which exodermal apoplastic barriers develop strongly depends on environmental cues such as drought, anoxia, salinity, heavy metals or nutrient stresses (Enstone, Peterson, 2005; Enstone et al., 2003; Hose et al., 2001). The cultivation of maize seedlings in aeroponic conditions induces the formation of an exodermis in primary roots (Hachez et al., 2006, 2012; Zimmermann et al., 2000), leading to a reduction of L_{pr} by a factor 1.5 to 3.6 compared to hydroponic culture. Furthermore, water deficit is known to promote or intensify the development of root apoplastic barriers (both endodermis and exodermis) that tend to develop closer to the tip (Enstone, Peterson, 2005; Hose et al., 2001; Karahara et al., 2004; Perumalla, Peterson, 1986; Vandeleur et al., 2009).

1.3.3 Regulation by water channels

Plants have the ability to rapidly alter their L_{pr} in a span of a few minutes to a few hours (Cochard et al., 2007; Hachez et al., 2012; Javot et al., 2003; Lopez et al., 2003; Moshelion et al., 2002). This fine regulation is under metabolic control and may be accounted for by changes in cell membrane permeability triggered by the expression and specific activation of water channel proteins known as aquaporins (Cochard et al., 2007; Maurel, Chrispeels, 2001; Maurel et al., 2008). Plant aquaporins are found in all subcellular compartments forming or derived from the secretory pathway (Maurel et al., 2008) as well as in some organelles such as chloroplasts (Maurel et al., 2008; Uehlein et al., 2008). Among aquaporin subfamilies, Plasma Membrane Intrinsic Proteins (PIPs) mostly localize in the plasma membrane where they control the bulk of the cell membrane water movement as shown by numerous pharmacological and reverse genetics evidences (Hachez et al., 2006; Martre et al., 2002; Siefritz et al., 2002; Tournaire-Roux et al., 2003).

In roots, the contribution of aquaporins to the total root water flow ranges from 20 to 80% (Javot et al., 2003; Maurel, Chrispeels, 2001) as assessed by the use of aquaporin inhibitors (Tournaire-Roux

1. WATER FLOW IN THE SOIL-ROOT DOMAIN

et al., 2003; Tyerman et al., 1999; Ye, Steudle, 2006) or by reverse genetics approaches (reviewed by Hachez et al. (2006)). In plants, silencing of PIP isoforms (by RNAi or knockout mutants) generally results in a lowered hydraulic conductivity of root cell plasma membrane (denoted as L_{pcell}) (Javot et al., 2003; Kaldenhoff et al., 1998; Martre et al., 2002; Siefritz et al., 2002). Arabidopsis transgenic lines in which expression of several PIP isoforms had been knocked out compensated for a 3- to 5-fold decrease in L_{pcell} by increasing the root/leaf dry mass ratio, so that the overall L_{pr} tended to remain the same (Kaldenhoff et al., 1998; Martre et al., 2002). However, an increase of the root/shoot mass ratio was not found to be a general trend as different plant species used different ways to cope with such reduction in L_{pcell} (reviewed by Hachez et al. (2006)).

L_{pcell} also tends to increase from the root surface towards the endodermis and this further supports the importance of the cell-to-cell path in mediating radial root water flow (Bramley et al., 2009). This increase in conductance of the cell-to-cell path could serve as a compensatory mechanism to the decreasing apoplastic space available as water radially progresses towards the stele.

Regulation of aquaporin expression and activity is of prime importance as it allows a fast adaptation of the cell membrane hydraulics to the cell ever changing surrounding environment. Multiple levels of regulation have been unraveled and novel mechanisms are still to be discovered (Chaumont, Moshelion, 2005; Maurel et al., 2010).

Expression of aquaporins is under a tight transcriptional control by a variety of environmental or hormonal cues of biotic or abiotic origin. Such transcriptional control allows the plant to cope with adverse or changing environmental conditions that impact soil water availability, evapotranspiration rate or plant water uptake ability (Alexandersson et al., 2005; Maathuis et al., 2003). Long-term abiotic stresses such as drought, cold, and salinity usually induce a marked drop in L_{pr} , mostly achieved through down-regulation of aquaporin expression and activity although some upregulated isoforms have been identified (Alexandersson et al., 2005; Jang et al., 2004).

Whereas concomitant down regulation of L_{pr} and L_{pcell} is usually expected upon stress, this is actually not always the case and both parameters can vary independently (Hachez et al., 2012; Sutka et al., 2011; Vandeleur et al., 2009). In response to stress, L_{pcell} may even

increase, as a result of an increase in aquaporin expression and activity, while L_{pr} may decrease or remain unchanged (Hachez et al., 2012; Vandeleur et al., 2009). One plausible explanation for such discrepancies between L_{pcell} and L_{pr} behavior, would be that the increase in cortex cell conductivity is insufficient to compensate for the drop in L_{pr} due to the presence of other control points acting as bottlenecks to water flow, most likely at locations where membranes are crossed (as discussed by Hachez et al. (2012)).

Once synthesized, PIP protein amount in the plasma membrane is modulated by regulation of their subcellular localization. Constitutive cycling of PIPs between the plasma membrane and endomembrane compartments has been demonstrated (Li et al., 2011; Luu et al., 2011). Modulation of this cycling presents a way to rapidly modulate PIP abundance at the plasma membrane in response to stress (Boursiac et al., 2008; Li et al., 2011). In addition to that, PIP subcellular localization can also be regulated by specific physical interaction between different isoforms (Zelazny et al., 2007).

The opening or closure of the aquaporin pore (gating) is also controlled by cytosolic calcium or pH, both of which trigger conformational changes occluding the pore (Boursiac et al., 2008; Törnroth-Horsefield et al., 2006; Tournaire-Roux et al., 2003). Other factors possibly affecting the gating behavior involve methylation, acetylation, phosphorylation, heteromerization, pressure pulses, solute gradients and temperature (for review, see Chaumont, Moshelion (2005), and Maurel et al. (2010)). Finally, hormonal signals also control aquaporin expression and L_{pr} . Abscisic acid (ABA), a well-known stress hormone, has long-lasting effects on plant water status (Nagel et al., 1994; Parent et al., 2009; Thompson et al., 2007). Root hydraulic properties indeed respond to application of exogenous ABA, the most common effect being an increase in L_{pr} (Aroca et al., 2006; Mahdieh, Mostajeran, 2009; Ruiz-Lozano et al., 2009; Zhang, Zhang, 1995). As inferred from a study on transgenic maize lines impaired in the regulation of ABA biosynthesis, this increase of L_{pr} occurs via the up-regulation of aquaporin activity. However ABA can actually trigger either an up- or a down-regulation of aquaporin expression/activity, depending on time, dose (exogenously applied or not) or species (Hose et al., 2000; Martinez-Ballesta et al., 2003; Parent et al., 2009).

1.3.4 *Interplay between root anatomy and aquaporin activity*

The changes in root anatomy described earlier may be accompanied by a concomitant adjustment of aquaporin expression/activity. Expression of root aquaporins has been detected in the vicinity of apoplastic barriers where they presumably facilitate a transmembrane flow of water (Hachez et al., 2006, 2012; Vandeleur et al., 2009). Such a phenomenon has been recently reported in maize where a correlation between exodermis suberization and PIP protein localization could be detected (Hachez et al., 2012). Plants which were grown under aeroponic conditions and which developed a hypodermis with Casparian bands, effectively forcing more water to flow through the membranous uptake path, showed increased levels of some PIP isoforms in the vicinity of the apoplastic barrier when compared to roots lacking such suberized exodermis. However, a similar correlation between suberization pattern and root hydraulic properties (of the endodermis) could not be observed in *Arabidopsis* (Sutka et al., 2011).

Interestingly ABA has been shown to induce suberin biosynthesis in *Arabidopsis* roots and the genes involved in this process were up-regulated by this hormone in *Agrobacterium*-induced tumors developing a suberization of their cell walls (Duan, Schuler, 2005; Efetova et al., 2007). These observations suggest that root suberization might be induced by ABA, whose role in regulating aquaporin expression level and activity has been demonstrated, as discussed in the previous section. The interplay between endogenous ABA levels, extent of root suberization and aquaporin expression and activity clearly deserves further characterization.

Root radial water conductivity is therefore controlled by several processes acting either on the long term (developmentally-driven or in response to lasting adverse environmental conditions) or on the short term (e.g. in response to diurnal variation to transpiration demand). The interplay between both type of processes and their relative contributions seem to be highly dependent on the plant species and the growing conditions. Altogether, this multilevel regulation of root water conductivity could confer a high plasticity and adaptation potential of the root water uptake mechanisms.

1.4 Control of the axial water flow

1.4.1 *Cavitation onset*

As stated earlier, most of the plant water movement takes place in the interconnected network of xylem vessels. The hydraulic continuity of this vascular network can be locally disrupted, as xylem vessels under tension are threatened by the nucleation of small gas bubbles whose rapid expansion (embolism) leads to cavitation. Because the conductivity of embolized vessels drops to zero, the movement of water is forced to flow through the remaining adjacent and non-cavitated vessels (Peirce, 1936; Sperry et al., 1988b; Tyree, Sperry, 1989). As a result, the flow rate and friction in the remaining vessels increases and, by virtue of the Ohm's analogy, the water potential downstream of the cavitation site decreases. This might increase the likelihood of cavitation in the system in a feed-forward way, unless the remaining vessels are less prone to cavitation. As long as the tension in the xylem is maintained (or increases, due to a lesser availability of water in the soil) an increasing number of vessels are likely to become more prone to embolization (fig. 1.1.D). The relation between xylem tension and the proportion of embolized vessels describes a plant's susceptibility to cavitation.

The susceptibility to cavitation has been shown to have various effects on the plant water status, ranging from changes in leaf conductivity (Johnson et al., 2012) and stomatal conductance (Cochard, 2002; Zufferey et al., 2011) to lowering plant yield (Cochard et al., 2007). It remains controversial whether the axial water movement is the weak link of the hydraulic flow in the soil-plant-atmosphere continuum. It is indeed often assumed that in crop plants the limiting factor is the radial component (Steudle, Peterson, 1998). More experiments are therefore required to clarify the functional importance of cavitation events.

1.4.2 *Cavitation avoidance*

Although xylem cavitation is essentially a passive phenomenon, plants use two strategies to keep some level of control. The first strategy embraces all plant features that influence its ability to prevent cavitation. The existence of a control at this level is demonstrated by the variability of the susceptibility to cavitation between plant species (Pockman, Sperry, 2000; Sperry, Ikeda, 1997), cultivars (Cochard et al., 2007; Li

1. WATER FLOW IN THE SOIL-ROOT DOMAIN

et al., 2009) and even organs, where roots have been shown to be more susceptible to cavitation than stem (Hacke, Sauter, 1996; Hacke et al., 2000; Sperry, Ikeda, 1997).

In several instances, differences in cavitation susceptibility have been linked to differences in xylem wall (and pits) structure in both angiosperms (Christman et al., 2012; Herbette, Cochard, 2010) and gymnosperms (Delzon et al., 2010; Hacke, Jansen, 2009). Such structural features are thought to influence gas leakage from an embolized vessel and the formation of nucleation sites in functional adjacent vessels (Delzon et al., 2010; Jarbeau et al., 1995; Tyree, Sperry, 1989). A recent hypothesis states that the total surface of the pit membrane is negatively correlated with cavitation avoidance (Christman et al., 2012). In addition, cavitation can weaken xylem vessels and render them more prone to further cavitation, a phenomenon that does not occur to the same extent in all plant species (Hacke et al., 2001; Stiller, Sperry, 2002).

Other options to restrict cavitation susceptibility are to avoid excessive increase in xylem tension. The surface ratio between the roots and the leaves appears to be a key factor controlling the maintenance of a low tension. For example, an undersized root system (relative to the leaf evaporative surface) would lead to an increase in xylem tension and a greater susceptibility to cavitation (Hacke et al., 2000; Sperry et al., 2002; Sperry et al., 1998). Similarly, isohydric stomatal behaviors preventing the variation of the plant water potential (Tardieu, Simonneau, 1998) are also likely to reduce the risk of cavitation.

1.4.3 *Cavitation recovery*

The second strategy relates to the restoration of the lost hydraulic conductivity through the refilling of embolized vessels. The osmotically-driven pressure build-up that can occur in the root at very low transpiration flow (viz. during the night or winter) is the first mechanism supporting this strategy. Provided the xylem pressure rises above a threshold value which depends on the xylem diameter (Yang, Tyree, 1992), the gas present in the embolized vessel may dissolve into the water that is pushed into the vessels until they are refilled (Sperry et al., 1988a,b; Sperry, Saliendra, 1994; Sperry et al., 1987). The extent and frequency of pressure-driven refilling vary widely between species.

Xylem refilling under tension (i.e. while the plant is transpiring), has been observed in several species and environmental conditions (McCully et al., 1998; McCully, 1999; Zufferey et al., 2011). This discovery caused lively debates within the scientific community but it seems now accepted that *novel refilling* (Hacke, Sperry, 2003) does indeed occur. Nonetheless, the mechanisms remain unclear and several theories coexist (Clearwater, Goldstein, 2005; Holbrook, Zwieniecki, 1999). Figure 1.3 illustrates the conceptual framework proposed by Zwieniecki, Holbrook (2009) to “provoke discussion, organize existing information and provide a useful guidelines for future studies of xylem refilling under tension”. In this framework, active transport of solutes from neighboring parenchyma cells to the embolized vessels generates an osmotic flow of water into the vessel forming high osmotic droplets at the wall surface. The expression of specific aquaporin isoforms appears to be involved in this osmotic flow (Secchi et al., 2011; Secchi, Zwieniecki, 2010, 2011). The partially hydrophobic xylem walls prevent water from the embolized vessel to leak to the neighboring vessel under tension, while small gas-filled channels in the vessel wall enable the exit of gas trapped in the embolized vessel. Finally, additional supply of water in vapor phase from the neighboring vessel is proposed as a novel pathway for refilling.

The hydraulic conductivity of the network of xylem vessels appears therefore as a complex and dynamic variable in the soil-plant continuum. Its complexity lays in the very different nature of the many components that contribute to its regulation. The active solute transport and the multiple paths for water entry and gas exit during refilling deserve more attention as these processes are extremely important in controlling plant long distance water movement.

1. WATER FLOW IN THE SOIL-ROOT DOMAIN

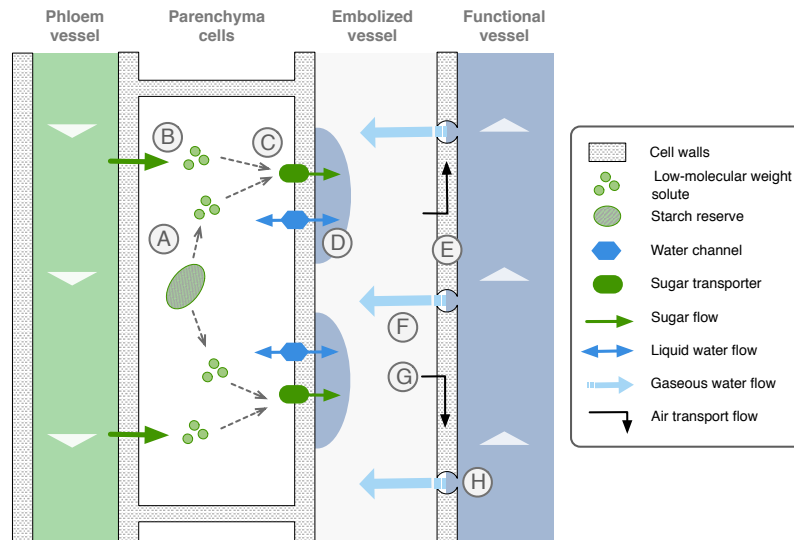


Figure 1.3: Scenario for xylem refilling under tension. Starch (**A**) and phloem (**B**) serve as sources of low-molecular weight solutes that are actively transported into the embolized vessel (**C**). The accumulation of solutes results in water movement from xylem parenchyma cells by osmosis, forming droplets with high osmotic activity on internal vessel walls (**D**). The partially non-wettable walls of xylem conduits prevent these droplets from being removed by suction from still-functioning vessels (**E**). Condensation of water vapor provides a second pathway by which water refills cavitated conduits, allowing adjacent conduits to provide water for refilling (**F**). As the high osmotic droplets grow inside the vessel, the embolus is removed by forcing gas into solution, and by pushing gas through small pores through the vessel walls to intercellular spaces (**G**). The flared opening of the bordered pit chamber acts like a check valve until the lumen is filled, thus preventing contact with the highly wettable bordered pit membranes (**H**). Reconnection occurs once the pressure in the lumen exceeds that of the entry threshold into the bordered pit chambers. A hydrophobic layer within pit membranes might provide the needed connectivity among multiple bordered pits. (Figure reproduced following Zwieniecki, Holbrook (2009), with permission from Elsevier)

1.5 Root architecture

1.5.1 *Root system architecture and the potential for water uptake*

Root systems are structured and ever changing populations of roots of different types (Eshel, Waisel, 1996). Much of their structure arise from growth and branching processes, the latter being responsible for their tree-like topological structure. The mechanisms that lead to the formation of a meristem or a new branch are under strong genetic control (Péret et al., 2009). However, growth and branching respond to global and local environmental cues, including soil water potential (Hodge, 2004; Pregitzer et al., 1993; Zhu et al., 2005), which provides an additional control of water flow. There are indeed several ways by which root architecture influences the ability of root systems to take up water.

Firstly, the tree-like topological structure of root systems impacts how water tension generated in the shoot organs propagates simultaneously to thousands of individual roots, which influences their hydraulic conductivities (see sections above) and the local driving force for water uptake.

Secondly, roots belong to a hierarchy of root types whose features (e.g. diameter, axial conductance or growth rate are often assumed to decrease with the root order) affect their impedance to radial and axial water flow (Rewald, Ephrath, 2011). As root architecture is developing, the total root size increases, but the relative proportions of the different root types change as well, leading to a complex evolution of the root systems hydraulic properties.

Thirdly, roots comprise a succession of segments of increasing age from the tip to the base. As roots segments get older, the deposition of apoplastic barriers decreases their radial conductivity, while the maturation of xylem vessels increases their axial conductivity (Dousan et al., 1998; Hachez et al., 2006; Steudle, Frensch, 1989). Young segments located behind the elongation zone appear to be sites of peak absorption while older segments are thought to be mainly conductive pipes for the water absorbed by more distal segments and branches (Boyer, 1995). One has to note, however, that the relation between segment age and segment position is not absolute and depends on root growth rate (Lecompte et al., 2001).

The coupling of root architecture with the hydraulic features of root segments has been referred to as the *hydraulic architecture* of a root system (Doussan et al., 1998). It has been shown that radial and axial water flows in individual segments can be estimated simultaneously for all segments of a root system using the Ohm's analogy, which turns into a system of multiple linear equations whose structure is set by the hydraulic architecture of the root system (Doussan et al., 1998; Landsberg, Fowkes, 1978). This finding led to a family of models that formalize the strong relationship between root architecture, hydraulic properties and water uptake capacity of root systems (Doussan et al., 2006; Javaux et al., 2008).

1.5.2 Root placement and the availability of water

In addition to size and topology, root architecture also embraces the three-dimensional localization of root segments in the soil. Root placement is at the core of the water flow dynamics from the soil to the plant, because soil moisture is usually not uniform and varies in space and time under the influence of the environment and of the root system itself (Draye et al., 2010).

The most recognized contribution of root system architecture to water uptake is certainly the root system ability to explore deep soil layers that contain water reserves during critical phenological phases. In a crop stand, where strong horizontal competition with neighboring plants is occurring, it is generally assumed that a deeper root system gives access to more water (King et al., 2003), although the optimal exploration strategy should also depend on the scenario of climate, soil water and plant water use over the whole season. Indeed, multiple studies have highlighted the link between rooting depth and drought resistance in a panel of species such as vegetables (Johnson et al., 2000), cereals (Bernier et al., 2009; Hammer et al., 2009; Henry et al., 2011; Reynolds et al., 2006; Shen et al., 2001; Steele et al., 2007; Wasson et al., 2012), trees (Nagarajah, Ratnasuriya, 1981; Pinheiro et al., 2005), grasses (Marcum et al., 1995) or legumes (Kashiwagi et al., 2006).

Several traits contribute to rooting depth, including root insertion angles and gravitropism (Hammer et al., 2009), timing of axial roots emission and penetration ability of hard subsoil (Lynch, Brown, 2012). Recent work has also shown that an increased proportion of

root cortical aerenchyma leads to a substantial decrease in root maintenance respiration (Zhu et al., 2010), which is thought to account for more than 50% of the global assimilate consumption (Nielsen et al., 1998). By decreasing the maintenance cost, an increased allocation of assimilates to primary root growth can be achieved, leading to deeper rooting and improved resistance to water deficit under both control and drought conditions. Traits influencing root depth appear to be under the control of multiples genes (Bernier et al., 2009; de Dorlodot et al., 2007; Johnson et al., 2000; Reynolds et al., 2006; Shen et al., 2001; Steele et al., 2007), indicating some potential for improvement.

A less recognized contribution of root system architecture to water uptake relates to the ability of root systems to shape soil moisture gradients in a way that optimizes water flow from the bulk soil to the root. During the growing season, evaporation and drainage create pronounced vertical water potential gradients that are modified by the spatial patterns of root water uptake in a way that orients water flow to the depleted areas close to roots. However, parts of the root system that are surrounded by zones with high root length densities (RLD) can fail to attract water from the bulk soil if they are unable to decrease the soil water potential below that of the surrounding zone. In this context, the gravitropic behavior of crown roots in cereals may contribute to keep vertical *low-RLD channels* between crown roots, in which capillary rise occurs and that is capable of supplying water to the upper layers. Finally, root system extension also contributes to the placement of young segments in new soil regions and ensure strong soil-root water potential gradients near the most conductive root segments.

1.6 Integration of water flow in the soil-plant domain

Our understanding of the hydraulic behavior at the whole plant (or crop) scale is much less advanced. The complexity of the whole system raised numerous discussions about the main resistance to water flow in the soil-plant domain. Analyses of the plant hydraulic conductance in soils coupled with simplistic or inaccurate assumptions led to apparently contradictory conclusions on the main resistance (in the cortex, the xylem, or the rhizosphere). Several authors found that under wet soil conditions, soil conductivity is much higher than root radial conductivity, and vice-versa (Arya et al., 1975; Gardner, Ehlig,

1. WATER FLOW IN THE SOIL-ROOT DOMAIN

1962; Newman, 1969b; Passioura, 1980). A comparison of root and soil conductances suggested that there is an important range of soil moisture where both of them can locally limit water uptake (fig. (fig. 1.4). Therefore, understanding how these controls cooperate (e.g. additive, feedback of feedforward actions) has become pivotal for predicting the patterns of water uptake and the development of soil moisture gradients.

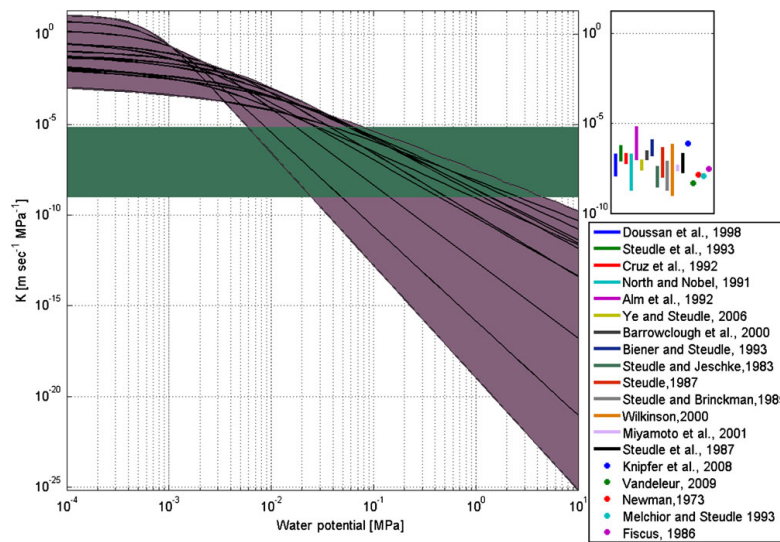


Figure 1.4: Envelopes of typical soil conductivity curves (blue area) and apparent root conductivity values (green area) redrawn from the literature. The upper right plot represents root conductivity values from 19 studies. (Figure reproduced following Draye et al. (2010), with permission from Oxford University Press)

The major perspective in the area of root water uptake is therefore to bridge the gap between local controls or regulatory mechanisms and water flow within the soil-plant domain. For this to happen, we need to build a *systems view* integrating the regulation of the driving force, the hydraulics of the soil-plant domain at different scales and the additional regulation layer provided by shoot-root signaling. Hopefully, novel tools are being developed that will move research in this direction. This section introduces some of these tools and illustrates with a few

examples how such integration can help elaborating and validating new hypotheses.

1.6.1 *Novel techniques supporting integration*

The practical difficulties in capturing the water dynamics of the whole system, that are largely responsible for the low pace of progress at the system scale, are now being addressed with novel experimental approaches that support the integration of root architecture with 2- or 3-D soil water content. Neutron tomography (Carminati et al., 2010; Esser et al., 2010) and nuclear magnetic resonance (Borisjuk et al., 2012; Jahnke et al., 2009) but also X-ray computer tomography (Mairhofer et al., 2012) and light transmission imaging (Garrigues et al., 2006) enable the visualization of root growth and the impact of water uptake on the soil properties and soil moisture distribution. Coupled with tracer experiments and detailed measurements of the plant water potential and xylem fluxes, these techniques are expected to help analyzing how plant and soil resistances are distributed, develop and affect water flow.

In parallel to experimental techniques, novel integrated modeling approaches have been recently proposed. These rely on the coupling of a 3D physical model of water flow in the soil with a bio-physical model of plant water flow based on the root hydraulic architecture (Doussan et al., 2006). The R-SWMS model (Javaux et al., 2008) performs this coupling using Richard's equation for the soil compartment (see above), and defining the sink term for each soil voxel (typically having a volume lower than 1 cm^3) based on the solution of Doussan's equations for the root segments present in the voxel (Doussan et al., 2006). The latter equations are solved using, for each segment, the local values of the soil water potential that satisfy Richard's equations. An iterative numerical algorithm is used to find the 3D water flows in the whole soil-plant domain that satisfy both models. Using this type of model, it is possible to consider the different controls that have been discussed above. For example, the radial conductivity can be set to change with root order and segment age (Doussan et al., 1998) or the axial conductivity can decrease with xylem water potential using a susceptibility function (Li et al., 2009).

1. WATER FLOW IN THE SOIL-ROOT DOMAIN

1.6.2 The need for integration in plant physiology studies

The appeal of deciphering cellular mechanisms underlying local conductivities should not draw the attention away from the fact that their effect on the local water flow is largely dependent on the hydraulic state of the whole system. For example, the effect of aquaporin activity on the radial conductivity of deep roots is likely to be marginal under well watered conditions in the upper soil layers, while it would make a strong contribution to water uptake when water has been depleted from the upper soil layers. Understanding the regulation of local controls may thus require consideration of other parts of the system.

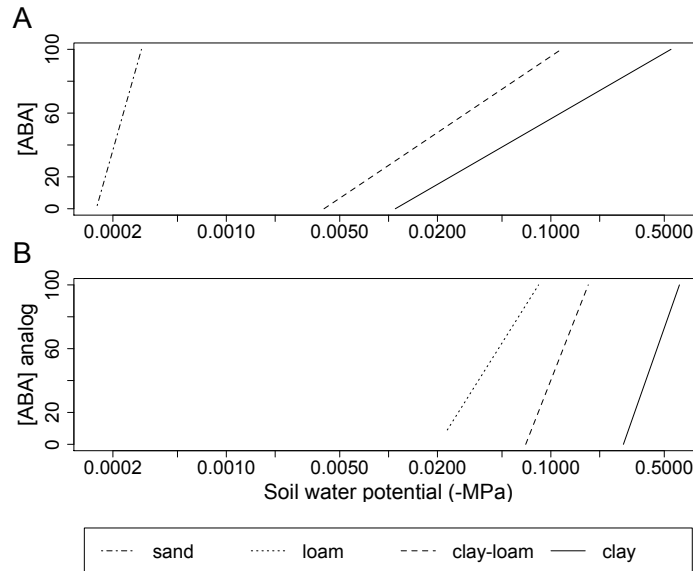


Figure 1.5: Evolution of xylem concentration of ABA (**A**, experimental) and a hypothetical stress factor (**B**, simulation) with decreasing soil water potential. Re-drawn from Dodd et al. (2010) (A) and Draye et al. (2010) (B)

Recent experiments on ABA signaling during root zone drying indicated that the response of root xylem ABA concentration to decreasing soil water potential varied with the texture of the soil substrate (fig. 1.5.A, Dodd et al. (2010)). The mechanisms responsible for this substrate dependence were not clearly understood. Interest-

ingly, independent simulation experiments with the R-SWMS model indicated that the concentration of a stress factor (called *ABA analog*) in the xylem sap would follow very similar trends and substrate dependency (fig. 1.5.B, Draye et al. (2010)). The explanation proposed in the modeling study relied on the hydraulic specificities of soil substrates (see above). In particular, the conductivity of the sand substrate (semi-dashed lines) is likely to drop before that of the clay loam substrate (dashed lines) in the vicinity of the roots, leading to a local water deficit (and ABA production) at higher soil water potential in the sand substrate. Although this hypothesis remains to be tested, this example indicates that an integration of the soil and plant hydraulic properties may provide new hypotheses for plant physiological experiments.

1.6.3 Integration helps understand water uptake patterns

When soil moisture content is unevenly distributed and relatively low, a small part of the root system located in a wetter zone may acquire a large part of the soil water, essentially because the soil hydraulic conductivity and soil-root potential gradient are higher in the wetter zones. In this situation, water is not extracted proportionally to RLD and it is said that a lack of uptake in certain root zones is compensated for by increased uptake in wetter zone (Jarvis, 2010). Similar deviations from the proportionality of uptake to RLD are expected to occur when the xylem conductivity is reduced (Draye et al., 2010).

This compensation phenomenon is a passive process which results from the redistribution of soil and plant water and arises intrinsically from the physical laws underlying water flow in the SPAC (as discussed in the previous sections). However, such compensation is also determined indirectly by root placement and hydraulic architecture. It follows that differences between water extraction patterns of different genotypes that result from compensation and can be explained by pure physical laws should not require complex biological explanations (see examples in Draye et al. (2010)). Using an integrated approach, it becomes possible to extract the part of the variation that can be accounted for by simple compensation, and to isolate the part of variation for which a specific biological explanation is needed.

1.6.4 *Integration helps to find where and when controls are effective*

As mentioned above, the radial flow of water is unlikely to be uniform over the entire root system surface, nor is the axial flow through all root segments. It follows that the many controls or regulatory processes that have been discussed in this chapter are unlikely to operate equally at all locations within the soil-plant domain. Depending on the situation, this heterogeneity may or may not be relevant. The case of xylem cavitation, which impedes the rate of water uptake under dry soil conditions and high evaporative demand is one example where this heterogeneity matters. The hydraulic effect of xylem embolism has mostly been analyzed using the susceptibility to cavitation curves that quantify the loss of axial conductance, usually at the shoot or whole plant level. However, because the soil-plant system is not hydraulically uniform, cavitation may be more important in some parts of the system than in other, and this is likely to be reflected in the patterns of water uptake and in the evolution of soil water potential.

To illustrate the benefits of integration, xylem cavitation was implemented in the R-SWMS model using a Weibull function that simulates the loss of xylem conductivity in response to the xylem water potential (Li et al., 2009). Simulations with maize and with a day-night sinusoidal transpiration demand in a globally wet soil reproduced the expected decrease of transpiration (fig. 1.6). Interestingly, the simulations indicated that cavitation occurred preferentially in the distal part of deep crown roots (not shown), which was not an intuitive result. Obviously, additional experiments are needed to determine whether this prediction matches the reality, or if our understanding of soil-plant hydraulics (as formalized in the model) needs further refinement. Nevertheless, if the prediction turned to be experimentally valid, failure to account for this asymmetric occurrence of cavitation would lead to inaccurate predictions on the spatial distribution of water uptake.

1.7 Future outlooks

The last decade has seen an increasing awareness that soil and plant hydraulics (and not only root length density) play an important quantitative role in water capture, especially in drought-prone environments (Bernier et al., 2009; de Dordot et al., 2007; Lynch, 2007). This shift of emphasis was made possible thanks to the accumulation of new

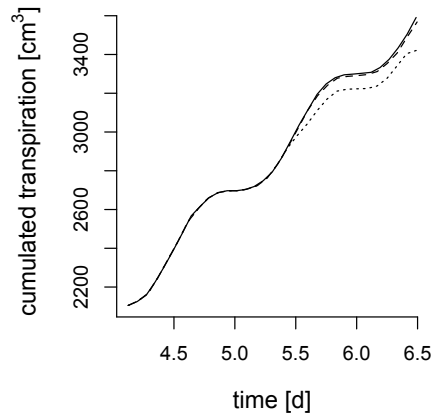


Figure 1.6: Cumulated transpiration rate for a plant with (dotted line) and without (dashed line) cavitation of the xylem vessels, as compared to potential transpiration (plain line).

data on the molecular and cellular processes controlling water flow in the plant and to the development of novel tools allowing the integration of water flow in all compartments and at different scales.

The major perspective in the area of root water uptake is therefore to rely on this development to bridge the gap between local controls or regulatory mechanisms and water flow within the soil-plant domain. For this to happen, we need to build a *systems view* integrating the regulation of the driving force, the hydraulics of the soil-plant domain at different scales and the additional regulatory layer provided by shoot-root signaling. In particular, there is a need for plant biologists and soil hydrologists to develop together their understanding of water flow in the soil-plant system.

In this context, developing a holistic view of the mechanisms controlling the distribution of water uptake (spatial and temporal) will be crucial for our understanding of plant water use and soil water availability, mainly because water uptake at any given time sets the limits to future modifies water availability in the next time step (feed-forward). Being able to separate between the contributions of the many controls to water flow during the crop cycle will be especially

1. WATER FLOW IN THE SOIL-ROOT DOMAIN

important in predicting the water availability to plants with promising traits.

Functional-Structural Plant Models (FSPM) are likely to play a pivotal role in future research, especially because they offer a unique mathematical framework to integrate, in a quantitative way, molecular, physiological, biophysical and hydrological data relating to important aspects of plant water use as phenology, assimilation, growth and long-distance signaling (Godin, Sinoquet, 2005). The relevance of models considering the flow of water to individual rootlets of a complete root system has long been questioned in soil physics, primarily because the precise geometry of the root system is impossible to capture (King et al., 2003; Molz, Remson, 1970). As exploration tools, however, such models have a great potential since they enable visual, intuitive and quantitative appreciation of the hydraulic behavior of root systems in their soil environment.

PART III

QUANTIFICATION
OF COMPLEX
ROOT SYSTEMS

This second part of the thesis presents new tools and methods developed for the analysis of root images.

The first chapter of this section presents a new image analysis toolbox, SmartRoot. The software and its underlying algorithms will be presented as well as two illustrative applications.

In the second chapter, we will demonstrate the use of SmartRoot in the context of soil-root interaction research. A new method to vectorize complex root systems grown in rhizotrons will be presented.



[...] any non-specialist faced with an image analysis problem rapidly realizes that a unique image transformation usually fails to solve it.

PIERRE SOILLE

PRELIMINARY CONCEPTS



IT IS NOW WIDELY ACCEPTED that root system architecture (RSA) is a fundamental component of agricultural and natural ecosystems productivity (Hammer et al., 2009; Hodge et al., 2009; Lynch, 1995).

Understanding the availability of a given resource for the plant requires the the integration of soil and roots bio-physical constraints. On the one side, the *potential* availability for the plant depends on the resource distribution in the soil and its mobility. On the other side, the *actual* resource availability is further constrained by the root system architecture (RSA, including morphology and topology) and the root placement in the soil domain (spatial correlation between the roots and the resource) (Draye et al., 2010; Ge et al., 2000; Lobet et al., 2012). However, root and soil constraints do not add independently and emerging behaviors are likely to arise from the existence of feed-back or feed-forward loops inside the soil-root system. Therefore, detailed datasets containing root system architecture, root placement and soil resource dynamics are required to improve our understanding of resource capture by plant roots.

Concurrently, recent progress in our understanding of the molecular bases of root growth and development in model systems (de Smet et al., 2006; Péret et al., 2009) and novel insights on the role of RSA in field resource capture (Draye et al., 2010) yield new prospects of manipulating RSA in crop species (de Dorlodot et al., 2007). This situation reinforces the need for robust, evolutive and adaptable root phenotyping solutions (hardware and software).

Nowadays, new imaging technologies such as magnetic resonance imaging (Jahnke et al., 2009) and X-ray computed tomography (Carmignati et al., 2009; Mooney et al., 2011) are being developed to extract RSA information from soil cores. However, classical imaging using flatbed scanners or cameras remains most widely used. Digital imaging is indeed affordable, features a wide range of image resolution, can be adapted to an array of experimental systems (e.g. hydroponics, aeroponics, gel plates, gellan gum or transparent soil (Downie et

2. PRELIMINARY CONCEPTS

al., 2012)) and has been extended to time-lapse and 3D applications (Clark et al., 2011; French et al., 2009; Hund et al., 2009; Iyer-Pascuzzi et al., 2010; Yazdanbakhsh, Fisahn, 2009).

In the same time, the interest in RSA phenotyping has gradually evolved from static and global traits (e.g. root mass or length density) to dynamic and local traits (e.g. growth rates, tropisms, insertion angles) (de Dorlodot et al., 2007; Ge et al., 2000). Accordingly, a panel of softwares have been implemented which target specific traits and experimental constraints (reviewed recently in French et al. (2009) and Le Bot et al. (2010), presented in the table 2.1). These software can be assigned to manual, semi-automated and fully automated methods according to the amount of user interaction.

In manual methods, users typically draw the skeleton of the root system using freehand graphical tools, as in DART (Le Bot et al., 2010) or WinRHIZO Tron (Regent Instruments, 2011). These methods exclude software generated errors and should provide accurate estimation of most local and global traits, but are highly time consuming. They are often the only solution for complex root systems and for rhizotron images.

Semi-automated methods usually combine automated thresholding and skeletonization algorithms with some extent of user intervention, mainly to re-touch and annotate software-generated root structures, as in EZ-Rhizo (Armengaud et al., 2009) and RootReader2D (Clark et al., 2012). The number of errors is usually negligible with seedling images but increases with the amount of root overlap. In principle, many traits can be estimated accurately if the software is used with the type of images and RSA for which it was designed.

Finally, automated methods rely on pre-defined procedures to perform image analysis without any user interaction. Such methods use specialized algorithms and tend to be application-specific, unlike manual or semi-automated methods that generate explicit root structure information. The number of errors is kept to a minimum as long as the type of root system and images fit the requirements of the software. Examples of automated methods include WinRhizo (length and topology, Arsenault et al. (1995)), RootTrace (growth, gravitropism and branching, French et al. (2009)) and a recent system developed at Duke University (various descriptors, Iyer-Pascuzzi et al. (2010)).

Table 2.1: Available root image analysis softwares (Monday 10th December, 2012). For a more complete review, see <http://www.root-image-analysis.org>. OS = Operating system. *All* refers to the three main OS: Windows Mac OS and Linux.

Software	Measurement	Licence	OS	Automation	Reference
RootFlowRT	Growth	Freeware	All	Automated	van der Weele et al. (2003)
KineRoot	Growth	Freeware	All	Automated	Basu et al. (2007)
RootTrace	Growth	Freeware	Windows	Automated	French et al. (2009)
Growth Explorer	Growth	Freeware	Windows	Automated	Basu, Pal (2012)
RootDetection	Length	Freeware	Windows	Automated	-
RootLM	Length	Freeware	All	Automated	Qi et al. (2007)
GIA Root	Architecture	Freeware	All	Automated	Galkovskiy et al. (2012)
RootReader2D	Architecture	Freeware	All	Semi-Auto.	Clark et al. (2012)
SmartRoot	Architecture	Freeware	All	Semi-Auto.	Lobet et al. (2011)
EZ-Rhizo	Architecture	Freeware	Windows	Semi-Auto.	Armengaud et al. (2009)
DART	Architecture	Freeware	All	Manual	Le Bot et al. (2010)
RootFly	Architecture	Freeware	Windows	Manual	-
WinRhizo	Architecture	Commercial	Windows	Automated	Arsenault et al. (1995)
WinRhizo Tron	Architecture	Commercial	Windows	Manual	-
RootSnap!	Architecture	Commercial	Windows	Semi-Auto.	-
RootTrak	Tomography	Freeware	Windows	Semi-Auto.	Mairhofer et al. (2012)
Cell-o-Tape	Morphology	Freeware	Windows	Manual	French et al. (2012)
RootScan	Morphology	Freeware	All	Automated	Burton et al. (2012)
SkyeRoot	Architecture	Commercial	Windows	Automated	-

2. PRELIMINARY CONCEPTS

In line with the distinction between methods, it is often the case that some areas of root images lend themselves to automated analysis better than other areas where the image quality is lower or where the amount of root overlap is higher and for which semi-automated or manual methods would perform better. Sometimes, a spatial segmentation of images even arises from the experimental design as with areas (or periods) where root growth is obviously altered by local (or transient) conditions. As long as the research focus is on local or dynamic traits (e.g. growth rate, growing and branching angles, diameter or inter-branch distance), a sampling-based processing strategy would be applicable to the areas of interest. In terms of efficiency, working on subsets of root systems would indeed allow one to devote more attention to the subset, or to handle more (or more complex) systems at constant cost.

In this section, we will first present SmartRoot, a new image analysis toolbox that speeds up the quantification of root growth and architecture of complex root system. The second chapter in the section will demonstrate the utility of SmartRoot in the context of soil-root interaction research and will detail a new method to vectorize complete root system of mature plant grown in rhizotrons.

A NOVEL IMAGE ANALYSIS TOOLBOX ENABLING QUANTITATIVE ANALYSIS OF ROOT SYSTEM ARCHITECTURE



This chapter is a modified version of a research article entitled:

Lobet, G., Pagès, L. & Draye, X. 2011. A Novel Image Analysis Toolbox Enabling Quantitative Analysis of Root System Architecture. *Plant Physiology*, 157, pp.29–39.

IN THIS SECTION, we introduce a novel, multi-purpose and semi-automated image analysis toolbox (SmartRoot) that speeds up the quantification of root growth and architecture of complex root systems and from a wide variety of applications.

The software combines a highly intuitive user interface with a new tracing algorithm and supports sampling-based image processing. SmartRoot is a platform independent software (Windows, MacOS, Linux) implemented as a plugin for the popular ImageJ software (Abramoff et al., 2004; *ImageJ*) and relies on established cross-platform standards (Java, SQL and XML).

Some of its features are illustrated with a time-lapse analysis of cluster root formation in lupin (*Lupinus albus*) and with an architectural analysis of maize root systems (*Zea mays*).

3.1 Results and discussions

3.1.1 *Multi-dimensional representations of roots*

SmartRoot shares some features with Geographic Information Systems (GIS) in particular the ability to capture, store, present and process data that are linked to location. As with GIS, information is stored in separate data layers. The first layer comprises the source image viz. the 2D-array of raw pixels values. The second layer contains all root morphological information in a vector format, with individual roots approximated by segmented lines (fig. 3.1). A third data layer contains the topological relationships between roots, while the fourth data layer contains user- or software-generated annotations or beacons inserted along roots.

A consequence of the vector representation of roots is that any position along a root has two corresponding sets of coordinates: the classical $[x, y]$ absolute coordinates and very intuitive $[r, d]$ relative coordinates specifying the root identifier $[r]$ and the (geodesic) distance to the root base $[d]$. Using the second coordinate system, it is easy to calculate inter-branch distances, to combine physical dimensions with topological information and to match corresponding positions on successive images in a time-lapse analysis (see below).

The information stored in data layers is displayed on the graphical user interface (GUI) as a separate set of six Photoshop-like layers containing the source image, the skeleton (segmented line) of individual roots, the nodes of the segmented lines, the border of individual roots, their area, a geodesic ruler along each root and a visual representation of the annotations and beacons.

Although invisible to the user, the separation between data layers and GUI layers disconnects the design of the GUI from any constraints relating to data structure (and vice-versa) and has proven to be instrumental in the evolution of SmartRoot since its first implementation.

3.1.2 *Root tracing principle*

SmartRoot features an automated individual root tracing algorithm triggered by a mouse click anywhere along the root in the image source GUI layer. It determines the centre (midline) of the root near the picked position and proceeds with the stepwise construction of a

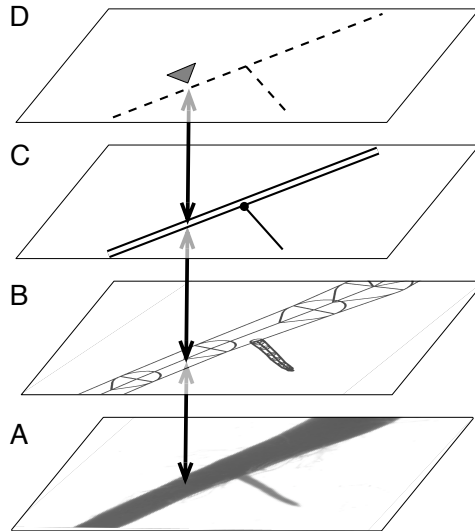


Figure 3.1: SmartRoot stores information in four separate data layers. **A.** Source image (raster). **B.** Morphology (vectorial). **C.** Topology (= parent root ; = branch root ; = connection). **D.** Annotations (illustrated here with a beacon, see text). The double arrows indicate matching position in different coordinate systems.

segmented line approximating the root midline, progressing forwards and backwards to the tip and basis of the root. The algorithm estimates the root diameter at each node of the segmented line and uses this information to set the orientation of the segmented line (from the root base of the root tip). Afterwards, a name is given to the root (see above, the (r) coordinate). This interactive procedure is at the core of the sampling-based processing mentioned in the introduction.

SmartRoot uses adaptive distances between nodes, increasing the node density for tiny roots and in curved regions of roots in order to maintain the accuracy of the segmented representation of the roots while minimizing the number of nodes (fig. 3.2). Indeed, large roots tend to show smaller curvature than small ones and can be therefore represented with fewer nodes. The implementation of adaptive distances is detailed below (see Step 1). As it is used hereafter, the term node denotes the intersection of successive segments of the segmented line. It is thus different from topological nodes referring to the branching points along the roots.

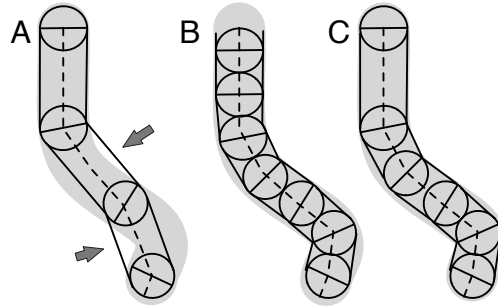


Figure 3.2: Effect of the distance between nodes (circles) on the accuracy of the segmented line (dashed) approaching a curvilinear root object (gray). **A.** Large and fixed distance between nodes. Arrows point to poorly represented regions of the root. **B.** Small and fixed distance between nodes. **C.** Adaptive internode distances lead to parsimonious segmented lines.

The optimal placement of nodes occurs during the segmented line construction and proceeds as follows (fig. 3.3):

Step 1: Before adding a new node to the segmented line, the algorithm investigates the pixel values along a search path, consisting of an arc of circle centered on the current node and oriented opposite the previous node (fig. 3.4.A). The initial amplitude of the arc is set to 90 to increase the likelihood of finding the prolongation of the root while avoiding branches or neighboring roots. The initial radius (L_i) of this arc is set at two times the diameter of the current node.

Step 2: Pixel values along the search path are compared against a threshold value adjusted to local greyscale gradients (for details see the supplemental PDF 1). If more than one candidate position are detected, the best one is selected based on diameter similarity with the current node (fig. 3.4.A).

Step 3: If the algorithm does not find a candidate position for the next node (fig. 3.4.B), it changes the search path amplitude to 120 and decreases the arc radius (fig. 3.4.C). If this fails, the algorithm considers that the end of the root has been reached and the tracing in that direction stops.

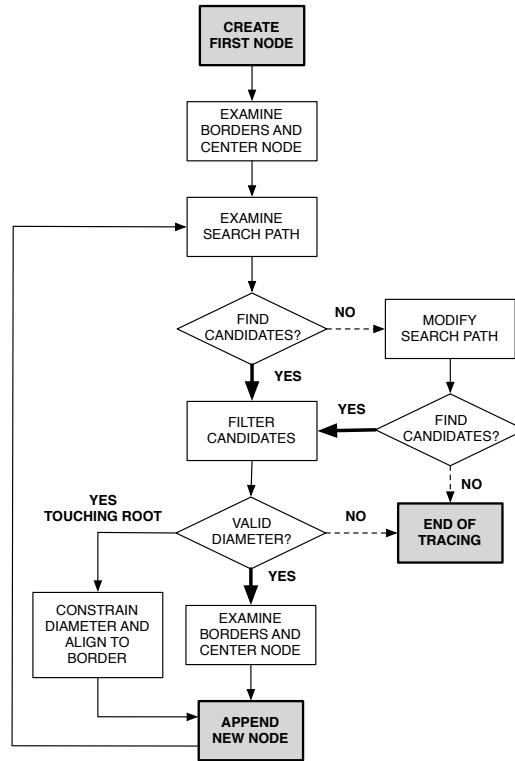


Figure 3.3: Diagram of SmartRoot tracing algorithm

Step 4: The algorithm then seeks for multiple points (fig. 3.5) along root borders near the candidate position to localise root borders with a sub-pixel resolution (comparing interpolated pixel values to the local threshold determined previously (fig. 3.6)). This procedure increases the accuracy of diameter estimation of tiny roots or in highly branched regions (for discussion on diameter estimation accuracy, see supplemental PDF 2). The distance between borders at the candidate position is then tested against three conditions.

- If that distance is smaller than 0.8 times the diameter of the previous node, the tracing stops. This condition aims at finding the very end of thick roots which have a long and conical shaped apex.

- If that distance is larger than 1.5 times the diameter of the previous one, it is considered that a neighbor root has come into contact with the root being traced, thereby creating an apparent diameter increase. A new node with a diameter equal to that of the current node and aligned to the closest root border is then created.
- If that distance is larger than 4.0 times the diameter of the previous node (fig. 3.7) the tracing stops. This condition occurs when the basipetal tracing of a lateral root reaches the junction with the parent root. The test may lead to different types of errors that are discussed in supplemental PDF 3, but which can be easily corrected manually.
- Otherwise, a new node with a diameter equal to the inter-border distance is created at equidistance of the two borders.

Newly created nodes are appended to the segmented line and the construction proceeds until the algorithm stops.

The parameters of the algorithm have been determined empirically using a wide range of root system architectures and image qualities. They can be taken as fairly generic although they could still be optimized for specific images.

The user can edit the newly created root by simple drag-and-drop actions on the different nodes (e.g. adding, moving, deleting or adjusting diameters). As the editing takes place in the nodes layer, it does not modify the source image and makes this operation very intuitive. Several roots can be picked and traced at once by stretching a line drawing tool across them.

3.1.3 Topology

Topological relationships can be set by attaching lateral roots to their parent. This information is used typically to calculate branching or insertion angles, position of insertion and inter-lateral distances. It is also very useful for monitoring the sequence of lateral root formation by individual parent roots in a series of time-lapse images. The topological information is also part of the specification of root types (primary, first order,...) and provides the shortest path connecting a root to the root-shoot junction.

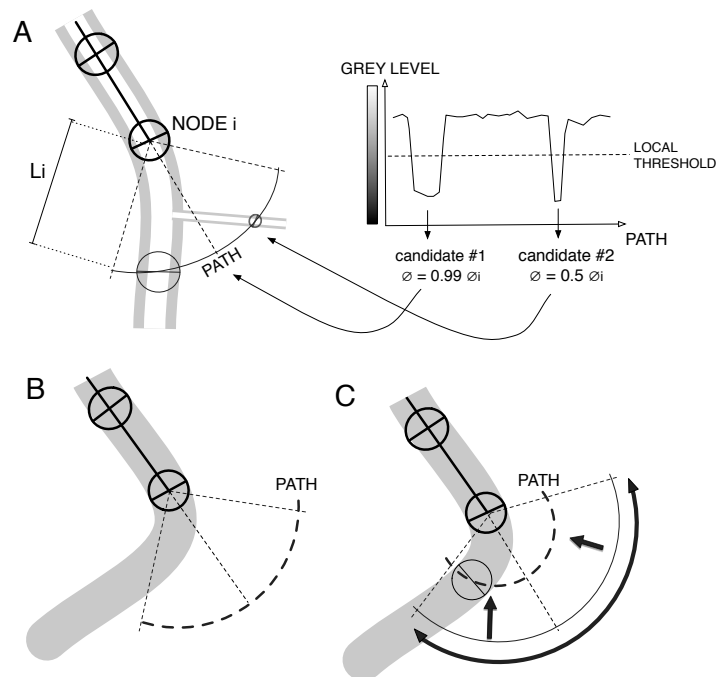


Figure 3.4: Illustration of the stepwise construction of the segmented line. **A.** Pixel values are evaluated along a 90 arc centered in front of the last node (NODE i). The resulting profile is compared against a local threshold (see text). The candidate positions are filtered based on their diameter similarity with NODE i diameter (here, the candidate 2 is excluded). **B.** This algorithm fails when the root curvature is too strong. **C.** Increasing the amplitude and decreasing the radius of the arc allows the search algorithm to find the successor node.

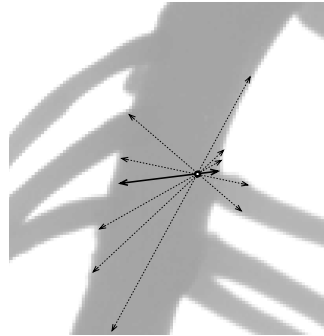


Figure 3.5: Illustration of the multipoint border search and centering algorithm. The open circle represents the initial position of the node. The dashed arrows represent the different trajectories used to find the root border. The plain arrow represents the shortest segment containing the node and joining root borders. This segment is used to estimate the local root diameter and to re-center the node on the root axis.

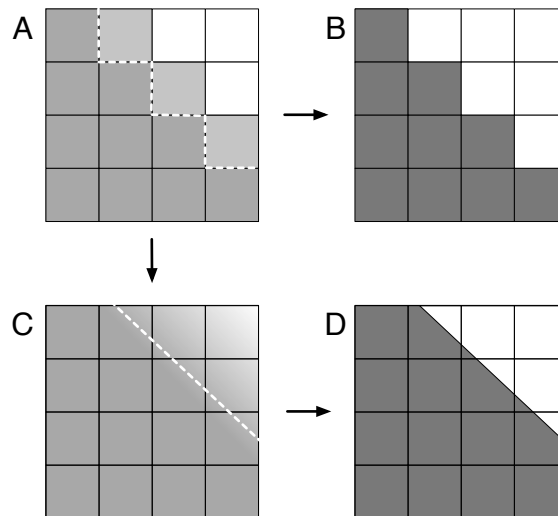


Figure 3.6: Consequences of sub-pixel resolution on the variability of diameter estimation. **A.** Close-up of the original image, near the border of a root. The dashed line marks the position of the threshold limit between root and background pixels. **B.** Segmented image after discrete thresholding. **C.** Interpolation of grey levels of A generates a smooth transition between root and background pixels. The position of the threshold limit can be approximated locally with a line. **D.** Segmented image after thresholding of the interpolated image.

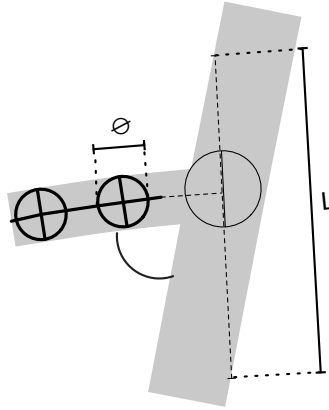


Figure 3.7: Detection of root junctions. A sudden increase of the orthogonal distance between the end of the segment and the closest borders marks the termination of the segmented line construction (see text).

Due to the large number of laterals along a parent root, SmartRoot features an algorithm to detect, trace and attach most laterals of an already traced parent root (for discussion on tracing time of laterals, see supplemental PDF 4).

This algorithm creates a search path parallel to the root border, at a distance arbitrarily set to the root diameter. Similarly to the root tracing algorithm, pixel values along this search path are compared against their local threshold value and a new lateral root is created whenever a satisfying position is found (fig. 3.8). For every new lateral built, a number of optional exclusion criteria (such as diameter, insertion angle and length of the newly build root) are evaluated. This filtering reduces the number of false positives but may eventually lead to a small number of false negatives (missed laterals). Adjusting the settings of the filtering reduces significantly the number of errors.

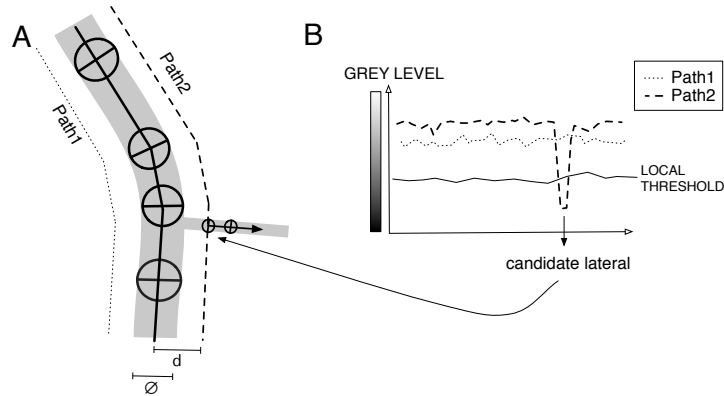


Figure 3.8: Lateral root detection algorithm. **A.** The algorithm creates search paths parallel to each root border, at a distance arbitrarily set to the local root diameter ($d = \varnothing$). **B.** As for the root tracing algorithm, pixel values along this search path are compared against their local threshold value and a new lateral root is created whenever a satisfying position is found.

3.1.4 Root annotations

The $[r, d]$ coordinate system mentioned above enables the referencing of virtually any type of information with specific longitudinal positions along roots. This referencing is implemented in SmartRoot through annotation tools designed for various purposes. The study of cluster root formation given below illustrates this capability.

Annotations can be used to point to the most distant lateral along a root, whose distance to the tip can be used as a proxy to the root growth rate (Lecompte et al., 2001; Pagès et al., 2010). This annotation is automatically added / updated when a new most distal lateral is added to a root. Annotations can be used in pairs to delineate regions along the root, as needed in experiments involving heterogeneous nutrient supply, where a separate morphological analysis of regions submitted to different conditions is desirable. Annotations can also be used as simple beacons to request subsequent exportation of local information (direction, diameter, distance to the tip, path to the root system origin) (see below). Finally, annotations can also be used as a generic, free text commenting tool.

3.1.5 Time series analysis

A major feature of SmartRoot is the ability to handle sequences of time-lapse images, thereby supporting root growth and development analyses. The general principle of time-lapse handling is that information stored across different images (e.g. annotation, branches or length) and corresponding to different time points, can be cross-linked, displayed on a single image (generally the last of the time-series) and exported in a single database query (see below).

The merging of information across different images is performed in the $[r, d]$ coordinates system and is therefore independent from cartesian coordinates (fig. 3.9). SmartRoot has therefore the ability to handle time-stamped images of root systems grown in liquid or air, where successive images are generally not superposable. This requires that the roots of interest be traced on every image of the image sequence and be coherently identified. As this can be tedious with complex images, the graphical user interface offers several intuitive viewing tools to navigate simultaneously along a root across different images.

When plants are grown on solid medium (e.g. *Arabidopsis thaliana* in agar plates), the root system structure is generally well conserved and is only augmented from one image to the next. In such cases, the tracings stored in a source image can be imported in a target image, either in a forward way, the imported tracings being augmented in the target image, or in a backward way, the imported tracings being cut or deleted to match the target image. If the source and seed images are not perfectly aligned, the root system structure of the source image can be registered on the target image through a linear transformation (translation and rotation) carried out using three user specified landmarks (Thévenaz et al., 1998).

3.1.6 Data handling

Information generated using SmartRoot can be exported as built-in tables to any SQL-compliant external database system for further analysis. This capability has been successfully used with Microsoft Access and MySQL database systems. At present, built-in tables include a table of node coordinates and diameter, a table of root global data (length and topological information), a table of annotations and a table of root length densities (as shown in table 3.1). This basic set of infor-

3. A NOVEL ROOT IMAGE ANALYSIS TOOLBOX

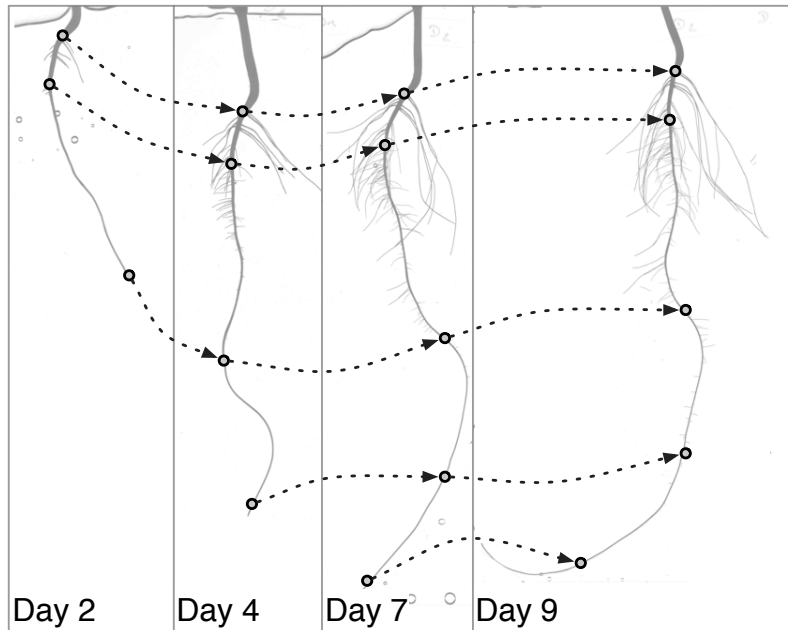


Figure 3.9: Analysis of time-lapse image sequences of plants grown in liquid or air medium (when root systems at different time points cannot be superposed). Corresponding positions are established based on the $[r, d]$ coordinates (see text).

mation is generic enough to allow the computation of most variables used in root morphological analysis: growth, gravitropic behaviour (tip angle as a function of time), wavy patterns (distance between positions having the same direction), radial growth (diameter as a function of longitudinal position and time), morphological response to localised or transient environments, lateral root density,... From a technical point of view, many of those variables can be accessed transparently using SQL views defined once in the external database system.

More recently, SmartRoot has been enriched with the possibility to export data to CSV files, which removes the need for database configuration and provide an easier to access to the data.

Table 3.1: Examples of export options in SmartRoot. The root length density export was designed for rhizotron images acquired as described in (Busch et al., 2006; Cheng et al., 1991). ID, identifier

Export options	Export data
Global root data	image filename root ID length surface volume branching order topological position number of children branching density position of first and last child on the root axis insertion angle insertion point
All marks	image filename root ID annotation type position along the root annotation value
Nodes data	image filename root ID node coordinates node diameter position along the root
Root length density	image filename x-y coordinates of the considered area root length density in this area

3.1.7 Image requirements (type and quality)

Many aspects of image quality (including resolution, contrast and background noise) are known to affect image processing output. Not surprisingly, the best results are obtained with high resolution images as captured using a flat bed (transparency) scanner. This technology potentially provides pictures of high quality (Smit et al., 2000) but is time-consuming and may not be suitable for high-throughput image acquisition. Images of lower quality (e.g. camera pictures) can be analysed with SmartRoot, as long as roots are at least two- to four-pixel wide (see supplemental PDF 2 for a discussion of accuracy). Due to the adaptive thresholding used by the tracing algorithm, background noise and contrast are usually not an issue. The software has been positively evaluated using pictures from different experimental setups, such as aeroponics, petriplates, or rhizotrons. SmartRoot reads the most popular image file types (jpg, gif, tif and bmp). Image processing is carried out in the greyscale space, with roots appearing darker than background. Colour images are automatically transformed to greyscale and grey level inversion is performed if required.

3.1.8 Example 1: Architectural analysis of *Zea mays*

We first illustrate the capabilities of SmartRoot with an architectural analysis as part of a modeling study of carbohydrate competition between the various root types of maize appearing during the first two weeks after germination. SmartRoot was used to estimate growth and branching parameters (growth rates, lateral root density, inter-lateral distances and branching angles) of the various maize root types (primary, seminal, crown and first order lateral roots, named after Hochholdinger et al. (2004)) in aeroponics.

Twelve maize plants were grown in aeroponics and their root system photographed at daily intervals during fifteen days. The resolution and quality of the images were low, with an uneven and noisy background (fig. 3.10.A). The primary, seminal and crown roots were traced on each picture of the time-lapse sequences using the line selection tools and the laterals were traced only on the last picture of the sequence using automated lateral root tracing (fig. 3.10.B). Two datasets were established: one containing time-series of root length (primary and seminal) and a second containing a near-complete architectural description of the root system at the end of the experiment.

Using the first dataset, the growth rate of the primary, seminal and crown roots were calculated. Insertion angles (fig. 3.11.A), inter-branch distances (fig. 3.11.B), root diameters (fig. 3.11.C) and the length of the apical unbranched zone (LAUZ) were retrieved from the second dataset. The growth rates of lateral roots were estimated with the SAS software (SAS Institute Inc., Cary, NC, USA) based on their length, their position on the parent axis and the growth rate of the parent axis (Hackett, Rose, 1972; Lecompte et al., 2001), assuming lateral root initiation in maize is almost acropetal (Lloret, Casero, 2002). A summary of the architectural parameters is given in table 3.2. These parameters (mean value and standard deviation) were used to execute a root architecture model (RootTyp, Pagès et al. (2004)) to simulate virtual and dynamic root systems useful for the carbohydrate competition analysis (not shown).

This example made extensive use of SmartRoot tools supporting time-series and topological analysis. It illustrates the possibility of extracting an information-rich dataset from very simple experiments, even with low quality pictures.

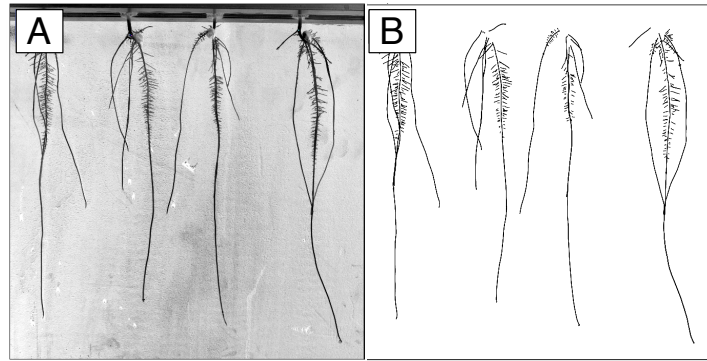


Figure 3.10: Analysis of 15-day old maize root systems grown in aeroponics. **A.** Low resolution source image from a CCD camera. **B.** Representation of root midlines representation after tracing

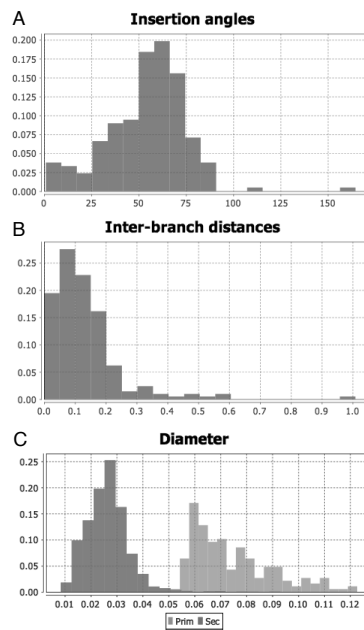


Figure 3.11: Histograms generated with the graph builder tool box of SmartRoot (maize example). **A.** Insertion angle. **B.** Inter-branches distances. **C.** Diameter (dark grey: first order laterals; light grey: primary roots).

3. A NOVEL ROOT IMAGE ANALYSIS TOOLBOX

Table 3.2: Architectural data. Summary of the architectural data of 15-days old maize plants grown in aeroponic obtained with SmartRoot (mean \pm s.e.m.). Crown roots were about 2 cm long at the end of the experiment and were not analyzed. LAUZ = Length of Apical Unbranched Zone; LR = Lateral Root. Roots are named according to Hochholdinger et al. (2004). Growth rate of LR is estimated in their early linear growth phase. The validity of the insertion angle is questionable since images are 2D projections of 3D root systems.

PRIMARY	
Growth rate [mm/d]	37.0 ± 0.2
Diameter [mm]	1.4 ± 0.3
Branching density [LR/cm]	5.9 ± 2.3
LAUZ [mm]	146.8 ± 54.8
SEMINALS	
Growth rate [mm/d]	31.0 ± 0.6
Diameter [mm]	0.9 ± 0.4
LATERALS	
Growth rate [mm/d]	0.6 ± 0.17
Diameter [mm]	0.48 ± 0.16
Insertion angle [$^{\circ}$]	65.6 ± 14.3

3.1.9 Example 2: Time-lapse analysis of cluster root formation in *Lupinus albus*

This second example illustrates a sampling-based processing and the possibilities offered by the annotation tool. In several species, compact clusters of short roots, first described by Purnell (1960), are produced in discrete regions along first order laterals, called proteoid roots. Cluster roots increase phosphorus acquisition and enhance survival of these species on their native low-P-soils (for review, see Shane, Lambers (2005)). Little is known about the acquisition of proteoid root identity nor about the mechanisms which trigger the initiation of clusters along proteoid roots. It is currently thought that a systemic signal is involved, leading to discrete events of synchronous cluster root formation (Skene, 2000; Watt, Evans, 1999). In order to explore the temporal dynamics of cluster root formation and to identify growth and morphological features that are singular to proteoid roots, the root systems of twelve lupin (*Lupinus albus*) plants grown in aeroponics have been scanned at daily intervals during sixteen days. The resulting time-lapse sequences have been analyzed with SmartRoot.

Despite the high quality of the images, carrying out this type of analysis using standard skeleton-based algorithms would be hampered by the high degree of root overlapping, unless a prohibitively long manual separation of roots is made prior to scanning. This, fortunately, is a typical situation where sampling parts of the root system would be a practical way to escape root separation while providing the data required (fig. 3.12).

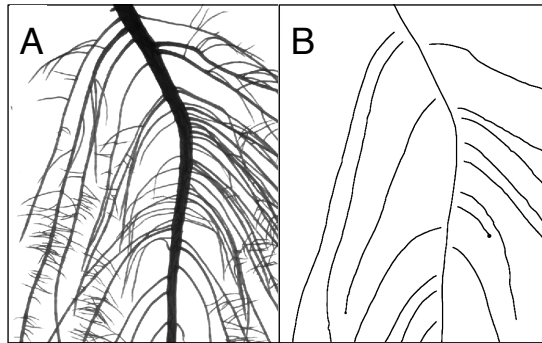


Figure 3.12: Analysis of a 16-day old lupin root system grown in aeroponics. **A.** High resolution (600 DPI) source image from a flat-bed scanner. **B.** Representation of the midline of selected roots after tracing.

Thirty first-order lateral roots randomly selected on each plant were retraced in all images from their emergence till the end of the experiment. When a lateral turned out to be a proteoid root, the position of its clusters were recorded over time using interval annotation tools (fig. 3.13). The final dataset comprised a set of informations for individual lateral roots: length over time, diameter and position of the clusters (if any). This dataset was exported to a Microsoft Access database and analyzed with the SAS software (SAS Institute Inc., Cary, NC, USA).

Significant differences were found between proteoid and non-proteoid roots for growth rates (respectively 0.76 cm.d^{-1} and 0.27 cm.d^{-1} , $p\text{-value} < 0.001$, $t\text{-test}$) and diameters (respectively 0.059 cm and 0.039 cm , $p\text{-value} < 0.001$, $t\text{-test}$) (fig. 3.14). Besides, proteoid roots tended to form only during the first four days after germination while non-proteoid root formation continued over time (fig. 3.15). These mor-

3. A NOVEL ROOT IMAGE ANALYSIS TOOLBOX

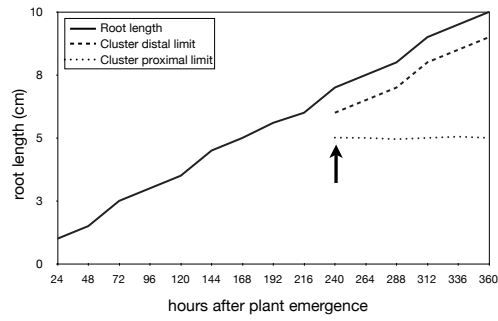


Figure 3.13: Evolution of a single proteoid root containing a single, long-lived root cluster (lupin example): length of the proteoid root (plain line), emergence of the root cluster (arrow) and evolution of the cluster boundaries (dashed lines).

phological differences suggest that proteoid root identity is already established when the lateral root emerges from the primary root (or that roots with a low growth potential lose the ability to form clusters).

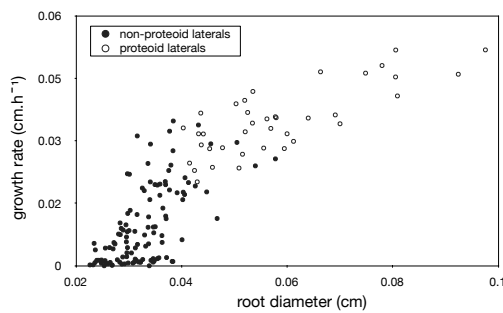


Figure 3.14: Relationship between growth rates and diameter of lateral roots (lupin example). A clear discrimination is seen between non proteoid (open circles) and proteoid roots (closed circles).

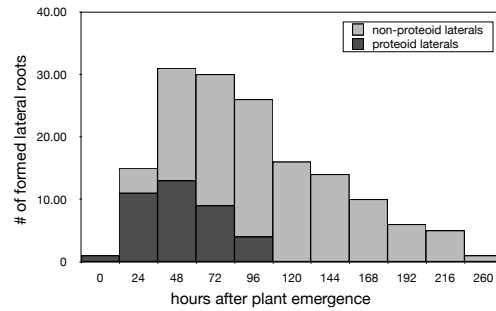


Figure 3.15: Histogram of the timing of lateral root formation (lupin example). Proteoid roots are in dark grey and non-proteoid roots in light grey.

From the same dataset, the number of clusters for individual plants was counted over time, with a temporal resolution of one day (fig. 3.16). This analysis revealed a continuous pattern of cluster root formation at the plant level, which does not fully support the systemic signaling hypothesis generating flushes of cluster root formation. However, the temporal resolution of our analysis does not allow to exclude the possibility of synchronous formation of clusters with a daily (or sub-daily) frequency. Several features of SmartRoot have been instrumental in this experiment: the annotation tools to export cluster boundaries; the sampling-based processing to enable analysis of images overcrowded in roots; the viewing tools for the reliable identification the selected laterals throughout the image sequence.

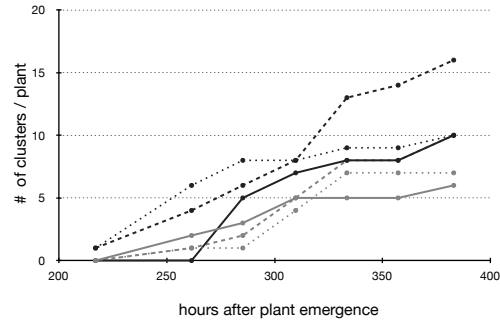


Figure 3.16: Sequence of cluster root formation (cumulative) (lupin example). The graph shows the emergence of new clusters on proteoid roots of six different plants.

3.2 Conclusions

We have presented a novel software supporting in depth characterization of root morphology, geometry and topology from images or time-lapse image sequences. The software uses several algorithms designed for root tracing and has been validated on a wide range of image spatial resolution, noise and contrast. The strengths and weaknesses of SmartRoot are listed in Table 3.3 and discussed hereafter.

Currently available imaging tools developed for the analysis of root system architecture share the same type of workflow: automated analysis followed (sometimes) by manual editing. This strategy leads itself to medium- to high-throughput handling of root images, but tends to be restrictive on the complexity of the root systems that can be analyzed. With branched root systems presenting a large degree of overlap, the user has to manipulate individual roots in the scanner tray prior to scanning or perform an intensive editing of the root skeleton. This reduces the throughput of the analysis and ultimately leads to restricting root studies to the young seedling stage.

The design of SmartRoot was largely influenced by Yoav Waisel's perspective that root systems consist of populations of roots of different types, ages, topological and spatial locations (Eshel, Waisel, 1996).

Table 3.3: Summary of the strengths and weaknesses of SmartRoot.

Weaknesses	Strengths
	Sampling-based analysis
Lack of global parameters	
Time of user interaction → depending on depth of analysis	Low requirements → on image quality, plant type or age
Batch analysis not supported	Time-series handling
Color management not supported	Annotation
	Vector-based representation of roots
	Database connection
	Platform independent
	Highly interactive

The focus was therefore placed on individual root behavior rather than on cumulated variables that are more difficult to interpret. Here, we introduce an innovative type of workflow, based on root system sampling at the time of image analysis. With this approach, manipulating roots prior to imaging is no longer required since parts of the root system where image quality or root overlapping would preclude accurate analysis or imply intensive editing can simply be discarded. The analysis can also be focused on specific root types, which may not be easily recognized by an algorithm, or can be performed stepwise, starting with an evaluation of cheap variables and proceeding with deeper analysis only where needed. The throughput of image processing using SmartRoot will therefore depend on the type of root system, quality of image and desired information (see supplementary material for an evaluation of processing time). A direct consequence of this sampling strategy is an inability to efficiently estimate variables such as total root length, at which most root analysis software are usually very good.

A further innovation of SmartRoot, compared to many root imaging software, is the vectorial representation of roots. This representation enables the most useful capabilities/features of the software

3. A NOVEL ROOT IMAGE ANALYSIS TOOLBOX

which support the sampling strategy: intuitive editing and annotation, navigation in a time-lapse sequence of non-superposable images and an object-oriented data structure allowing an explicit topological description of root systems.

A classical issue in the analysis of root systems image is the discrimination between root branching and root overlapping. Initially, this issue attracted attention because overlaps create biases in the estimation of the total root length (Arsenault et al., 1995). The problem becomes more complicated if the scope of the analysis extends to the recognition of individual roots, in which case the crossing root segments must also be correctly connected. All software that we know, including SmartRoot, attempt to recognize a finite list of situations which they handle in an approximate way. There remains here an important area for the development of more generic algorithms, integrating, for instance, advances in neuron imaging. There are increasing reports of using color images to ease the separation of roots from extraneous objects on the image (substrate particles) or to analyze root health. SmartRoot currently lacks color management, however the multilayer approach will make it easy to implement the stacking of additional raster layers providing data in other range of the electromagnetic spectrum (mainly visible and fluorescence).

To some extent, further developments may come from biomedical imaging, where neuron tracing and cell tracking algorithms have become popular (Meijering et al., 2004). Indeed, neurons and root systems share a similar tree-like structure and the displacement of cells shows parallel behaviors with growing root meristems. Preliminary testing indicates that those methods are not directly applicable on root images that are very different from those obtained in biomedical sciences. However, tracing and tracking tools used for neurons and cells rely on different image analysis concepts and those are worth being investigated in the root domain.

SmartRoot is a platform-independent freeware available at www.uclouvain.be/en-smartroot.

3.3 Material and methods

3.3.1 *Experience 1*

Plants (*Zea mays*, genotype B73) were grown in aeroponic with a modified Hoagland's solution (doubled Fe content, see annex A). The pictures, seven megapixels in size, were taken with a regular CCD camera (Canon EOS 450D) every two days in a small black chamber build inside the greenhouse.

3.3.2 *Experience 2*

Plants (*Lupinus albus*) were grown in aeroponic system with the same nutrient solution as Johnson *et al.* (1994). Daily pictures were taken during sixteen days with a flat bed scanner (Microtek 9600XL), at a resolution of 300 DPI.

3.4 Supplemental data

All supplemental data are available online at <http://www.plantphysiol.org/content/157/1/29.full>

NOVEL SCANNING PROCEDURE ENABLING THE VECTORIZATION OF ENTIRE ROOT SYSTEM



This chapter is a modified version of a method paper currently submitted under the title:

Lobet, G. & Draye, X. Multi-layer scanning procedure enabling the vectorization of entire rhizotron-grown root system. Submitted to BMC Plant Methods.

FEW TECHNIQUES ALLOW the simultaneous acquisition of precise soil and root information. Among the classical techniques, growing plants in rhizotrons is widely used in root research. This technique provides an easy way to observe the growth and development of a large number of plants in a soil-like substrate (Neumann et al., 2009). Moreover, rhizotrons allow some level of soil observation, as with the light transmission imaging (Garrigues et al., 2006). These techniques enable a fine analysis of soil-root relations, given that sufficient information is obtained about the plant and the soil.

The description of the root system of plants grown in rhizotron is often performed by recording the visible roots on the outer surface of the rhizotron (manual drawing or scanner, *in-situ* images), or by removing the plant from the rhizotron and scanning its root system (*ex-situ* images). These methods yield complementary informations about the root system architecture, but neither of them provide precise data about the root morphology, topology and placement that is required for a local analysis of soil-root interactions.

We propose here a new method, referred hereafter as the *hybrid method* that combines the strengths of existing techniques and software in order to generate detailed and spatially correct digital versions of entire root systems.

4.1 Results and discussions

The general principle of the method is to extract as much local information as possible from *ex-situ* imaging of large root system fragments and use the global information from *in-situ* imaging to reconstruct entire root systems.

In practice, major root axes appearing at the rhizotron transparent side are manually traced on an acetate sheet superimposed on the rhizotron (fig. 4.1.A). The rhizotron is then opened and the root system is extracted and split into parts where root overlap is minimized (fig. 4.1.B and C). In monocots, one would typically split the root system in first order roots (primary, seminal, adventitious) while in dicots, one would separate the tap root from its large branches.

The acetate sheet (obtained *in situ*) is then attached on the glass of the scanner (fig. 4.1.D) and, one by one, each root part is laid on the scanner, aligned to its corresponding tracing and scanned (fig. 4.1.E). The whole scanning procedure yields a set of high resolution registered images where roots (1) are positioned as in the rhizotron and (2) display a much reduced degree of root overlap. The subsequent tracing of the roots is realized with SmartRoot (fig. 4.1.F) on the individual images and the resulting morphological datasets are combined into a unique and complete vectorized root system.

The ability of the method to generate vectorized versions of entire root systems and its utility in the framework of soil-root-interaction research is demonstrated with the analysis of water uptake dynamics in maize. Plants were grown in thin rhizotrons under non-limiting conditions until emergence of the sixth leaf. The nutrient solution supply was then interrupted and the evolution of the 2D soil water content was monitored during three days using light transmission imaging (Garrigues et al., 2006).

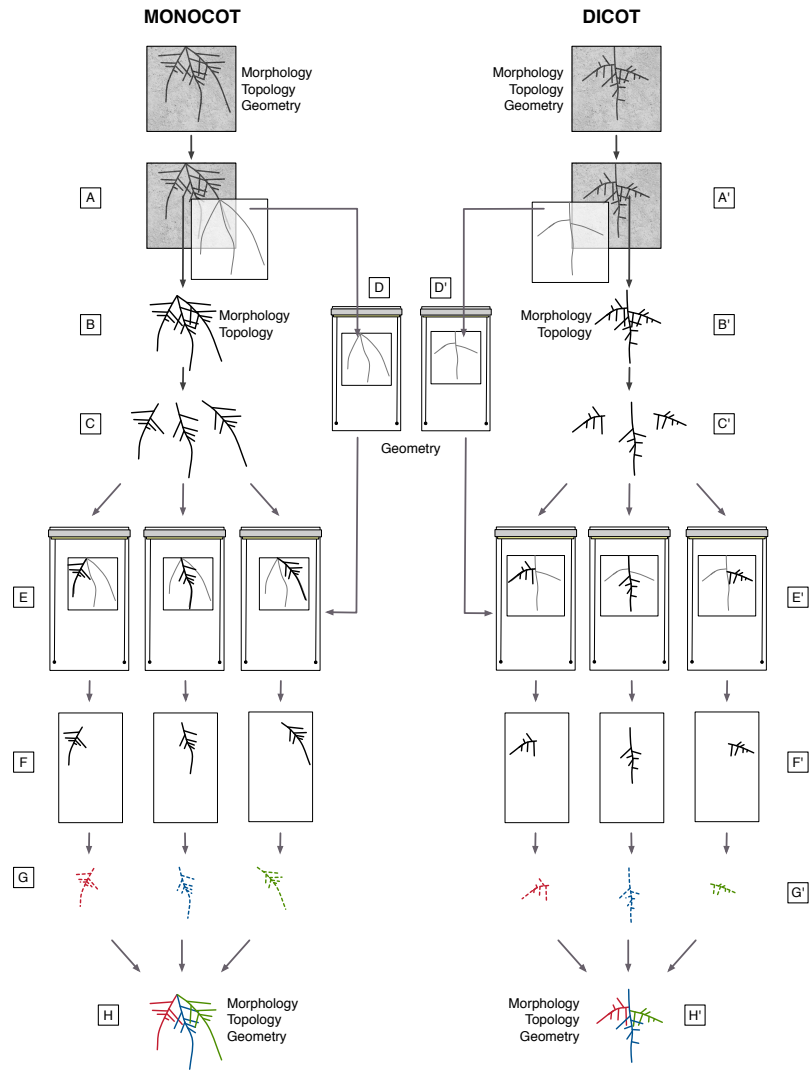


Figure 4.1: Procedure to vectorize an entire root system. **A.** Thick and easy to recognize parts of the root system are manually traced on a transparent sheet at the rhizotron surface. **B.** The entire root system is extracted and cleaned. **C.** The different parts are dissociated. **D.** The transparent sheet is laid on the surface of the scanner. **E.** Each root axis is successively placed on the scanner according to the drawing and scanned. **F.** As a result, every root system is contained in a set of several images. **G.** Every root image is traced with SmartRoot. **H.** The different tracing are regroup into a single vectorized root system using SmartRoot.

4. DIGITIZING ROOT SYSTEMS

4.1.1 Step 1: Architectural analysis of complex root systems

The hybrid method was successfully used to create vectorized versions of entire root systems of 20-day old maize plants having 2-3 seminal roots and 2-4 adventitious roots (fig. 4.2A-E). To validate the accuracy of the method, the total root area estimated for 52 plants were compared with the area obtained from classical *ex-situ* images (similar to the one presented in the figure (fig. 4.2.A) using GiA Roots (fig. 4.3) (Galkovskyi et al., 2012). The high correlation coefficient (linear regression with intercept forced to zero, $r^2=0.96$) between the two methods indicates that the results obtained with the hybrid method are within the range of classically obtained data. It is interesting to see that values obtained with GiA Roots tend to be overestimated compared to the hybrid method. This is probably due to the quality of the original root images and the subsequent errors generated during the GiA Roots thresholding/skeletonizing steps (fig. 4.4).

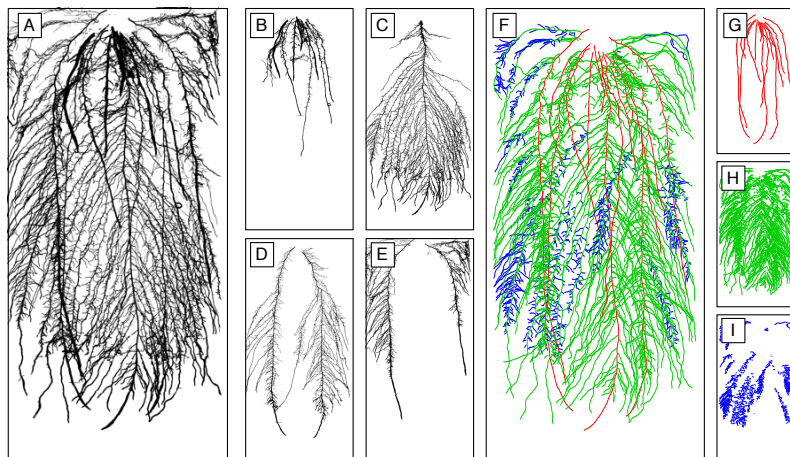


Figure 4.2: Example of vectorized maize root system. **A.** Complete scan. **B-E.** Individual root scans. **F.** Entire vectorized root system. **G-I.** Vectorized root system by root order. **F-I.** Different colors represent different root orders: red = first root order, green = second root order, blue = third root order.

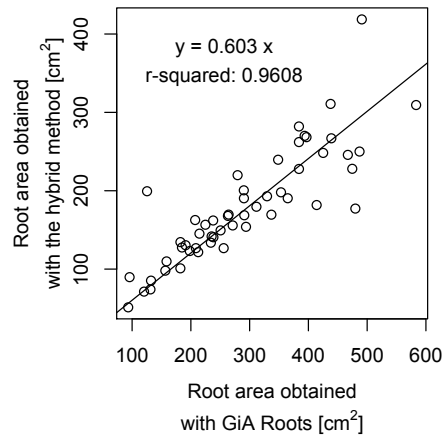


Figure 4.3: Comparison of the total root surface obtained with a classical root scan analysis (performed with GiA Roots (Galkovskiy et al., 2012)) and the hybrid method. The linear regression was forced to zero.

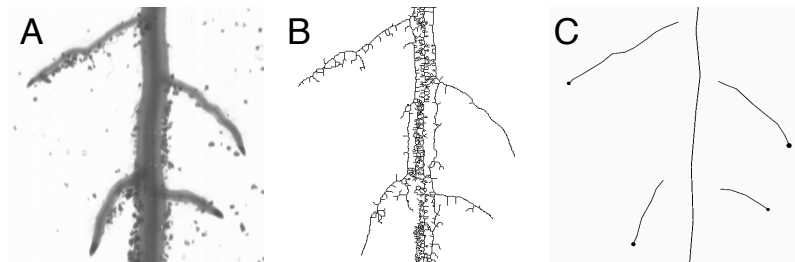


Figure 4.4: Skeleton comparison between GiA Roots and SmartRoot. **A.** Original image. **B.** Skeleton obtained with GiA Root. **C.** Skeleton obtained with SmartRoot.

4. DIGITIZING ROOT SYSTEMS

The dataset resulting from the hybrid method was analyzed using common statistical software (data presented here were analyzed using *R R: A Language and Environment for Statistical Computing*). Figure 6 highlights some of the information that can be extracted from the SmartRoot database: a complete representation of the root system (by root orders, fig. 6.A), a representation of the total root surface distal any position in the root system (fig. 4.5.B), the comparison of the root length 1D profiles of the different root orders (fig. 4.5.C), the comparison of the root diameters for the different root orders (fig. 4.5.D), the contribution of the different root orders to the global root surface (fig. 4.5.E) and the changes in orientation of the roots along their axis.

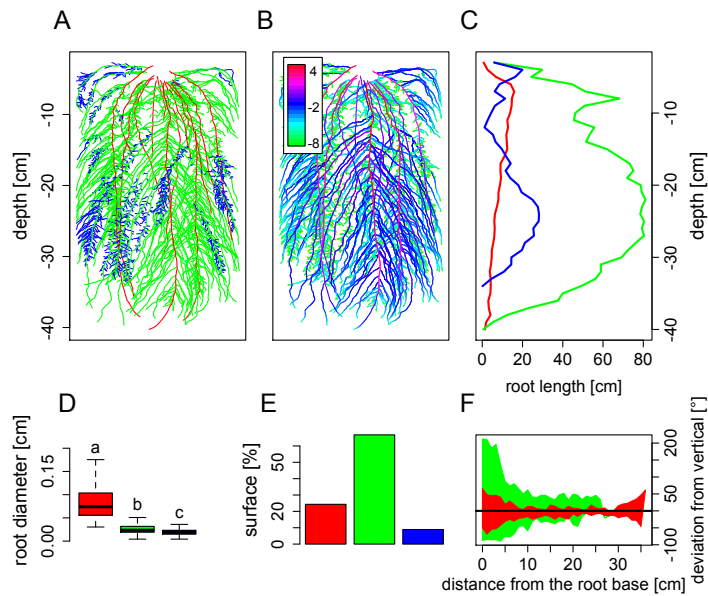


Figure 4.5: Root system architecture results. **A.** Entire vectorized root system. **B.** Total root surface distal any position in the root system (scale is in $\log(\text{cm}^2)$). **C.** Root length profiles for the different root orders. **D.** Comparison of the root diameters for the different root orders (values suffixed with the same letter are not significantly different at $p < 0.01$, t-test). **E.** Surface proportion of the different root orders. **F.** Orientation of the roots along their root axis. The horizontal black line highlight the vertical direction. In all the figures (except B), different colors represent different root order: red = 1, green = 2, blue = 3.

4.1.2 Step 2: Local analysis of root-soil interactions

As mentioned earlier, a detailed description of root system architecture (including root placement) and quantification of the distribution of the observed resources in the soil domain is required to analyze the interplay between root systems and their environment (Draye et al., 2010; Ge et al., 2000; Lobet et al., 2012). Because the vectorized root system is spatially registered on the rhizotron surface, the architectural information can be combined with any 2D description of soil resources. Here, we crossed the SmartRoot dataset with 2D maps of soil water content obtained with the light transmission imaging technique (Garrigues et al., 2006).

Figure 4.6.A shows the temporal evolution of the soil water content for as a function of the distance to the closest root. This estimation combines the root placement information and the local evolution of soil water content around individual roots. The figure highlighted the strong water content gradient appearing at the vicinity of the roots (fig. 4.6.A, red area). This non-linear decrease of water content at the proximity of the roots results to a higher resistance to the water flow compared to the bulk soil and can ultimately lead to local hydraulic isolation of the root system (Gardner, 1965; Lobet et al., 2012) and to reduction in the transpiration rate (fig. 4.6.A). Additionally, the same figure shows the apparition of a refilling process occurring during the second night between the bulk soil and the dry region close to the roots (fig. 4.6.B, arrow). This example highlights the usefulness of the method in the framework of soil-root interaction analysis at a local scale (in this example, at the centimeter scale).

Depending on the size and complexity of the root system, this method can be time consuming and is not amenable even to moderate throughput. In our example, the image acquisition step (cleaning and scanning) took between 20 to 50 minutes per root system. The time required for root tracing with SmartRoot ranged from 1 to 4 hours. Nevertheless, the methodology proves to be a valuable tools to analyze complex root systems since, to the authors knowledge, no other methods today is able to extract such detailed dataset from entire root systems well beyond the seedling stage.

4. DIGITIZING ROOT SYSTEMS

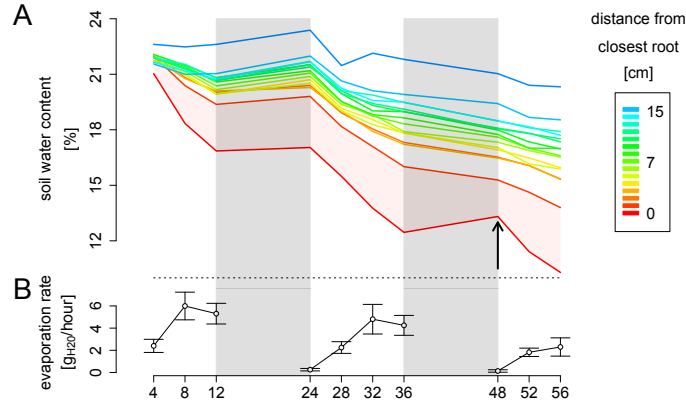


Figure 4.6: **A.** Evolution of transpiration rate. **B.** Evolution of the soil water content at different distances from the roots (0-15 cm). Red area highlight the difference in soil water content between the root and the first centimeter of soil. Grey area represent the night (no measurements). The arrow highlight the water redistribution in the soil occurring at night.

4.2 Conclusions

We have presented a new method based on a multiple scan approach to vectorize entire root systems grown in rhizotrons. This method combines the strengths of two classical methods: *in situ* recording of root placement and *ex situ* high resolution scanning of root system fragments. The method yields ultimately a rich dataset containing detailed informations on every root (position, morphology and topology) which can be easily crossed with spatial soil information data to analyze the interplay between the root system and local soil conditions. The method has been successfully used to vectorize root systems of 20-day old maize plants and has been used for the analysis of spatial root water uptake patterns.

Despite the time required by the method (both root scan and image analysis), we believe that it opens new perspectives for root-soil research. It proved an affordable way to precisely describe complex root system architecture and their interplay with their direct environment. We are currently using it for the validation and exploitation of functional-structural plant models that simulate water and nutrient

movement in the soil-root domain (Couvreur et al., 2012; Javaux et al., 2008; Schröder et al., 2009). Using the digital structure created with the hybrid method, these models could be used to analyze *in silico* the water dynamics of the system.

The hybrid approach is neither bound to a specific acquisition device nor to a specific image analysis software. It provides a framework which should be improved with future technical advances (e.g. faster scanners) and software developments (e.g. increased tracing automation). Following the root tracing protocol described by Le Bot et al. (2010) the method could also be extended to the temporal analysis of root growth and its merging with relevant local soil conditions (e.g. soil water content and mechanical impedance).

4.3 Methods

4.3.1 Hybrid method

Maize plants (B73) were grown during 20 days in thin rhizotrons (Lobet, Draye, 2012) made of transparent acrylic filled with a mix of white sand (98.5%) and clay (Bentone SA, 1.4%). The substrate was maintained at field capacity with a modified Hoagland solution. In order to increase the number of roots growing along the rhizotron surface, rhizotrons were stored at an angle of $\approx 35^\circ$.

In situ tracing of the root axis

At the end of the growing period, before removal of the plant from the rhizotrons, the visible roots were manually traced on a transparent sheet placed on the rhizotron surface (fig. 4.1.A). Different roots orders were drawn using different colors for an easier placement of the roots on the scanner. We used light colors that do not appear on the final scan.

Root system preparation

After the tracing, rhizotrons were open and plants were taken out. Root systems were separated from the shoot and cleaned from the substrate (fig. 4.1.B). Root cleaning was performed by soaking them during 5 minutes into water with a mild detergent. Finer soil particles still attached to the root were removed using a small painting brush. Plant were stored in a 50% ethanol solution before the scanning procedure.

4. DIGITIZING ROOT SYSTEMS

Root scanning procedure

The scanning procedure was performed with a custom flat bed scanner whose scanning window can be filled with water to enable an easier positioning of the roots (fig. 4.7.A and C). The scanner (Medion 3600 DPI) was customized in house in such way that the light source and the sensor on both side of a large water container ((fig. 4.7.B, 21 x 60 cm). The transparent film with the root tracing was first fixed at the bottom of the scanner with transparent adhesive paper (fig. 4.7.B). Then, the root system was split into fragments that were scanned individually.

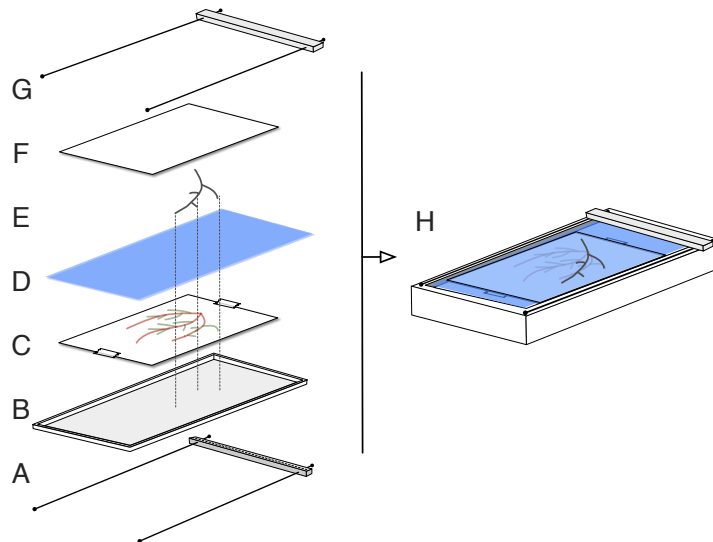


Figure 4.7: Scanning procedure. **A.** Captor mounted on conveyers. **B.** Transparent water container. **C.** Transparent sheet with the root tracing. **D.** Water. **E.** Part of root system. **F.** Transparent sheet for reduction of shading effect. **G.** Light source mounted on conveyers. **H.** Complete scanning setup. Parts of root systems are replaced according to the root tracing (dotted lines).

Each fragment (usually corresponding to a first order roots) was placed on the scanning window according to its position on the root tracing (fig. 4.1.C-E). Since every one of these roots is different (in length and shape), the correct position of every axis is found easily. Once the fragment was positioned, its lateral roots were carefully

untangled (with a painting brush if needed). The use of a submersible scanning window streamlined the process as the roots tended to recover their initial shape in the water. A transparent plastic sheet was placed on the water surface to improve image quality and reduce shadows around the roots (fig. 4.7.E). The scan was done with a 600 DPI resolution. The same procedure was repeated for every fragment of the root system. The final output of the scanning was therefore an image set of x images, where x is the number of fragments of the root system.

Root vectorization

Every root image was analyzed using the root image analysis software SmartRoot (fig. 4.1.F, Lobet et al. (2011)). The software enables a semi-automated tracing of individual roots and generates morphological and topological informations. In order to streamline the tracing of complete root systems, several new tools were implemented in SmartRoot which allow the user to performed grouped action on multiple roots:

Root list panel A new tool was implemented to be able to view the different roots as a hierarchical list (every root order being nested in its parent node). This tool allows a fast observation of basic root statistics and an easy selection of multiple roots.

Action on multiple roots Complementary to the multiple root selection tool in the root list panel, the possibility to perform actions on multiple roots was implemented. These actions include deleting roots, attaching them to a single parent or finding lateral roots.

Import multiple files A new import function was implemented to allow the import of multiple datafile to a single image. This tool enables the reconstruction of a completed root system from individual images.

The use of the root list panel combined with the action on multiple roots streamlines the root tracing process for individual images. The multiple import option enables the merging of multiple root tracing on a single image.

4. DIGITIZING ROOT SYSTEMS

4.3.2 Local analysis of root-soil interactions

Time series of 2D maps of soil water content (fig. 4.8.A) were obtained using the light transmission imaging technique Garrigues et al., 2006. Briefly, the technique relies on the relationship between the water content of the substrate and its light transmission Tidwell, Glass, 1994. Using this principle, the 2D soil water content distribution was obtained by placing every rhizotron between a light source (light tubes, 36W, Sylvania Standard F36W/33-640-T8) and a regular CCD camera (Canon EOS 450D with a lens Canon EF 50mm 1:1.8). The time series consisted in a picture every four hours during three days.

The obtained time-series were analyzed by crossing the data contained in the images with the vectorized root system (fig. 9B and C). More precisely, this was achieved by (1) reducing the image to 50 x 50 pixels so that every pixels had a size of 1 cm², (2) finding, for every pixel, the closest root (euclidian distance) (fig. 4.8.C) and (3) creating a new database containing the information about the root and the soil. Root growth was assumed to be negligible during the three days of measurement.

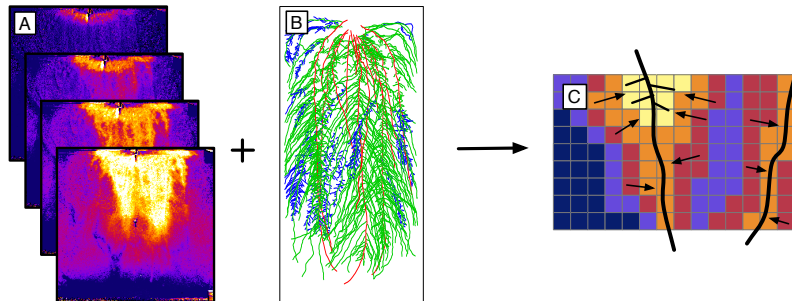


Figure 4.8: Local uptake analysis. **A.** Time-series images of soil water content. **B.** Vectorized root system. **C.** Local analysis of the variation in the soil water content using the information obtained with the vectorized root system.

PART *IV*

MONITORING SOIL
WATER CONTENT
IN THE SOIL-ROOT
DOMAIN

In this section we will present a new experimental platform that allows the simultaneous observation of the evolution of soil water content and root system growth and development of 20 plants. We will present and discuss the experimental results obtained with the platform.

The first chapter will present an analysis of the role of morphological root features in the water content distribution.

The second chapter will present a new type of analysis that combines *in vivo* and *in silico* experiment to unravel the contribution of plant hydraulic features in the uptake dynamic.



Water is the driving force of all nature.

LEONARDO DA VINCI

PRELIMINARY CONCEPTS

5

AS DISCUSSED IN CHAPTER 1, the acquisition of water is a key process in the plant life. Focusing on plant constraints, the water availability is restricted by the root system architecture (the connection between roots and their position in the soil) and the hydraulic properties of its constitutive root segments (axial conductance, K_h , and radial conductivity, K_r). Root system architecture is therefore a potential target for the improvement of water use and capture by plants (Tuberosa, 2012).

5.1 Architectural traits

5.1.1 *Root system size*

The total size of the root system is a first important feature in the uptake process. Large root systems are often associated with large leaf area, so that plants with an important root area tend to transpire and extract more water from the soil. In drought-prone environments, having a large root system could therefore be detrimental for the plant if all the soil water is extracted early in the season (Kholová et al., 2010; Palta et al., 2011; Zaman-Allah et al., 2011a).

Additionally to the absolute size of the root system, its relative size, compared to the shoot, is thought to have an influence on the global plant water status. For a given transpiration demand (and leaf area), the size of the root system directly influences the tension in xylem vessels. If the demand set by the shoot cannot be met by the roots, xylem tension is likely to increase leading to an increase in the likelihood of cavitation (Hacke et al., 2000; Sperry et al., 2002; Sperry et al., 1998).

5.1.2 *Root system shape*

Next to the root system size, the volume of soil explored by the roots restricts the quantity of water potentially available for transpiration. Although water is a mobile and rapidly moving soil resource, an adequate placement of the roots in the soil domain is required for an

efficient water uptake process. In particular, the root system depth, and therefore the ability of the plant to access deep soil water, has been linked in numerous occasions to the drought resistance strategies (Bernier et al., 2009; Henry et al., 2012, 2011; Hund et al., 2009; Steele et al., 2007).

5.1.3 *Root distribution*

Recent work put forward the fact that not only having roots in deep soil layers is important for water acquisition, but that the root length density (the amount of root per soil volume) in deep soil layers was correlated with better transpiration maintenance and drought resistance in the field (Henry et al., 2011; Wasson et al., 2012). Moreover, root length density in the surface layer often exceeds the one required to extract all the water contained in the soil ($1\text{cm}/\text{cm}^3$, Passioura (1983)). Decreasing the proportion of roots in the upper soil layers and therefore decreasing the corresponding carbon cost is therefore thought to be beneficial in drought prone environment (Wasson et al., 2012).

5.2 Hydraulic properties

The root system hydraulic architecture (Doussan et al., 1998), defined by the integration of the root system architecture and of the radial and axial hydraulic properties of its composing root segments, has been shown to influence the distribution of the uptake sites along the roots (Draye et al., 2010).

Radial and axial hydraulic properties of the roots are known to be highly regulated by the plant. Radial conductance is influenced, on the long term, by the number of cell layers, the formation of apoplastic barriers (Enstone et al., 2003) and, on the short term, by the regulation of aquaporins activity (Maurel et al., 2008). Similarly, the formation and maturation of xylem vessels impact root axial conductivity on the long term, while the management of cavitation events (avoidance and/or recovery) influences it on the short term (Sperry et al., 2002). However, despite numerous studies on both components of the hydraulic architecture, their respective contribution to the water uptake process at the plant scale is still not fully understood (Bramley et al., 2009; Lobet et al., 2012).

In the following chapters, we will attempt to link experimentally the morphological and hydraulic features of roots to the water uptake dynamics. In the first chapter of this section, we will present a new experimental platform allowing the simultaneous observation of root system development and of the evolution of soil water content. The platform has been used to assess the role of various root system descriptors such as the root system size or the distribution of roots in the soil profile in the uptake dynamic. In the second chapter, the influence of contrasted hydraulic properties on the formation soil water content patterns will be tested using the functional-structural root water uptake model R-SWMS.

USING LIGHT TRANSMISSION IMAGING TO IDENTIFY ROOT ARCHITECTURAL FEATURES INFLUENCING WATER UPTAKE



THE SIMULTANEOUS OBSERVATION of soil water content and root system architecture is a challenging task. Indeed, most available techniques focus on either components of the system and very few on both.

The monitoring of soil water, on the one hand, relies on techniques such as time domain reflectometry (Robinson et al., 2003; Walker et al., 2004), electrical resistance tomography (Cassiani et al., 2006; Kemna et al., 2002; Vanderborght et al., 2005) or, more recently, ground penetrating radar (Lambot et al., 2004a,b; Lambot et al., 2008) and neutron radiography (Esser et al., 2010). These techniques usually provide, at different scales, a distribution of the water content in the soil domain but can hardly be linked to root distribution in the soil or single root architecture.

On the other hand, root observation in the soil can be done using techniques recently brought to the plant science community such as magnetic resonance imaging (Jahnke et al., 2009) or x-ray computed tomography (Mooney et al., 2011). However, these techniques require heavy equipments and expertise and are usually not suitable for the analysis of a large number of plants.

The use of rhizotrons is a popular method for the observation of root growth and development. A couple of years ago, Garrigues et al. (2006) introduced light transmission imaging (LTI) to quickly observe soil water content variation in rhizotrons. In our experiments, we used LTI to monitor changes soil water content arising from water uptake by maize plants. The obtained water depletion patterns were used to evaluate the quantitative influence of different root architectural parameters on the water uptake dynamics.

6.1 Material and methods

6.1.1 Experimental procedure

Each experiment was run during 25 days (fig. 6.1). The experimental setup was made of 24 transparent acrylic rhizotrons (inner volume = 480 x 480 x 4 mm, Lobet, Draye (2012)). Rhizotrons were filled with the substrate (described below), saturated in nutrient solution (see annexe A) and left overnight for drainage. Sterilized seeds were germinated in petri dishes at 25°C and transplanted into the rhizotrons when the hypocotyl was 1cm long.

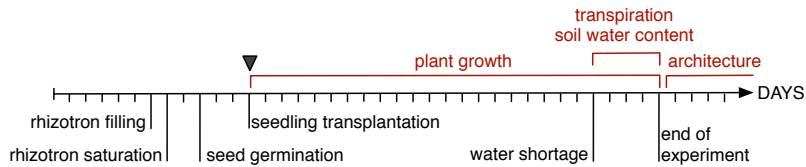


Figure 6.1: Time line of the light transmission imaging experiments. Black triangle indicates the beginning of the experiment. Experimental measurements are in red.

Rhizotrons were placed in a greenhouse at an angle of approximately 35° (Berntson, Woodward, 1992; Busch et al., 2006) and supplied with 6 ml of modified Hoagland solution every 2 hours (fig. 6.2). Phenological stages were recorded and a manual tracking of the root growth was made every two days during approximately 15 days (Cheng et al., 1991; Devienne-Baret et al., 2006).

After the emergence of the sixth leaf, the water supply was stopped to induce a three days-long water shortage episode (WSE). Pictures of the soil water content distribution were taken at regular interval during the WSE (7a.m., 11a.m., 3p.m., 7p.m.) using the light transmission imaging technique. For each plant, a sequence of twelve water content pictures was generated. During this period, plant growth and transpiration were recorded. After three days, the plant were taken out of the rhizotrons and the root systems were scanned (see chap. 4). During the whole experiment, light intensity was kept above 300 $\mu\text{mol.m}^{-2}.\text{sec}^{-1}$ between 7AM and 7 PM. Day/night temperature were fixed at 20°C/25°C.



Figure 6.2: Rhizotron storing device

In total twelve experiments were performed, between February 2009 and May 2011. All experiments were carried in Louvain-la-Neuve, Belgium ($+50^{\circ} 39' 59.91''$, $+4^{\circ} 37' 10.56''$). Only three experiments were used in this analysis. The other experiments were considered as preliminary tests. Table 6.1 presents the schedule for these experiments, the genotype used and the environmental conditions.

Table 6.1: Details of the different light transmission imaging experiments.

Date	Genotypes	#	temp. [$^{\circ}\text{C}$]	rel. hum. [%]	VPD [MPa]
Nov. 2009	B73+A188	6+6	24.9 ± 1.5	46.7 ± 3.8	1.7 ± 0.2
Feb. 2010	B73+A188	6+6	23.4 ± 2.9	40.9 ± 5.0	1.7 ± 0.4
Apr. 2010	B73+A188	6+6	26.6 ± 5.7	38.8 ± 7.4	2.3 ± 1.2

Plant material

Two genotypes were used for the experiments: B73 (Iowa State University) and A188 (Minnesota Agric Exp Stn). A188 was initially thought to be ABA overproducing (Parent et al., 2009) and were chosen for their (expected) altered root radial conductivity. It turned out no significant changes were observed between the different genotypes in terms of ABA production or development (data not shown, ABA dosed with the ABA-RIA method at the University of Lancaster).

6. LIGHT TRANSMISSION IMAGING

Light transmission imaging

Light transmission imaging (LTI) enables a fast acquisition of a 2D map of the soil water content (Garrigues et al., 2006). Briefly, the technique relies on the quantitative relationship between light transmission properties and water content of the substrate (Tidwell, Glass, 1994). The technique generates images where dry regions of the soil appears darker than the wet regions. The resulting dataset was composed of time series of 2D maps of soil water content.

The complete image acquisition and treatment process is detailed in the annex B. Briefly, the relationship between the quantity of light transmitted through the substrate and the soil water content was determined experimentally. This relation was used to transformed the pixel value of every rhizotron images into water content values. However, since compaction differences were observed between rhizotrons, the calibration curve of every rhizotron was corrected such as the water loss estimated from the LTI images was consistent with the mass balance measured experimentally (fig. 6.3).

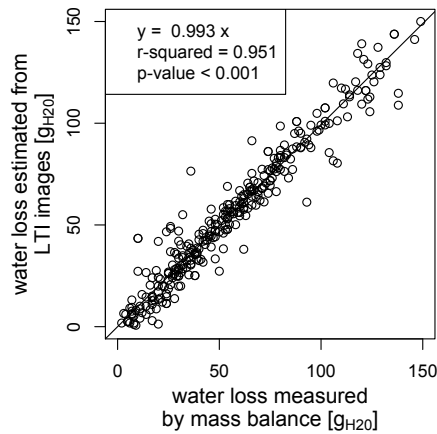


Figure 6.3: Comparison between the water loss measured by mass balance during the LTI experiment and the estimated from the light transmission images. These values are for all the rhizotrons.

Soil properties

The LTI technique is bound to a specific type of substrate. The chosen substrate must have a good light transmission and water retention. We used the substrate described by Garrigues et al. (2006), made of 98.5% of white sand (Flamingo Siberia) and 1.5% of hectorite, a white clay (Bentone HC, Necarbo). This substrate has a good water content / light transmission relation, a good water content retention capacity (fig. 6.4.A, determine with sand box and pressure plate experiments) and has a steep conductivity curve (fig. 6.4.B, Garrigues (2002)). Such properties makes it suitable for LTI.

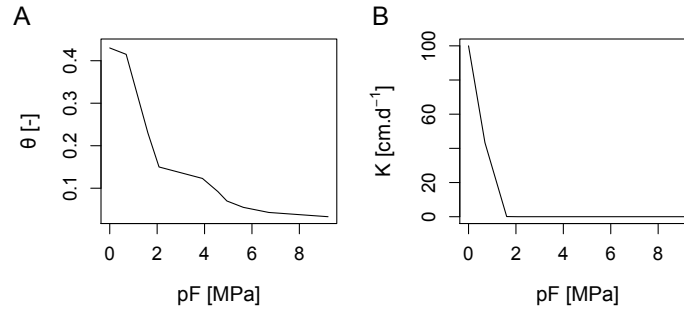


Figure 6.4: Soil hydraulic properties. **A.** Water retention curve as determined experimentally by the application of increasing suction to soil samples. **B.** Conductivity curve (Garrigues, 2002).

6.1.2 Plant and soil parameters

The final dataset used for the analysis of the LTI experiments comprises plant morphological features, total transpiration and evolutions of soil water content (see tab. 6.2). For the sake of notation simplification in the rest of the chapter, the different variables will be referred to by their acronym shown in the table 6.2. All root-related parameters were obtained from the vectorized root systems (see chap. 3 and 4) and computed using R..

6. LIGHT TRANSMISSION IMAGING

In order to analyse the effect of plant morphological features on the uptake dynamics, the evolution of soil water content of different plants were compared. Every light transmission image was divided in three horizontal layers for which average decrease in soil water content (SWC) was calculated (fig. 6.5). This method had to advantage to filter out local heterogeneities in the soil water content profiles (due to uneven substrate filling or soil disruption).

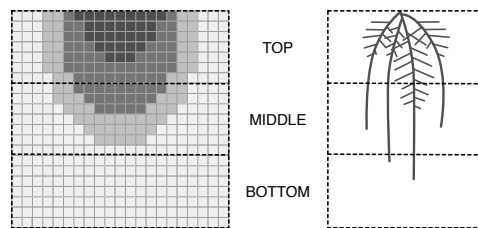


Figure 6.5: Soil and root system layers used for the computation of the different variables (see tab. 6.2).

6.1.3 Statistical analysis

Data processing and statistical analyses were performed using R (*R: A Language and Environment for Statistical Computing*).

6.2. Results and discussions

Table 6.2: Parameters used for the analysis of the light transmission imaging experiments. *Network* refers to the whole root system. PR = first-order root. SR = second-order root. Distri. = root distribution. Tr = transpiration. WCD = volumetric water content decrease

	Parameter name	Description	Unit
SIZE	rArea	projected root area	cm^2
	rsRatio	root / shoot area ratio	–
	nVol	total root network volume	cm^3
	nLength	total root length	cm
SHAPE	nWidth	root network maximal width	cm
	nDepth	root network maximal depth	cm
	nRatio	root network width/depth	–
	nConv	root network convex area	cm
DISTR.	pTop	% of roots length in the top layer	%
	pMid	% of roots length in the middle layer	%
	pBot	% of roots length in the bottom layer	%
	nBush	root network bushiness (nLength / nConv)	cm^{-1}
	tCumul	total transpiration	g_{H_2O}
SOIL	diff.hum.top	WCD in the top soil layer	%
	diff.hum.mid	WCD in the middle soil layer	%
	diff.hum.bot	WCD in the bottom soil layer	%

6.2 Results and discussions

6.2.1 Plant architecture

The different genotypes were compared using a multivariate analysis of variance (MANOVA) using the different root architectural parameters (tab. 6.2). The analysis revealed no significant global difference between the genotypes (p-value = 0.055), but small difference between some of the considered parameters were observed (fig. 6.6). However, since these differences were small compared to the residual variability, we decided to leave the genotypic effect aside of our analysis.

The large amplitude of values observed for each architectural variable was exploited to investigate the functional role of root traits in the patterns of water uptake (fig. 6.7).

6. LIGHT TRANSMISSION IMAGING

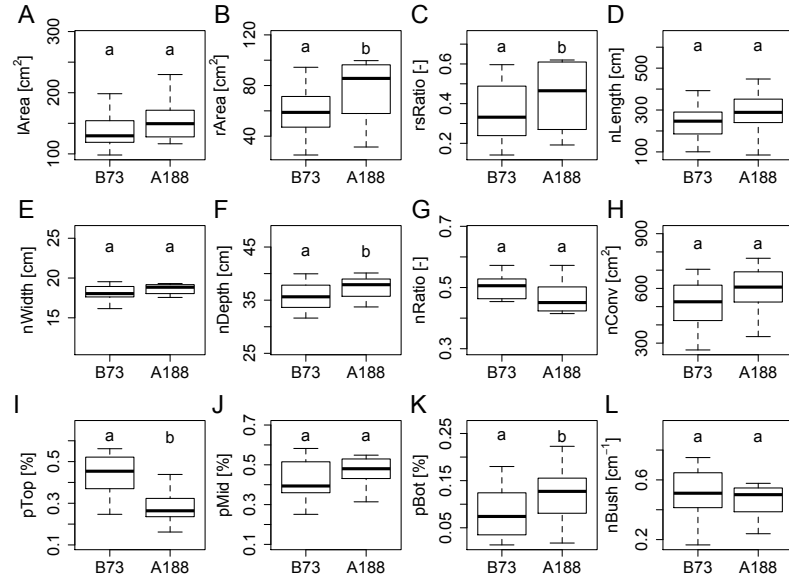


Figure 6.6: Comparison of architectural traits related to plant size between the different genotypes. **A.** Root area. **B.** Root-to-Shoot surface ratio. **C.** Root system length. **D.** Root system volume. **E.** Root system width. **F.** Root system depth. **G.** Root system depth / width ratio. **H.** Root system convex area. **I.** Proportion of root in the top layer. **J.** Proportion of root in the middle layer. **K.** Proportion of root in the bottom layer. **L.** Root system bushiness. Different letters indicates significant differences between genotypes (t-test, $p < 0.05$). Variables names are explained in the table 6.2

The many architectural parameters that were considered were not completely independent one from another. Figure 6.8 shows the correlation matrix of all variables. It can be observed that many descriptors, particularly the one related to the root exploration at depth (rArea, nDepth, pBot), are highly correlated. While this observation makes complete sense, we will have to pay attention to these correlations to avoid over-interpretation in the following analyses.

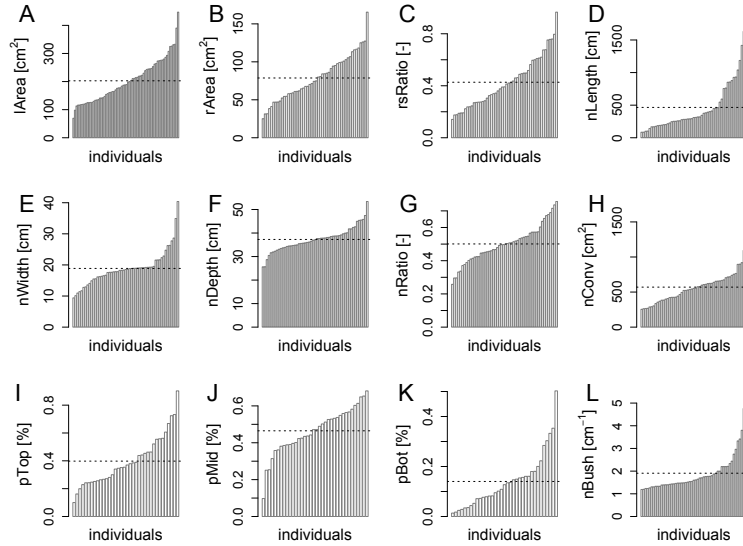


Figure 6.7: Parameters variability for all LTI experiments **A.** Leaf area. **B.** Root area. **C.** Root-to-Shoot area ratio. **D.** Root network length. **E.** Root network width **F.** Root network depth **G.** Root network width to depth ratio **H.** Root network convex area. **I.** Proportion of roots in the top layer. **J.** Proportion of roots in the middle layer. **K.** Proportion of roots in the bottom layer. **L.** Root network bushiness. Dotted line indicates the mean value of the variable. Variables names are explained in the table 6.2

6.2.2 General water content variations dynamics

During the water shortage episode, the patterns of soil drying followed a downward evolution (fig. 6.9). At the beginning of the experiment, decrease in SWC occurred only in the upper region of the soil, near the plant collar. SWC decrease extended downward as the water shortage episode went on. Similar progressive patterns were observed in previous experiments with narrow-leaf lupin (*Lupinus angustifolius*, Garrigues et al. (2006)) and was attributed to the progressive water extraction for the substrate.

6. LIGHT TRANSMISSION IMAGING

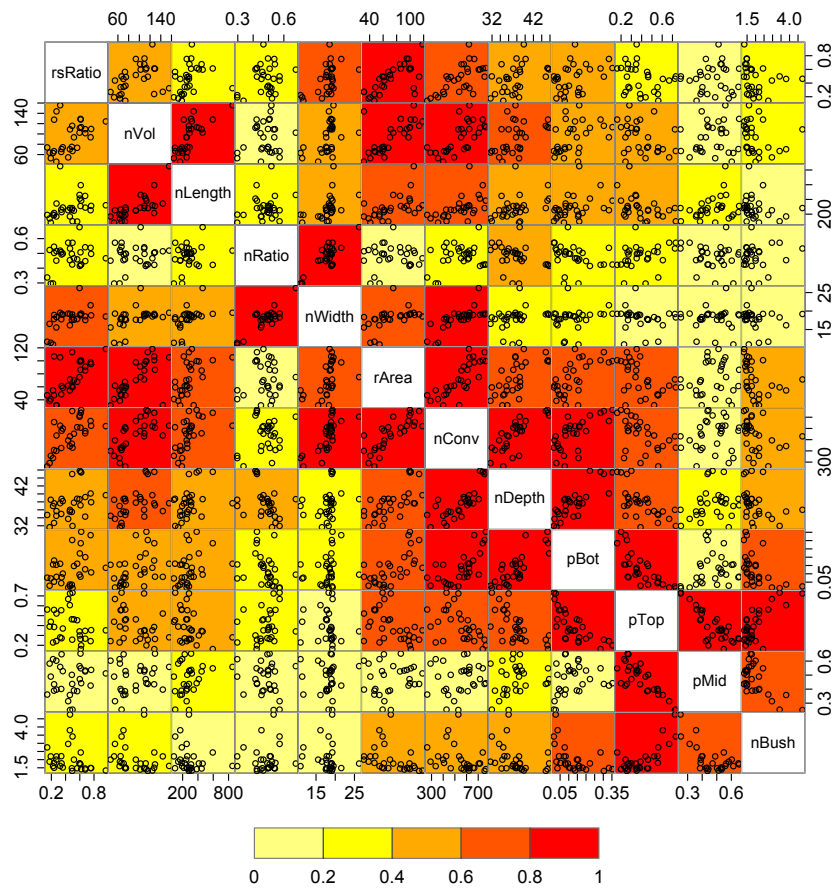


Figure 6.8: Correlation matrix of architectural features. Different color represent different r-squared values (cf. scale). Variables have been re-organised so the greater correlations lies on the diagonal. Units presented in the table 6.2

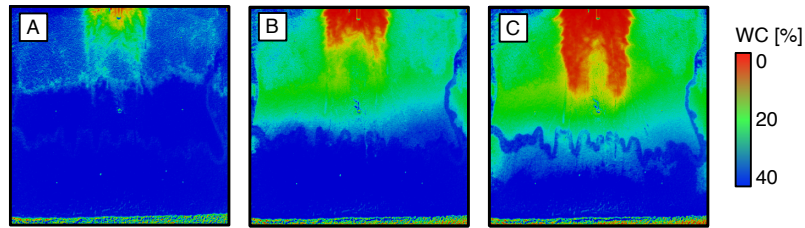


Figure 6.9: Images of soil water content evolution obtained with the light transmission imaging technique. **A.** First day. **B.** Second day. **C.** Third day. All pictures were taken at 7.00PM. WC: volumetric water content

The evolution of the SWC decrease in the three soil layers (top, middle and bottom) is shown on figure 6.10. In all layers, the SWC decreases progressively during the water shortage episode. In some cases, some small increases were observed (values below 0) and indicated that soil water redistribution occurred in the rhizotrons. This phenomenon typically happened during the night when the water flow decreases and the system evolves toward an equilibrium. Changes in soil water content were much smaller in the bottom layer of the rhizotrons.

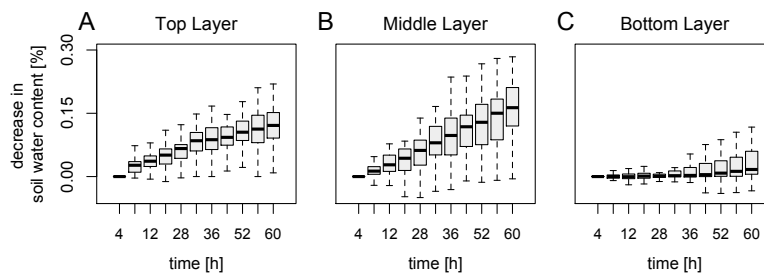


Figure 6.10: Evolution of the decrease in soil water content for **A** the top soil layer, **B** the middle soil layer and **C** the bottom soil layer.

6. LIGHT TRANSMISSION IMAGING

6.2.3 Effect of architectural traits on the soil water content distribution

In order to assess the influence of architectural traits on the SWC distribution, linear regressions were performed between each architectural variable (measured at the end of the experiment) and the cumulated decrease in SWC in each soil layer.

As expected, the total transpiration was tightly correlated with decrease in SWC in all layers (fig. 6.11). It as to be noticed that water extraction in the top soil layer was less correlated with transpiration. This observations is probably due to design of the rhizotron and the constant presence of a darker zone (not related to water extraction) around the seed and at the top of the rhizotrons.

For that reason, decrease in SWC values were normalized by the total transpiration of the plant. The r-squared coefficients obtained for the different regressions are shown in the table 6.3. Plots of the different regressions are shown in the figures 6.12 (top soil layer) and 6.13 (bottom soil layer). Results from the middle soil layer are not shown as no correlation were found for any of the parameters.

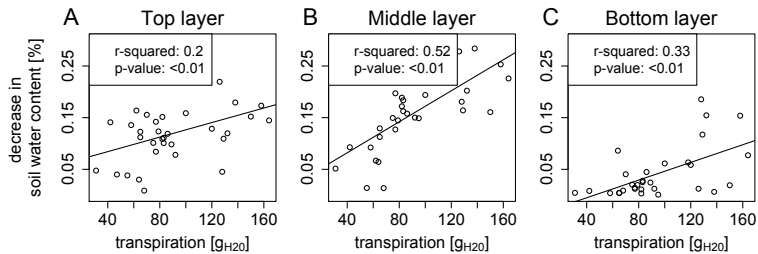


Figure 6.11: Effect of transpiration on the soil water content decrease. **A.** Effect on the top soil layer. **B.** Effect on the middle soil layer. **C.** Effect on the bottom soil layer.

Decrease in SWC in the top layer was slightly influenced by two architectural variables. Figures 6.12.D and F shows that the quantity of water taken from the top layer decreases with increasing root depth or root volume. The same observation, although very weak, could be

Table 6.3: R-squared values of the correlations between plant architectural parameters and soil water content. Water content decrease values were normalized by their corresponding total transpiration. Bold numbers highlight r-squared values higher than 0.1

	Parameter	Top	Middle	Bottom
SIZE	rArea	0.09	< 0.05	0.49
	rsRatio	< 0.05	< 0.05	0.082
	nLength	< 0.05	0.05	0.24
	nVol	0.12	0.05	0.19
SHAPE	nWidth	< 0.05	< 0.05	0.05
	nDepth	0.11	< 0.05	0.5
	nRatio	< 0.05	< 0.05	0.06
	nConv	0.06	< 0.05	0.43
DISTR.	pTop	< 0.05	0.09	< 0.05
	pMid	< 0.05	< 0.05	0.3
	pBot	0.09	0.09	0.7
	nBush	< 0.05	0.06	< 0.05

made for the root area (fig. 6.12.A) and the proportion of roots in the bottom layer (fig. 6.12.K). The similar dynamics between these parameters is consistent with their correlations (fig. 6.8) and with the fact that they all relate to the presence of roots in the bottom layer.

The inverse trend was observed for water extraction in the bottom soil layer. In this case, decrease in SWC was correlated positively with increasing parameters related to the rooting depth. Moreover, in contrast with the relations observed in the top soil layers, the coefficients of determination of the different regressions were much higher (fig. 6.13.A, F and K).

In order to investigate further the effect of the presence of roots in the deep soil layers, a second analysis was performed using a complete dataset including data for every time step of the water shortage episode.

The dataset was first subsampled by creating two plant groups with plants having low and high proportion of roots in the bottom soil layer (*pBot*). These groups were respectively renamed *shallow rooted* and *deep rooted*. The two groups were assembled by taking the plants

6. LIGHT TRANSMISSION IMAGING

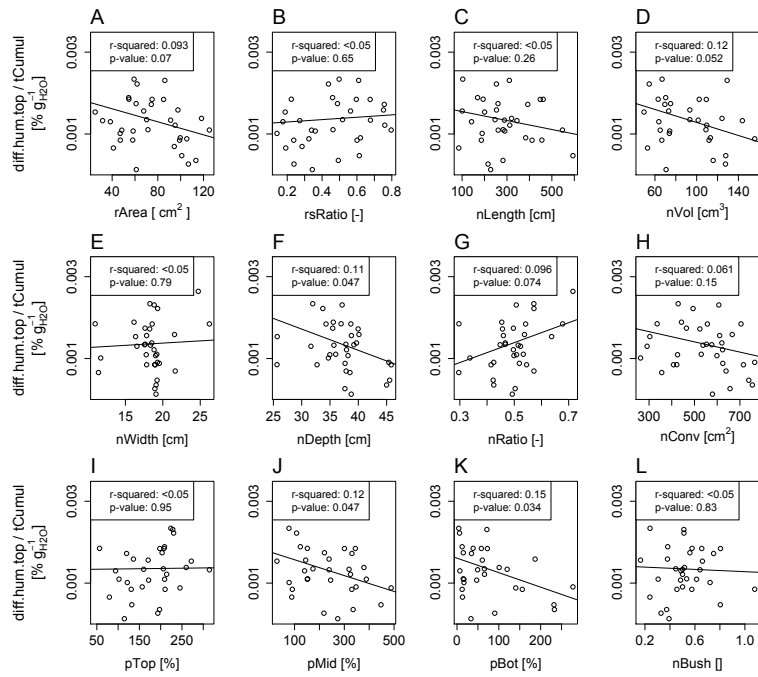


Figure 6.12: Correlations between water depletion in top soil layers and architectural traits. **A.** Leaf area. **B.** Root area. **C.** Root to shoot surface ratio. **D.** Root system total length. **E.** Root system width. **F.** Root system depth. **G.** Root system width to depth ratio. **H.** Root system convex area. **I.** Proportion of root in the top soil layer. **J.** Proportion of root in the top soil layer. **K.** Proportion of root in the top soil layer. **L.** Root system bushiness. **M.** Total transpiration.

6.2. Results and discussions

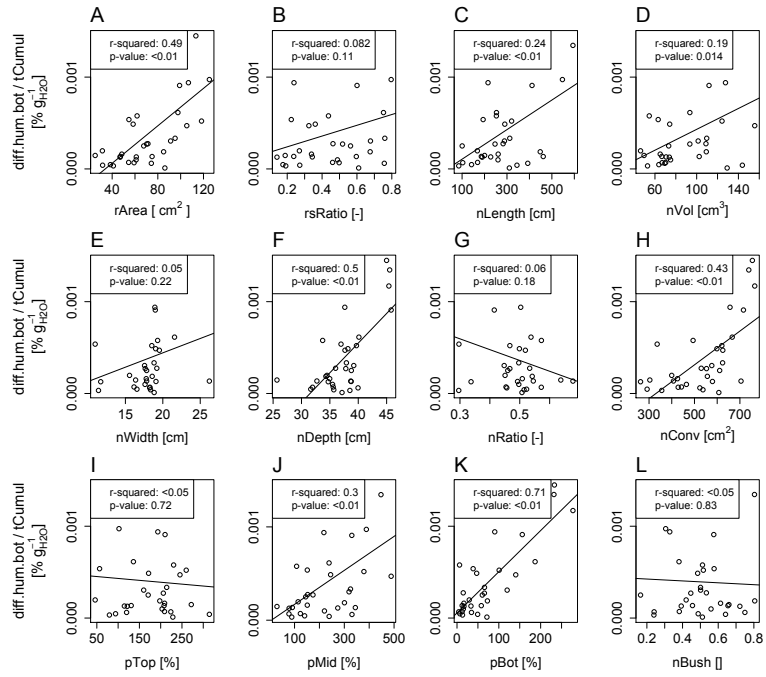


Figure 6.13: Correlations between decrease in water content in bottom soil layers and architectural traits. **A.** Leaf area. **B.** Root area. **C.** Root to shoot surface ratio. **D.** Root system total length. **E.** Root system width. **F.** Root system depth. **G.** Root system width to depth ratio. **H.** Root system convex area. **I.** Proportion of root in the top soil layer. **J.** Proportion of root in the top soil layer. **K.** Proportion of root in the top soil layer. **L.** Root system bushiness. **M.** Total transpiration. **N.** Leaf area * proportion of roots in the bottom soil layer.

6. LIGHT TRANSMISSION IMAGING

with $pBot$ values smaller than the 12th percentile and higher than the 74th percentile respectively. The mean $pBot$ values of the groups are presented on the figure 6.14C.

Decrease in SWC was then compared to the cumulative transpiration in the upper (top and middle) and bottom layers. In the upper layers, for similar transpiration values, deep rooted plants displayed a smaller decrease in SWC (fig. 6.14.A). On the contrary, in the bottom soil layer, decrease in SWC was more important for deep rooted plants (fig. 6.14.B). Similar evolutions were observed for other root parameters related to the rooting depth.

These results confirm that the size of the root system and the distribution of roots along the soil profile influence the water content variations throughout the soil profile. For a given transpiration, deep rooted plants induce a more distributed diminution of soil water content compared to shallow rooted ones. All other things being equal, since local water extraction happens more quickly in the latter ones, gradients in soil water content are likely to be much more important than for the former ones. As a consequence, small root systems might become hydraulically isolated from the bulk soil and experience faster water shortage. However, this hypothesis was not verified as no differences were observed in terms of transpiration between the different groups.

It has to be noted that these results do not necessarily bear correct information about the root water uptake *per se*. Since water redistribution occurs in the soil, following both horizontal and gravitational gradients, the observed patterns of decrease in SWC can not be directly linked to the effective sites of water uptake by the roots. Given the high saturated conductivity of the substrate and the important connectivity between different regions in the rhizotrons (fig. 6.4), the depletion patterns observed in our system could occur equally under homogeneous uptake across the whole root system or under uptake sites localized at the root apex. As a consequence, water movement in the soil should be explicitly considered in the analysis to be able to estimate local root uptake.

Most of the considered architecture features had no or little impact on the changes in SWC in the top and middle layers. This might be caused by the fact that all the plants in the experiment had enough roots to extract all the water contained in the soil. Passioura (1983) pos-

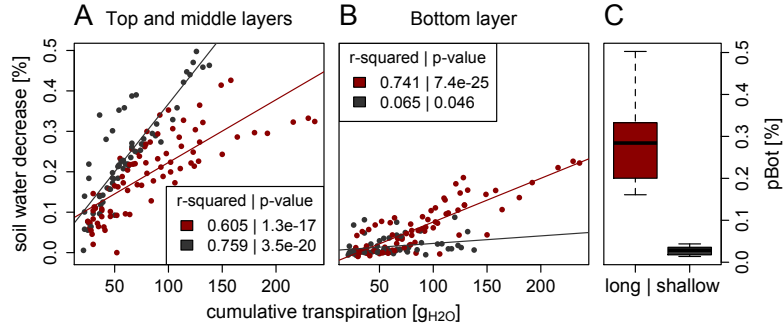


Figure 6.14: Response of soil water extraction in the different soil layer to plant cumulative transpiration for plants with contrasted proportion of roots in the bottom soil layer. **A.** Soil water content decrease in the top and middle soil layers. **B.** Soil water content decrease in the bottom layer. **C.** Proportion of roots in the bottom layer for the two groups used for the comparison. Red dots and bar: plants with a high proportion of roots in the bottom soil layer. Grey dots and bar: plants with a low proportion of roots in the bottom soil layer.

tulates that 1 cm of root length was sufficient to uptake all the water in 1 cm^3 of soil. Figure 6.15 shows that in the top and middle layers, most of the plant had a root length density higher than $1\text{cm}/\text{cm}^3$, which was not the case in the bottom soil layer. This might explain the lack of influence of the different root features in the upper layers.

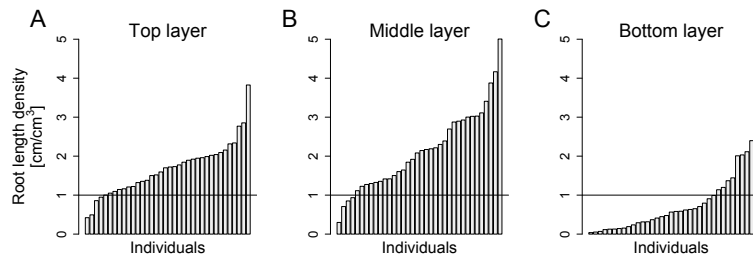


Figure 6.15: Root length density in the different soil layers. **A.** Top soil layer. **B.** Middle soil layer. **C.** Bottom soil layer. The horizontal line highlights a root length density value of 1.

6.3 Conclusions

In this chapter, we tried to explicitly link root morphological parameters with patterns of decrease in soil water content (SWC). Amongst the root parameters tested, only two, mostly related to the rooting depth, had some impact on water extraction in the top soil layer. The changes in water content were negatively correlated with the proportion of roots in the bottom soil layer and with the total root size. The same parameters were significantly affecting the water distribution in the bottom layer of the rhizotrons (last third). In that layer, however, correlations between root architectural features and the water depletion were positive.

By looking at the progressive decrease in SWC in different layers for plants with large and small proportion of roots in the bottom layer, we have found that the difference root architecture triggered different water uptake patterns. Deep root systems, in addition to being able to access deep soil water, induce a more diffuse water depletion in the surrounding soil than shallow ones. We hypothesize that this diffuse water depletion is beneficial for the plant since it reduces the gradient of water potential in the soil, which contributes to maintain a higher soil conductivity and secure water flow from the bulk soil to the root surface.

From a methodological point of view, our results confirmed the usefulness of the light transmission technique as a tool to study water movement in the soil-root domain. The experimental setup, originally used with six plants (Garrigues et al., 2006; Lobet, 2008), was successfully scaled up to allow the simultaneous monitoring of 20 plants. Moreover, the downstream analysis pipe was fully automated, making the technique a useful tool to observe the water uptake dynamic of a large number of plant.

However, our experiments also highlighted some weakness of the LTI technique. The method is bound to a very specific type of substrate that has very different properties than most cultivated soils (although we have been told the same type of soil is encountered in some region in Australia). Therefore, observations made in our experimental setup are likely to be different from field situations. Additionally, unlike other methods such as the neutron tomography (Carminati et al., 2010), the light transmission imaging does not allow the direct observation of water movement in the soil and roots.

COMBINING *IN VIVO* AND *IN SILICO* EXPERIMENTS TO EVALUATE THE INFLUENCE OF ROOT HYDRAULIC PROPERTIES ON THE WATER UPTAKE DYNAMICS.



This chapter is a modified version of a research article in preparation entitled:

Lobet G., Bhowmick S., Couvreur V., Javaux M., Ligeza A., Draye X. Combining *in vivo* and *in silico* experiments to decrypt root water uptake dynamics. In prep.

IN THE PREVIOUS CHAPTER, soil water depletion patterns obtained with the light transmission imaging (LTI) technique were analysed. As a result, root architectural features that have an impact on the variation of soil water content were identified. However, the analysis performed with LTI was limited by the fact that soil water movement was not considered and it was therefore not possible to infer the effective sites of water uptake by roots.

Contemporary to the development of new techniques to observe water flow in the SPAC, new computational models have been introduced that rely on an explicit representation of the root system architecture and of 3D water flow in the soil and root domains. Amongst these models, R-SWMS has seen an increasing development during the last few years (Couvreur et al., 2012; Javaux et al., 2008; Schröder et al., 2012; Schröder et al., 2009; Shroeder et al., 2008). The model uses measurable plant and soil properties and applies the physical laws of water transfer to reproduce water flow for virtually any type of soil and / or plant.

We present in this chapter a model-based approach to study the flow of water in the soil-root domain. The proposed methodology consists in running the R-SWMS model with an incomplete set of experimental data to simulate a complete dataset, comprising data that were not accessible experimentally. This strategy allowed us to estimate the actual water uptake or the xylem potential distribution during our experiments. The method was used to help understanding how different soil drying patterns observed experimentally arise, and assessing the contribution of changes in specific root hydraulic properties.

7.1 Methodology

7.1.1 General methodology

The approach used in this paper was to combine *in vivo* and *in silico* experiments in order to decrypt water flow in the soil-root domain (fig. 7.1). More precisely, LTI experiments (Garrigues et al., 2006) were designed to generate data that can serve as input for the R-SWMS model (fig. 7.1.A). These data include the root system architecture, the soil type and the environmental conditions (evaporative demand and initial soil water content). Root hydraulic properties were not acquired experimentally, but set to theoretical values found in the literature (fig. 7.1.B). In order to validate the results obtained by the model, the simulated and experimental water content distributions were compared (water content distribution, (fig. 7.1.C)). The model was then used to estimate variables that were not experimentally accessible, such as the actual root water uptake distribution (fig. 7.1.D).

7.1.2 Experiments

The experimental procedure was identical as the one described in the chapter 6. The only difference being that for this experiment, after a first water shortage episode (WSE1) of three days, the rhizotrons were resaturated in nutrient solution, left overnight for drainage and a second water shortage episode (WSE2) of three days was imposed to the plants (fig. 7.2). The same measurements were taken during both WSE. Experiment details is shown in the table 7.1.

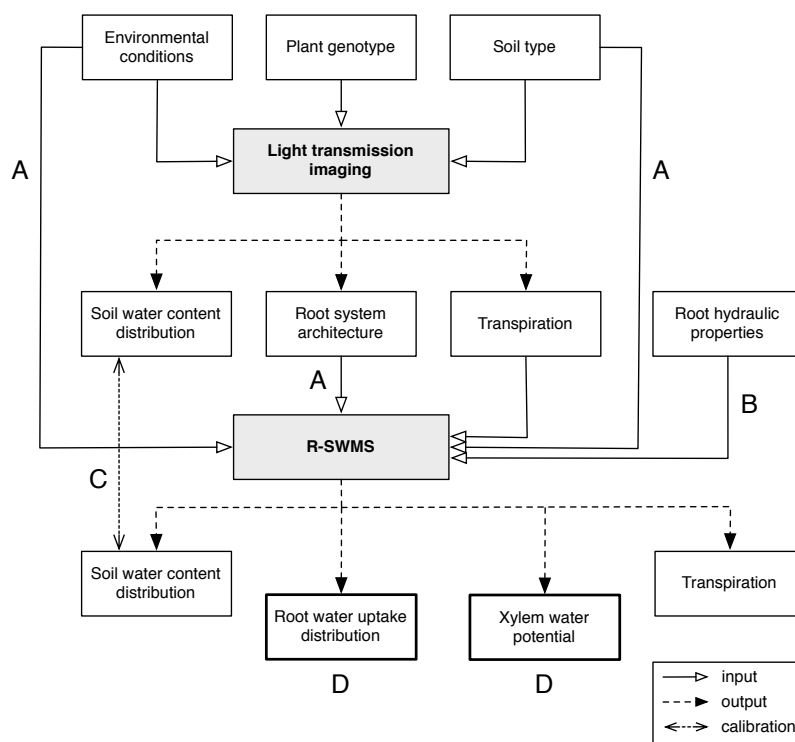


Figure 7.1: Methodology used to decrypt water flow in the soil-root domain using both experimental and modeling data. **A.** Experimental outputs serve as simulation inputs. **B.** Some simulation inputs are not acquired experimentally. **C.** Simulated and experimental output are compared to validate the simulations. **D.** Simulation outputs gives access to data that were not experimental accessible.

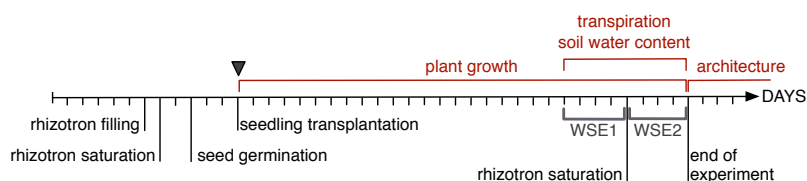


Figure 7.2: Timeline for the LTI-RSWMS experiment. The black triangle indicates the beginning of the experiment.

7. IN VIVO AND IN SILICO EXPERIMENTS

Table 7.1: Details of the light transmission imaging experiment for the two water shortage episodes.

WSE	Date	Gen.	#	temp. [°C]	rel. hum. [%]	VPD [MPa]
WSE1	Jan. 2012	B73	8	19.6 ± 2.1	53.4 ± 5.4	1.1 ± 0.2
WSE2	Feb. 2012	B73	8	21.5 ± 4.1	47.2 ± 4.2	1.4 ± 0.5

7.1.3 R-SWMS input data

The information contained in the root system database was used to generate input files for the model R-SWMS. The morphological and topological data were taken directly from the database while the root segment ages were inferred based on the root growth rates observed during the growth period preceding the water shortage episode. Similarly as previous R-SWMS simulations (Couvreur et al., 2012; Javaux et al., 2008), hydraulic properties of the roots were function of the root segment type and age (for details, see Doussan et al. (1998)).

Additional experimental data were also used as input parameters for the simulation done with R-SWMS. This included the transpiration values and the retention and conductivity curves of the substrate that were determined experimentally (fig. 7.3.A and B). It as to be noted that the substrate used has a very steep conductivity curve, with very high conductivity values at saturation and very low values above pF 4. Simulation were performed for one plant only, due to the relatively long computation times.

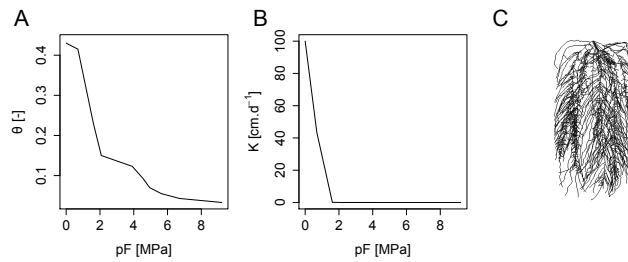


Figure 7.3: Parameters used for R-SWMS' simulations. **A.** Water retention curve determined by sand box and pressure plate experiments. **B.** Conductivity curve (Garrigues, 2002). **C.** Root system architecture

7.2 Results

7.2.1 Experimental results

Transpiration values for the two water shortage episode were compared (fig. 7.4). These data reveals significantly higher transpiration values for WSE2, due to an increase in the leaf area and in the environmental demand (see tab. 7.1).

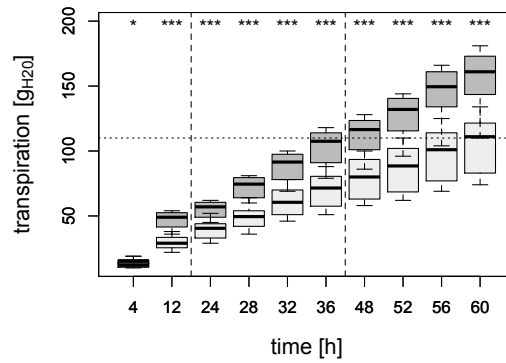


Figure 7.4: Cumulative transpiration [g_{H_2O}]. Light grey boxes: WSE1. Dark grey boxes: WSE2. Dashed lines indicates the limits of the different days. Dotted line highlight the same cumulative transpiration values for the first and second water shortage episode at different time step. t-test: - = not significant, * = $p < 0.05$, ** = $p < 0.01$, *** = $p < 0.001$.

Figure 7.5 shows the evolution of the water content in one rhizotron for the first (fig. 7.5.A-C) and second (fig. 7.5.D-F) water shortage episode. Similar data were obtained from the height plants used for the experiment. A first general observation reveals the appearance of a water depleted area at the collar level that extends downward in the profiles as the water shortage goes on. Such downward dynamic, triggered by the progressive water uptake, was observed in previous light transmission imaging experiments (Garrigues et al., 2006).

Visual comparison of the water content variations between WSE1 and WSE2 seems to reveal differences in soil drying patterns. During the second drought episode, the water depletion zone seems to extend more quickly, but, concurrently, the water depletion in the upper parts

7. IN VIVO AND IN SILICO EXPERIMENTS

of the rhizotrons, close to the plant collar, is more intense than for the first water shortage episode. This difference is more visible if the comparison is performed between the time step corresponding to the same amount of water extracted (fig. 7.4., horizontal dotted line). In such case, the comparison should be done between the figures 7.5.C and 7.5.E, which highlight the differences between soil drying patterns.

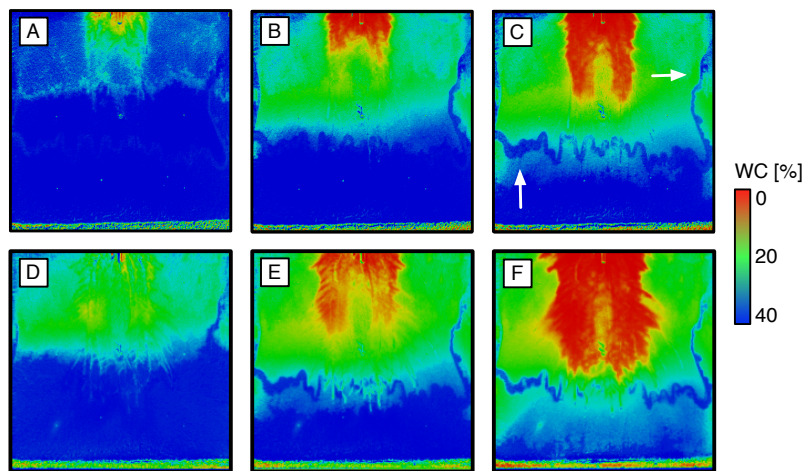


Figure 7.5: Volumetric water content (WC) profiles. A-C: First drought episode. D-F: Second drought episode. Pictures were taken every day at 11PM from the same plant.

In order to quantify the difference between the two WSE, we compared the decrease in soil water content (SWC) in three horizontal soil layers (respectively labeled as the top, middle and bottom layers, see chap. 6). This analysis method had the advantage to synthesize the main variation observed in the rhizotron into a few variables and to remove experimental noise such as the one observed on the figure 7.5.C (white arrows).

Figure 7.6 shows the evolution of the decrease in SWC in the different soil layers for the two WSE. Significant difference between WSE1 and WSE2 can be observed in all layers, with bigger decrease in SWC for WSE2.

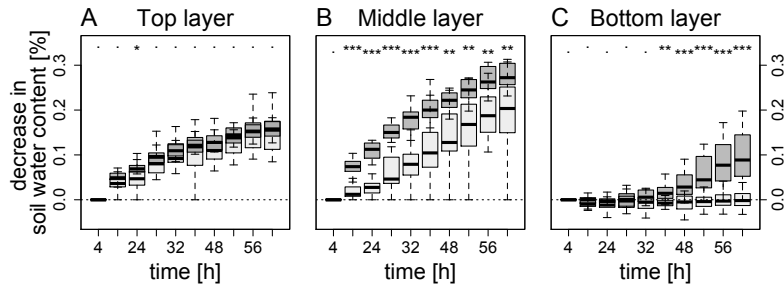


Figure 7.6: Experimental decrease in water content in the different soil layers and for the two water shortage episodes. **A.** Top soil layer. **B.** Middle soil layer. **C.** Bottom soil layer. Light grey boxes: first water shortage episode; Dark grey boxes: second water shortage episode. t-test to compare first and second water shortage episode: . = not significant, * = $p < 0.05$, ** = $p < 0.01$, *** = $p < 0.001$

7.2.2 Modeling results - WSE1

Figure 7.7 shows a visual comparison between the water content distribution obtained during WSE1 (fig. 7.7.B) and simulated by the model (fig. 7.7.A). Although local differences in soil water content can be observed (probably due to compaction variations in the experimental setup, fig. 7.7.A, white arrows), the general patterns (e.g. depth and width of the red area) seems to be correctly reproduced by the model.

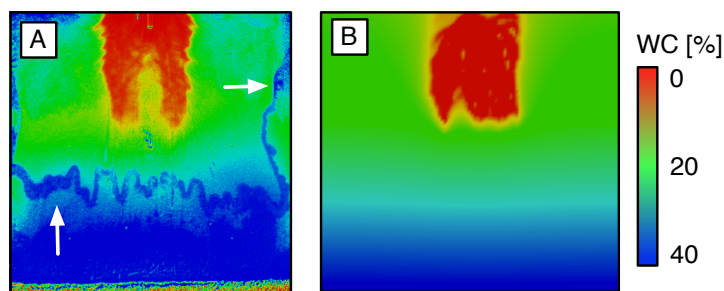


Figure 7.7: Visual comparison of water content distribution. **A.** Experimental results. **B.** Simulation results. White arrows represent local variation of water content due to soil compaction heterogeneity.

7. IN VIVO AND IN SILICO EXPERIMENTS

In order to quantitatively evaluate the simulation's result, we compared the simulated and experimental evolution of water content in the different soil layers (fig. 7.8). In the first two soil layers, the evolution of SWC obtained with the simulation falls within the range of experimental results obtained for WSE1 (fig. 7.8.A and B, light grey area). The simulation was not completely accurate since it overestimated to decrease in SWC in the bottom soil (fig. 7.8.C, light grey area). However, since most of the SWC variation seems to be reproduced, the model can be regarded as being a good approximation of the experimental data.

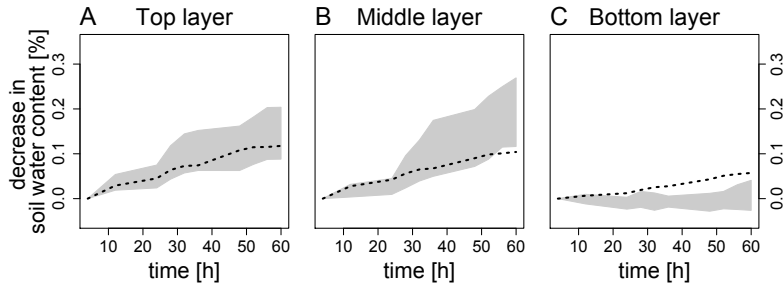


Figure 7.8: Comparison of the evolution decrease in SWC in the three soil layers obtained with the experimental results and the simulation for the first water shortage episode. **A.** Top soil layer. **B.** Middle soil layer. **C.** Bottom soil layer. Light and dark grey areas represent the range of experiment values for the first and second water shortage episode respectively (values obtained with eight plants, similarly as on figure 7.6). The bold dotted lines represent the evolution of the value obtained with the simulation results.

The modeling results were used to estimate variables that were not experimentally accessible. Figure 7.9 shows the parallel evolution of the (simulated) soil water content, water uptake distribution in the soil and xylem water potential distribution in the root system. In these simulations, it appears clearly that the different roots of the plant do not participate equally to the uptake process (fig. 7.9.D). The vast majority of the uptake is performed by the primary and the older secondary roots, whose axial conductivity (which reflect the maturation of the xylem vessels) is large enough to transmit the tension generated by transpiration.

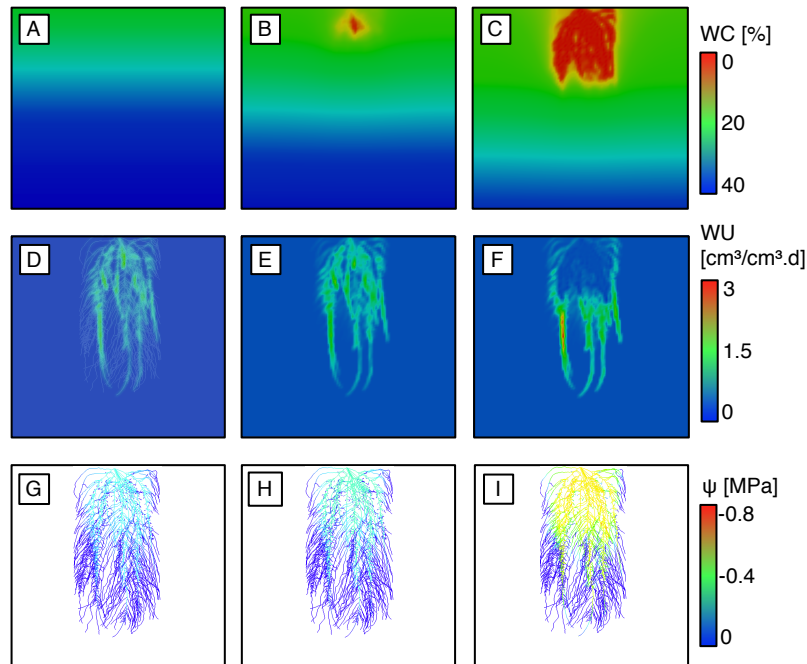


Figure 7.9: Comparison of water content and water uptake distribution. **A-C.** Volumetric water content (WC) distribution for two different time steps. **D-F.** Water uptake (WU) distribution for two time steps (expressed in cm^3 of water per cm^3 of soil per day). **G-I.** Xylem water potential (Ψ) distribution **A, D, G.** First time step of the simulation. **B, E, H.** Middle of the simulation. **C, F, I.** Last time step of the simulation.

At the beginning of the experiment (fig. 7.9.A and D), the water content distribution is uniform and water uptake occurs all over the root system. The lack of differences in the water uptake profile is a result of vertical water drainage in the highly conductive substrate. The emergence of dry zones where refill from the bulk soil becomes increasingly difficult, i.e. in the upper parts of the root system (fig. 7.9.B) leads to increased tension in the root xylem (fig. 7.9). In these zones, the soil water conductivity has decreased and the surrounding soil is not able to sustain the uptake flux anymore. Roots present in these zones are therefore less able to take up water and the uptake is forced to take place further down in the profile (fig. 7.9.D).

This dichotomy between the decrease in soil water content content and the actual water uptake is highlighted in the figure 7.10. No clear relationship can be found between the both variables. As a consequence, in our system, the decrease in soil water content can no be used as a proxy of root water uptake.

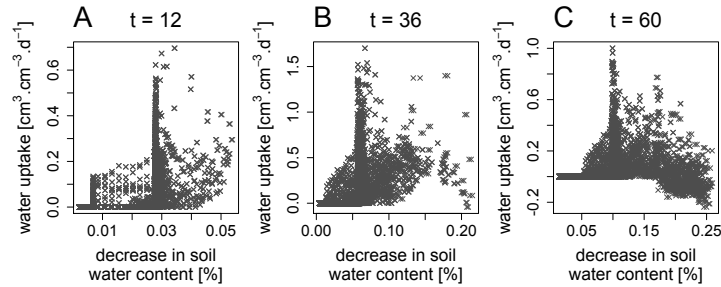


Figure 7.10: Water uptake as a function of decrease in volumetric soil water content. **A.** 12th of simulation. **B.** 36th hour of simulation. **C.** 60th hour of simulation.

7.2.3 Modeling results - WSE2

As shown on figure 7.4, the transpiration rate of the plant during the second water shortage episode was significantly higher than during the first water shortage episode. In order to assess whether increased transpiration would be sufficient to explain the evolution of the water content distribution, the model was run with the same parameters as for WSE1 except the transpiration demand, which was set to experimental results of WSE2 (fig. 7.11.A). This simulation will be referred hereafter as S1.

We also considered alternative hypotheses that might explain the differences observed between the water content patterns of the two WSEs: the onset of cavitation events and / or a decrease in radial conductivity.

On the one hand, cavitation occurring in roots subjected to important xylem tension (in this case due to an increased transpiration) is known to dramatically reduce the root axial conductances (Li et al., 2009; Sperry et al., 1998, 1996). Cavitation apparition was thus imple-

mented in R-SWMS at the root segment level using a Weibull function whose parameters were taken from previously published experimental data (fig. 7.11.B, Li et al. (2009)). This simulation will be referred hereafter as S3.

On the other hand, the root radial conductivity is thought to be tightly controlled by the plant in response to environmental conditions through the expression and regulation of water channels (aquaporins) (Chaumont, Moshelion, 2005). In particular, aquaporin gating (Hedfalk et al., 2006), which reduces the root radial conductivity, is known to occur in situations of local water deficit, presumably to prevent the back-flow of water from the root tissues to the soil solution (Ehlert et al., 2009; Javot, Maurel, 2002; Maurel et al., 2008). On the soil side, a loss of contact between the root and the surrounding soil, caused by root shrinkage during a drought episode, can lead to a drop in the rhizosphere conductivity (Carminati et al., 2012, 2009). It is likely that the succession of WSEs in our experiments has induced one or both of these situations. This hypothesis was tested with R-SWMS by decreasing the root radial conductivity by a factor two in all roots (fig. 7.11.C and D). This simulation will be referred hereafter as S2.

Finally, a simulation combining the three modifications was also made. This simulation will be referred hereafter as S4. Table 7.2 synthesize the different simulation performed and their corresponding parameters/

Table 7.2: R-SWMS simulation's parameters for WSE2.

Simulation	Transpiration	$K_r / 2$	Cavitation
S1	increased	No	No
S2	increased	Yes	No
S3	increased	No	Yes
S4	increased	Yes	Yes

The main results of the experiments and simulations for the second water shortage episode are shown on figure 7.12. Firstly, the comparison of the soil water content distribution indicates that the increase in transpiration is sufficient to represent roughly the uptake patterns observed experimentally (fig. 7.12.A). Secondly, the changes in the hydraulic properties of the root system (scenario S2-S4), despite having a

7. IN VIVO AND IN SILICO EXPERIMENTS

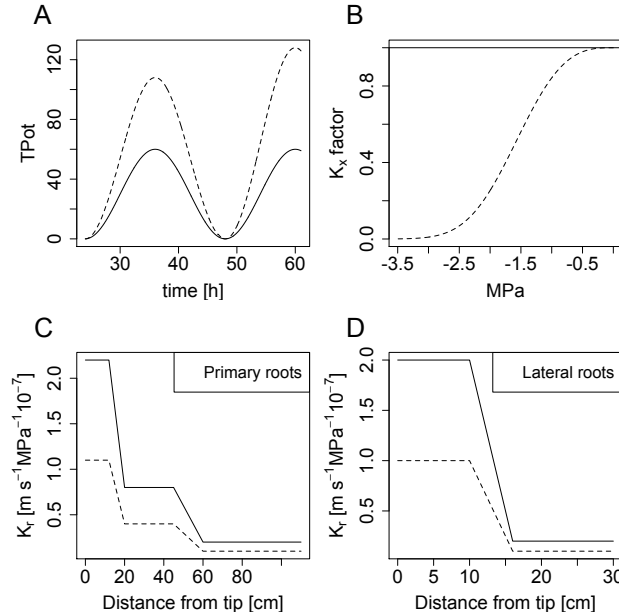


Figure 7.11: Parameter modifiers used in R-SWMS to simulate the second water shortage episode. **A.** Increased transpiration **B.** Effect of cavitation on K_x . **C.** Effect of reduced K_r on the primary roots. **D.** Effect of reduced K_r on the lateral roots. Plain and dashed lines represent the parameters for WSE1 and WSE2 respectively.

large effect on the xylem water potential distribution in the plant (fig. 7.12.I-L), induces only small changes in the soil water content distribution and uptake sites (fig. 7.12.A-H). More precisely, by looking at the evolution of the plant collar water potential during the water shortage episode, it can be observed that decreasing K_r leads to a increase in the xylem tension, while the onset of cavitation as the opposite effect (fig. 7.13). Combining the two modifications lead to an intermediate result.

It as to be noted that the difference observed in terms of xylem water potential might have important effects on the plant growth and development. For the scenario 2 and 4, around the hour 55, water potential even falls below the permanent wilting point, which is not viable for the plant. However, since the version of R-SWMS used for these simulation used a static root system (no growth or development),

the potential changes due to water potential decrease were not captured and did not affect the simulation.

A second interesting observation is that cavitation, at least in these simulations, appears to act as a conservation mechanism for the plant. By reducing K_x in the root system, the onset of cavitation limits the decrease in water potential observed for the other scenario without dramatically affecting the plant water uptake (fig. 7.12.G and K).

The lack of differences in the water content distribution due to changes in hydraulic properties were confirmed by comparing the evolution of SWC in the different soils layers for the different simulations. As shown on figure 7.14, only small differences were observed between the different scenarios. Moreover, unlike for WSE1, none of the scenario was able to satisfyingly fit the experimental results. In the top and middle soil layers, simulated results were smaller than the experimental ranges (fig. 7.14.A and B, dark grey area). Decrease in SWC in the bottom layer was better reproduced by the simulation.

7. IN VIVO AND IN SILICO EXPERIMENTS

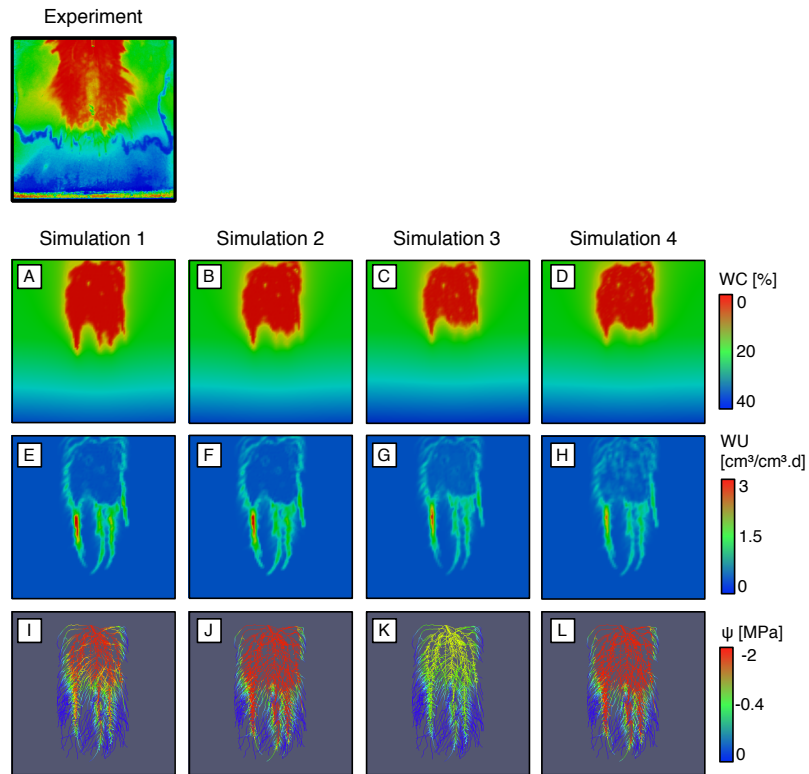


Figure 7.12: Visual comparison of the different simulation for the second drought episode at the last time step of the simulation. **A, E, I.** Increased transpiration. **B, F, J.** Increased transpiration & $K_r/2$. **C, G, K.** Increased transpiration & cavitation. **D, H, L.** Increased transpiration & $K_r/2$ & cavitation. **A-D.** Volumetric soil water content distribution. **E-H.** Water uptake distribution. **I-L.** Xylem water potential distribution. The top left panel show the corresponding experimental water content distribution. Images were taken at 15:00.

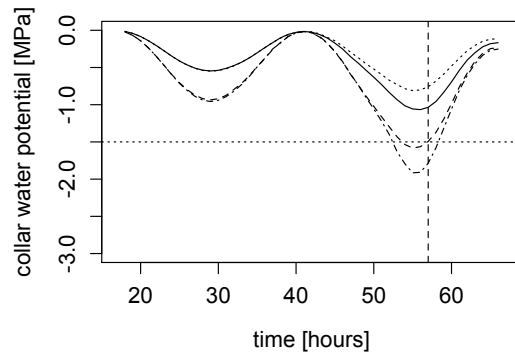


Figure 7.13: Evolution of the collar water potential for the different simulations. Plain line = S1. Dashed line = S2. Dotted line = S3. Dashed-dotted line = S4. Horizontal dotted line = permanent wilting point. Vertical dashed line = 15:00 on the last day. The evolution is shown for the two last days of the simulation

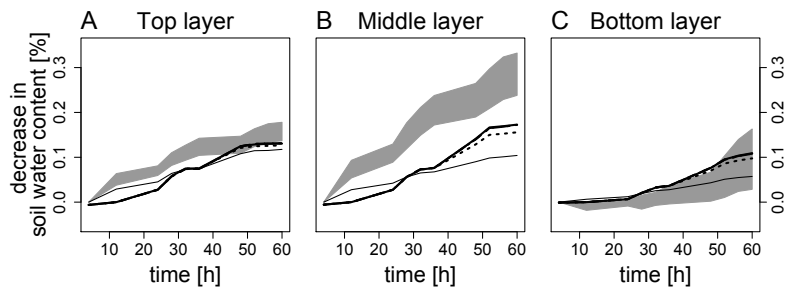


Figure 7.14: Comparison of the evolution decrease in SWC in the three soil layers obtained with the experimental results and the simulation for the second water shortage episode. **A.** Top soil layer. **B.** Middle soil layer. **C.** Bottom soil layer. Light and dark grey areas represent the range of experiment values for the first and second water shortage episode respectively. Simple plain line = simulation for WSE1. Bold plain line = S1. Bold dashed line = S2. Dotted line = S3. Dashed-dotted line = S4.

7.3 Discussion

7.3.1 *R-SWMS is able to represent the majority of the water content variation observed experimentally*

The model R-SWMS was successfully used to reproduce the main variations in soil water content observed experimentally using the LTI method. More precisely, the depth of the water depletion area, which is a relevant criteria in a context of plant breeding for drought tolerance (Bernier et al., 2009; King et al., 2003; Wasson et al., 2012), were correctly estimated for both water shortage episodes. However, the model failed at reproducing variations observed at a smaller scale.

7.3.2 *Water content can not be used as a proxy of water uptake*

As shown on the figures 7.9 and 7.12, the temporal variation of the soil water content distribution should not be used as a proxy of the distribution of root water uptake. In homogeneous soil conditions, root water uptake occurs across the whole root system, in as much as the roots are mature enough. However, as soon as heterogeneity arises in the soil profile, the uptake process takes place preferentially in the wetter regions of the soil. This compensation mechanism occurs as the soil is drying around the roots, its conductivity decreases and the remaining water content in the soil solution becomes increasingly difficult to extract. In physical terms, the soil sites that minimize the energy required for water flow into the plant moves gradually from the upper layers to the lower layers of the rhizotrons. However, despite the fact that the uptake takes place in the lower parts of the root system, no differences in soil water content are observed there, as a consequence of vertical soil water distribution.

Although the fact that this observation was made in artificial conditions, we believe it should stand true in natural conditions. The soil used in this experiment had a rather special conductivity curve, which makes it unlikely to recharge water depleted area. However, the conductivity of the wet zones allow the water to move along gravitational gradient and to redistribute vertically. In natural conditions, where the soil conductivity is likely to be different, the soil water re-distribution is expected to follow a smoother dynamics and the buffering action of the soil to be more important.

7.3.3 Changes in root hydraulic properties may not have significant effects on the soil water content distribution

Different hypotheses were tested using R-SWMS in order to reproduce the modified dynamics of water content changes that occurred during the second WSE. The simulation results suggested that most of the variation could be attributed to an increase of transpiration. Furthermore, the changes in root hydraulic properties had no or little effect on the uptake and soil water content distribution, despite pronounced differences in xylem water potential.

In a large range of situations, the limiting element to water flow in the soil-root system is the soil itself (Draye et al., 2010). In such situations, if the soil conductivity is lower than that of the root system, changes in the plant hydraulic properties may have no or little effect on the uptake dynamics, as was observed in our simulation.

On the plant side, the root radial conductivity is often thought to be the limiting factor to the water flow (Steudle, 2000; Steudle, Peterson, 1998). It is therefore expected that changes in K_r have a more important effect than changes in K_x , as it was also observed here.

7.3.4 Experimental water content distribution is not sufficient for the model calibration

Variations in soil water content appeared to be mildly sensible to changes in root hydraulic properties. In order to perform a better calibration of the model, in particular for the estimation of the hydraulic properties of the roots, more information about the experimental system are needed. As shown on the figure 7.13, xylem water potential is highly influenced by the hydraulics of the root system and could be used as an additional calibration variable. In practical, measuring the water potential of the first leaf (using a pressure bomb), at 15.00 on the last day of the experiment (fig. 7.13., dashed line) would theoretically give us a good information about the global water status of the plant and help calibrate the model.

7.4 Conclusions

In this chapter, we demonstrated the interest of combining *in vivo* and *in silico* experiment to analyse root water uptake dynamics in the soil-root system. The model was used as an analytical tool to access variable that were experimentally not measurable. The use of the model reveals an important dichotomy between the water content distribution in the soil and the root water uptake, which indicates that the former can not be used as a proxy to the latter. A second important observation was that changes in the major root hydraulic properties had no or little effect on the water uptake behaviour of the plant, probably due to an important buffering effect of the surrounding soil.

The availability of R-SWMS-like models open new perspective in plant water relation research. As an example, root sampling could be done at the end of the experiment, right after the scanning procedure to analyse the expression or level of molecules such as aquaporins or abscissic acid. R-SWMS could be used to assess the theoretical water potential at the sampling location, hence providing meaning full data about the effect of the environment on the expression/level of such molecules. However, further calibration (e.g. based on collar water potential) might be needed to secure the validity of the model to reproduce smaller or more local variations.

PART V

MODELING WATER
FLOWS IN THE
SOIL-PLANT-
ATMOSPHERE
CONTINUUM

This section is devoted to the modeling of water flow in the soil-plant-atmosphere continuum.

The first chapter will focus on the general presentation of the model PlaNet-Maize and the regulatory mechanisms acting on the water flow.

In the second chapter, we will present a first attempt to incorporate explicit long distance signaling (root to shoot) as a additional layer in the plant hydraulic regulation.



Essentially, all models are wrong, but some are useful.

GEORGE BOX

PRELIMINARY CONCEPTS



THE FLOW OF WATER in the soil-plant-atmosphere continuum is a passive process driven by water potential differences and enabled by the continuity of the liquid phase of water between the soil and the leaf mesophyll (Steudle, 2001). For a given driving force, the flow of water in the plant is set primarily, though not exclusively, by the radial conductance of the root system, the axial conductivity of the xylem and the leaf conductance.

The leaf conductance, which is largely determined by the density and aperture of the stomata, sets the maximum amount of water that can be transpired under a given environmental demand. Due to the obvious and major role of stomata, the mechanisms underlying their regulation have received much attention from the scientific community, leading to numerous experimental and modeling approaches (reviewed by Damour et al. (2010)).

The root radial conductance is a complex property reflecting the composite nature of water movement from the root surface to the xylem. It both depends on irreversible processes like the deposition of hydrophobic barriers in the endodermis and exodermis (Enstone et al., 2003), and on time-varying features like the activity of water channels (Javot, Maurel, 2002; Maurel et al., 2008). The crossing of root tissues is generally considered as an important limiting step in the water uptake process (Steudle, Peterson, 1998).

The axial conductivity of the xylem vessels is also a complex property which combines the structural features of the xylem, the dynamics of cavitation events occurring when the tension in the xylem is too large (Sperry et al., 1998) and the extent of embolized vessels refilling that occurs when the tension vanishes but possibly also under tension (Holbrook, Zwieniecki, 1999; McCully et al., 1998; Zwieniecki, Holbrook, 2009).

While the leaf conductance sets the amount of water extracted by the plant, the distribution of root axial conductivities and radial conductances throughout the root system (the *hydraulic architecture*) determines the sites of water uptake in the soil (Draye et al., 2010). This role of root hydraulic properties has often been considered as minor in comparison with root length density, but this should be reconsidered in view of recent data (Draye et al., 2010). Therefore, considering leaf, root and environmental factors simultaneously may be an important contribution if we aim to tailor plants with improved resistance to water deficit.

For many years, scientists have developed computer models to simulate how biological processes, described individually or at an organ scale, integrate and scale up in the soil-plant-atmosphere system. On the root side, models evolved from architectural models reproducing the root system shape and growth (Diggle, 1988; Lynch et al., 1997; Pagès et al., 1989) to functional-structural models simulating physical, chemical or physiological processes such as nutrient acquisition (Ge et al., 2000), carbon allocation (Bidel et al., 2000) or water uptake (Javaux et al., 2008; Somma et al., 1998). A similar trend was observed for shoot models (Fournier, Andrieu, 1998). While some models address simultaneously the root and shoot systems (Drouet, Pagès, 2003; Janott et al., 2011), the vast majority focus on either part of the plant and use simplified descriptions of the other. As of today, we are not aware of any model that simulates the water dynamics of a complete plant with a detailed description of each organ.

This situation led us to develop the PlaNet-Maize model, which simulates at a sub-organ resolution the growth and architecture, the water flows and the main hydraulic regulations of a whole maize plant. The model uses simplified rules for the production and allocation of assimilates to the different organs. The first chapter of this section presents the model and its use in the framework of the analysis of the regulation of the water flow in the SPAC. The second chapter presents and discusses a first attempt to implement ABA fluxes in PlaNet-Maize .

A MODELING APPROACH TO DETERMINE THE CONTRIBUTION OF PLANT HYDRAULIC CONDUCTIVITIES ON THE WATER UPTAKE DYNAMICS IN THE SPAC



This chapter is a modified version of a research paper in preparation:

Lobet, G., Pagès, L. & Draye, X. A modeling approach to determine the contribution of plant hydraulic conductivities to the water uptake dynamics in the soil-maize-atmosphere system.

The chapter is also based on a conference paper published as:

Lobet G., Pagès L., Draye X. A modeling approach to determine the contribution of plant hydraulic conductivities on the water uptake dynamics in the soil-plant-atmosphere system, 2012, to appear in proceedings of IEEE Plant Growth Modeling and Applications.

WE PRESENT IN THIS CHAPTER a new functional-structural plant model, PlaNet-Maize , with the purpose of investigating the effect of environmental and endogenous factors on the growth and water relations of the maize plant. This functional-structural model encompasses the entire soil-plant-atmosphere continuum with a sub-organ resolution. The model simulates the growth and development of an individual maize plant and the flux of water through the plant structure, from the rhizosphere to the leaf boundary layer. Leaf stomatal conductance and root radial and axial conductivities are considered as functions of local water potential. Finally, a simple carbon allocation rule is included in the model to allow the feedback effect of water deficit on plant growth.

9.1 Model description

9.1.1 General principles

PlaNet-Maize adheres to the principles of the metal-model PlaNet (Plant as a Network), developed by Loïc Pagès, that defines a building schema for the creation of various whole plant models. In PlaNet, the plant structure is viewed as a network of articles interconnected in a tree-like structure and localized in space. Articles are typically organs, but can be defined as smaller or larger entities. They have three fundamental behaviors: (1) they can grow and create new articles (morpho-generator), (2) they have their own metabolic activity (bio-reactor) and (3) they can transport substances from and to neighboring articles and environment (carrier). As articles are localized in space and in the network topology, these behaviors can be dependent on local environment information as well as on network-derived information.

Two types of articles are typically considered in PlaNet. The first are the segments, which make up the structure of the plant. The second are the meristems, which generate new segments and / or meristems and ensuring growth and branching. These two types of articles can be sub-grouped based on their botanical nature: stem, leaf or root. These six types of articles are sufficient to simulate the growth and development of a whole plant during the vegetative stage (fig. 9.1).

The PlaNet-Maize model follows PlaNet rules to simulate the growth and structure of a maize plant and includes modules specific to water movement and hydraulic regulatory processes. PlaNet-Maize was developed in Java and is integrated in the modeling platform CrossTalk (Draye, Pagès, 2006) that enables the coupling with environment models, the 3D visualization and the *in situ* interactive modification of the plant during a simulation (e.g. pruning).

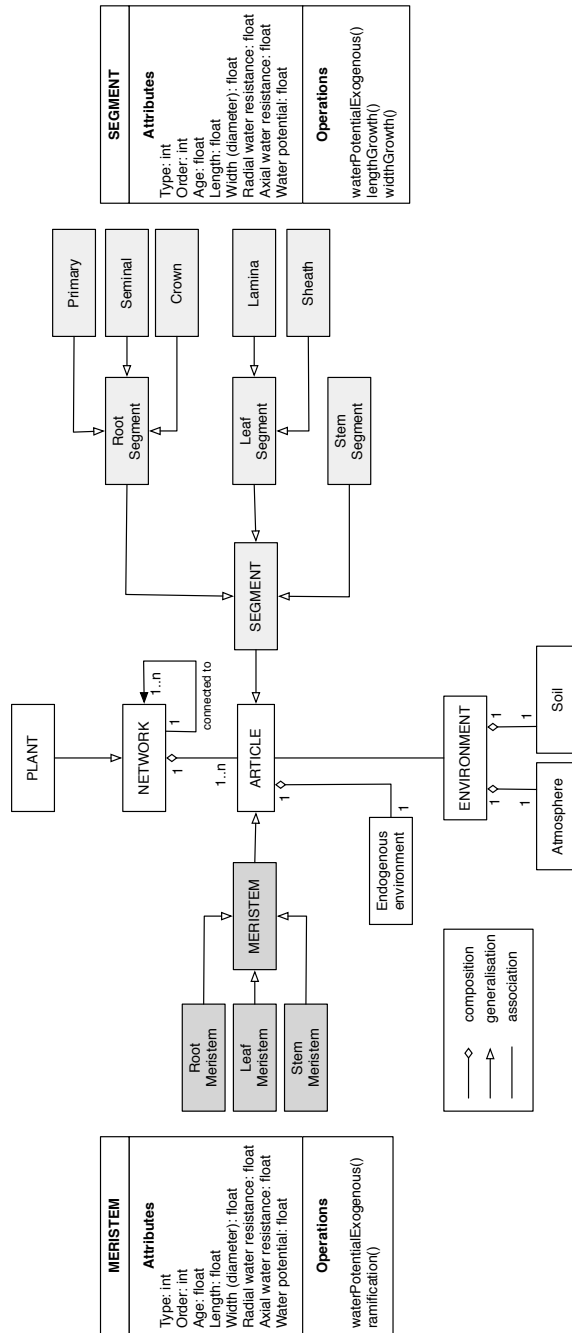


Figure 9.1: PlantNet-Maize UML scheme. Light grey boxes represent the segments classes. Dark grey boxes represent the meristem classes.

9. MODELING WATER FLOW AND ITS REGULATIONS.

9.1.2 Architecture module

Root system

The root system of PlaNet-Maize comprises four types of roots: the primary root (first embryonic root), the seminal roots (embryonic roots initiated from the scutelar node), the crown roots (shoot-born roots) and the first and second order lateral roots (Hochholdinger et al., 2004). Its implementation was inspired from previous root architecture models (Drouet, Pagès, 2003; Pagès et al., 2004) with the distinction that root axes in PlaNet-Maize originate from different types of organs (fig. 9.2.B). The primary and seminal roots arise from the seed while crown root meristems are initiated by the stem meristem. It follows that there is no single connection between the root system and the shoot and that preferential water flow may occur between crown roots and the leaf initiated at the same node.

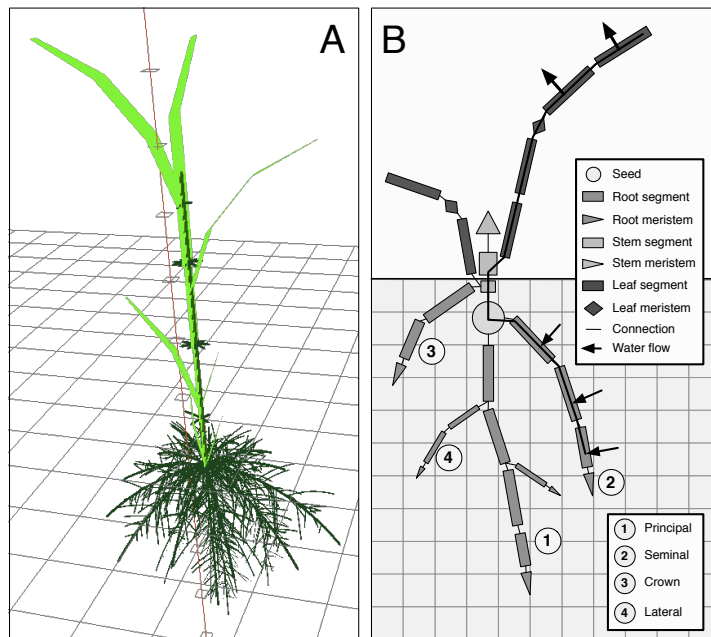


Figure 9.2: PlaNet-Maize representations. **A.** PlaNet-Maize visual output in CrossTalk. **B.** Schematic representation of the PlaNet-Maize structure.

Root elongation rate was computed as a function of the root meristem diameter (Drouet, Pagès, 2003; Mollier, Pellerin, 1999):

$$R_e = R_{emax} \left[1 - \exp\left(\frac{-b_{ed} \max(D_r - D_{r0}, 0)}{R_{emax}}\right) \right] \quad (9.1)$$

where R_e is the root elongation rate [$\text{cm} \cdot ^\circ\text{Cd}^{-1}$], R_{emax} is the maximal elongation rate [$\text{cm} \cdot ^\circ\text{Cd}^{-1}$], D_r is the meristem diameter [cm], D_{r0} is the minimal diameter below which elongation stops [cm] and b_{ed} is the initial slope of the relationship between root diameter and root elongation rate [$^\circ\text{Cd}$]. Parameters values were taken from Drouet, Pagès (2003).

Shoot system

The shoot architectural module of PlaNet-Maize was freely inspired from the model GRAAL where leaf and stem growth and development are determined by morphogenetic processes and are a functions of thermal time (Drouet, Pagès, 2003). Similarly as for the roots, leaves are made of successive segment articles. Every article is labeled as part of the sheath of the lamina. The leaf meristem is located at the junction between the sheath and the lamina (fig. 9.2.B).

9.1.3 Carbon module

A carbon module was implemented in PlaNet-Maize to allow various feedbacks between plant growth and the water dynamics. For the sake of simplicity, the carbon module was not implemented at the article but at the plant level. The module was divided into three processes: production, demand and allocation of assimilates.

Production

During the first steps of the simulation, the seed acts as a carbon source and its supply is computed at each time step according to the seed dry weight and a seed supply rate factor. When leaves start transpiring, the amount of carbon produced at each time step (C_{av}) is defined by the total amount of water transpired by the plant as in the model presented by Somma et al. (1998) and considering instantaneous water use efficiency values between 3.5 and 9.5 $\text{mg}_{\text{CO}_2}/\text{g}_{\text{H}_2\text{O}}$ (Allen et al., 2011). Finally, at each time step, exceeding carbon (see below) is stored and can be further released as a function of the total amount

of C available at the plant level and a reserve supply rate (Drouet, Pagès, 2003).

Demand

Carbon demand is divided into maintenance and growth demands. The maintenance demand is computed for every plant article such as:

$$C_m = mMQ10^{(T-T_{ref})/10} \Delta t \quad (9.2)$$

where C_m is the carbon maintenance demand [g_{CO_2}], M is the organ dry mass [g], m the specific maintenance cost [$g_{CO_2} \cdot g^{-1}DM$], $Q10$ is a temperature coefficient [-], T is the environmental temperature [$^{\circ}C$], T_{ref} is the temperature above which maintenance cost is more than proportional to the organ dry mass [$^{\circ}C$] and Δt is the length of the time steps [h] (Drouet, Pagès, 2003).

Similarly, the growth demand is defined for every article following the equation:

$$C_g = \frac{G_p}{g} \Delta t \quad (9.3)$$

where C_g is the carbon growth demand [g_{CO_2}], G_p is the potential growth in dry mass [g_{CO_2}], g is a growth conversion coefficient [-] and Δt is the length of the time step [h] (Drouet, Pagès, 2003). The dry mass of every article is a function of its volume and density, itself depending on the article age (Drouet, Pagès, 2003, 2007).

Allocation

The allocation of the available carbon (C_{av}) between all plant articles follows precise priority rules. C_{av} is used in priority to meet the whole plant maintenance demand, considered as an obligatory cost (Drouet, Pagès, 2003; Postma, Lynch, 2011b). The remaining C:

$$C_{avg} = C_{av} - C_m, \quad (9.4)$$

is divided between the root and the shoot according to a root-to-shoot C allocation ratio (Somma et al., 1998). In the shoot, priority is given to the leaf growth over the stem, while in the roots, priority is defined based on the potential growth rate of each root (*sink term*). Once this allocation is performed, a unique growth satisfaction coefficient is computed ($G_p \cdot C_{avg}^{-1}$, between 0 and 1). This coefficient will be used

(1) to define the actual growth of the different articles and (2) to define the initial diameter of newly created root meristems. As in the GRAAL model, if this diameter falls under a critical minimum value, the meristem is not initiated (Drouet, Pagès, 2003).

9.1.4 Water fluxes module

General principle

The network of articles intervening in the uptake and transport of water in the plant can be conveniently analyzed using the analogy with an electric circuit (Landsberg, Fowkes, 1978). In particular, radial water fluxes can be described using the equation:

$$J_r(z) = L_r[\psi_e(z) - \psi_x(z)]S \quad (9.5)$$

where $J_r(z)$ is the radial flux through root tissues or stomata [$\text{m}^3 \cdot \text{s}^{-1}$], $\psi_x(z)$ and $\psi_e(z)$ are respectively the xylem water potential of the article and of the environment [MPa], L_r is the article radial conductivity [$\text{m} \cdot \text{s}^{-1} \cdot \text{MPa}^{-1}$] and S is the article surface [m^2]. Similarly, the axial water flux can be described as follow:

$$J_h(z) = -K_h \frac{\Delta\psi_x(z)}{\Delta z} \quad (9.6)$$

where $J_h(z)$ is the axial flux between two articles [$\text{m}^3 \cdot \text{s}^{-1}$], $-K_h$ is the xylem conductance [$\text{m}^4 \cdot \text{s}^{-1} \cdot \text{MPa}^{-1}$], $\Delta\psi_x(z)$ is the water potential difference between the articles and Δz is the distance between these articles [m].

Finally, the Kirchhoff law, which states that *in* fluxes must equal *out* fluxes, is applied to every article:

$$\sum^k I_{kin} = \sum^k I_{kout} \quad (9.7)$$

The combination of these three equations has been successfully used to simulate water transfers in the soil-plant system in different models (Doussan et al., 2006; Javaux et al., 2008). In these models, at each time step, the equations are specified for every root segment and are assembled as a system of linear equations that is solvable at the whole root system level. In PlaNet-Maize, we generalized this formulation in order to apply it to the whole plant level (roots, stem and leaves).

Soil water depletion

The soil in PlaNet-Maize is implemented as a 3D grid of voxels with a mesh size of typically 1 cm³. Soil water depletion is simulated by removing the uptake of every root article from its enclosing voxel. The relationship between the soil water content and the soil water potential (θ -h curve) is defined using a Mualen-Van Genuchten equation (van Genuchten, 1980).

It has to be noted that the current implementation of water fluxes in the soil 3D domain does not follow Richard's equations (unlike traditional soil models like HYDRUS or R-SWMS). In PlaNet-Maize, horizontal redistribution of water in the bulk soil is obtained by the application of a mean smoothing operator on every soil element and its 8 horizontal neighbors. This operator may be modified to simulate different soil properties. Despite the fact that this method lacks physical basis, it has the advantage to mimic basic soil water movement at a minimum computational cost.

Hydraulic parameters

To the exception of the stomatal conductance, most of the conductances used in the water flux module remain poorly estimated. In addition, some of these conductances are expressed in different units. In particular, the root radial conductivity is expressed in [m.s⁻¹.MPa⁻¹] while the leaf radial conductivity (g_s) is expressed in [m³.m⁻².s⁻¹], which lead us to make some approximation in the model.

Root The root hydraulic properties described by Doussan et al. (1998) were used in this study. These properties (axial and radial) are functions of the root segment age and type (axis or lateral). These values have been used successfully in previous models (Doussan et al., 2006; Javaux et al., 2008).

Stem The stem radial conductivity was set to zero, assuming that the stem is not permeable to water. Its axial conductivity was calculated according to the Hagen-Poiseuille law,

$$K = \frac{\Pi r^4}{8\eta} \quad (9.8)$$

where K is the axial conductivity, r the radius of the xylem pipes and η the water dynamic viscosity (= 1.002 mPa.s). Xylem radius was

estimated to be 1.7% of the stem radius (Li et al., 2009). In our case, for the sake of simplicity, xylem vessels were considered as a single pipe.

Leaves As no quantitative data about the axial conductivity of the leaf were found in the literature, we set it empirically to a tenth of the stem axial conductivity.

As mentioned above, leaf radial conductivity values are generally based on the difference in relative humidity between the stomatal cavity and the atmosphere and do not fit the water flux resolution in PlaNet-Maize that are based on water potential differences. Therefore, we used the flux equation

$$L_r = \frac{\Delta\psi S}{J_{out}} \quad (9.9)$$

where $\Delta\psi$ is the water potential difference between the atmosphere and the leaf [MPa], S is the leaf area [cm²] and J_{out} the radial water flux [m.s⁻¹], with experimental data on water potential and flux (not shown), and could estimate the maximal leaf stomatal conductance to 3.10⁹m.s⁻¹.MPa⁻¹.

Hydraulic regulation of the plant

In order to investigate the contribution of varying hydraulic properties to the regulation of the water status of the plant, we introduced modifier functions that reduce the radial conductance of roots, the axial conductivity of the xylem (roots, stem and leaf) and the leaf radial conductance. These modifiers were calculated locally for each article as a function of its (xylem) water potential.

Leaf conductance (g_s) As stomata, which ranges from fully open to completely closed, ultimately define the transpiration demand, their regulation is therefore seen as the master control site in the transpiration flow. In PlaNet-Maize, stomatal closure is influenced by exogenous (light, temperature and vapor pressure deficit) and endogenous (leaf water potential) factors.

Diurnal variations in the leaves stomatal conductivity due to exogenous factors were implemented following Jarvis equations (Jarvis,

9. MODELING WATER FLOW AND ITS REGULATIONS.

1976):

$$g_s = g_{smax} * F_1(PAR) * F_2(T_a) * F_3(VPD) \quad (9.10)$$

where g_s is the leaf stomatal conductance [mm.s^{-1}] and g_{smax} is the maximum stomatal conductance of individual leaves under optimal conditions [mm.s^{-1}]. $F_1(PAR)$, $F_2(T_a)$ and $F_3(VPD)$ are environmental stress functions, with $0 \leq F_i(X) \leq 1$. In particular,

$$F_1(PAR) = \frac{PAR}{a_1} \quad (9.11)$$

$$F_2(T_a) = \frac{(T_a - T_L)(T_H - T_a)^{(T_H - a_2)/(a_2 - T_L)}}{(a_2 - T_L)(T_H - a_2)^{(T_H - a_2)/(a_2 - T_L)}} \quad (9.12)$$

$$F_3(VPD) = e^{-a_3 \cdot VPD} \quad (9.13)$$

where PAR is the average received photosynthetically active radiation by leaves [$\mu\text{mol.m}^{-2}\text{s}^{-1}$], T_a is the air temperature [$^{\circ}\text{C}$], T_H and T_L are the upper and lower temperature limits outside of which transpiration is assumed to cease [$^{\circ}\text{C}$], VPD is the vapor pressure deficit [MPa] and a_1 , a_2 , and a_3 are parameters [-]. We assumed that light interception is not influenced by leaf positioning and mutual shading, and is homogeneous for all leaves.

The influence of the leaf water potential on the leaf radial conductivity (fig. 9.3.A) was implemented in PlaNet-Maize following a Weibull function (Bohrer et al., 2005; Janott et al., 2011) following data from Cochard (2002):

$$f(\psi) = 1 - e^{-\left(-\frac{\psi}{b}\right)^c} \quad (9.14)$$

where b and c are curve parameters and ψ is the article water potential.

Root radial conductivity (K_r) The dynamic regulation of the root radial conductivity is mainly performed through the regulation of aquaporin activity (Javot, Maurel, 2002; Maurel et al., 2008), although quantitative data linking aquaporin activity with the root radial conductivity are generally not available. Aquaporin activity is down regulated during water deficit, yet it is not clear to what extent aquaporin activity influences K_r (Bramley et al., 2009). Therefore, the regulation of root radial conductivity was implemented in PlaNet-Maize following a logistic function bounded between 1 and 0.4

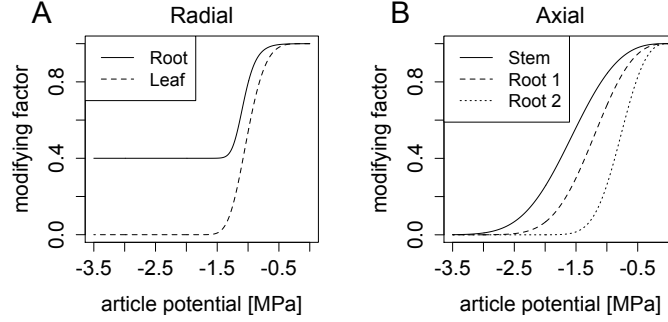


Figure 9.3: PlaNet-Maize conductivity modifiers. **A.** Modifiers for root/leaf radial conductivities. **B.** Modifiers for the axial conductance. PR = first order root. LR = lateral root.

(aquaporin regulation cannot reduce the root radial conductivity to zero):

$$f(\psi) = A + \frac{K - A}{(1 + Qe^{-B(\psi-M)})^{1/v}} \quad (9.15)$$

where A is the lower asymptote, K is the upper asymptote, B is the growth rate, $v > 0$ affects near which asymptote maximum growth occurs, Q depends on the value $f(0)$, M is the water potential of maximum transpiration if $Q = v$ and ψ is the current water potential. In this case, Weibull function could not be used since the function is bounded between 0.4 and 1 and not 0 and 1.

Axial conductance (K_x) Changes of axial conductance occur primarily under the influence of xylem cavitation and embolism repair (Peirce, 1936). The relationship between the tension in the xylem and the decrease in axial conductance is commonly described using Weibull functions (Sperry et al., 1988b; Tyree, Sperry, 1989) (see eq. 9.1.4). In PlaNet-Maize, the Weibull function was implemented in every article according to data from Li et al. (2009) and considering different curves for the different plant organs (stem > first order roots > second order roots) (fig. 9.3.B, Hacke et al. (2000)).

9. MODELING WATER FLOW AND ITS REGULATIONS.

9.1.5 Conditions for simulations

The aim of the simulations presented here was to understand the intimate processes by which the maize plant regulates its water uptake behavior (hence its water status) by modifying architectural and/or hydraulic traits. Four sets of simulations were performed. The first set (I, tab. 9.1) highlights the effect of the root-to-shoot surface ratio (RSSR) by changing the number of seminal roots for given hydraulic parameters and transpiration demand. The second set of simulations (II, tab. 9.1) focuses on the effect of conductivity modifiers. The third set (IIIa-d, tab. 9.1) simulates the influence of management practices (well-watered, water-stressed, deficit irrigation and partial root-zone drying). Finally, the last set (IVa-f, tab. 9.1) was used to analyze the sensitivity of the water flow regulation mechanisms.

Table 9.1: Conditions for simulations. PRD = partial root zone drying. RW = Rewatering. # of SR = number of seminal roots

Simulation	# of SR	regulation	carbon	water depletion
I	0-6	none	no	no
II	0-6	all	no	no
IIIa	4	all	yes	no
IIIb	4	all	yes	yes
IIIc	4	all	yes	PRD
IIId	4	all	yes	RW
IVa	4	enhanced g_s	yes	yes
IVb	4	inhibited g_s	yes	yes
IVc	4	enhanced K_r	yes	yes
IVd	4	inhibited K_r	yes	yes
IVe	4	enhanced K_x	yes	yes
IVf	4	inhibited K_x	yes	yes

In all simulations, the soil and atmosphere initial water potential were respectively -0.01 and -95 MPa. Environmental conditions (temperature, light and VPD) were set according to a summer day in the greenhouses in Louvain-la-Neuve (Belgium, $+50^{\circ} 39' 59.91''$, $+4^{\circ} 37' 10.56''$). A sandy soil with a low water retention capacity was considered in order to quickly observe water shortage for the plant. The time step was 1h for the plant development and 10 minutes for the water fluxes. Data were exported every 12 hours, from the 50th to the 350th hour of the simulations.

9.1.6 Model validation

The architectural and water flux modules were validated against experimental data independent of the one used to calibrate the model. PlaNet-Maize was able to reproduce realistic kinetics of root and shoot growth and water fluxes, integrated at the plant level (fig. 9.4).

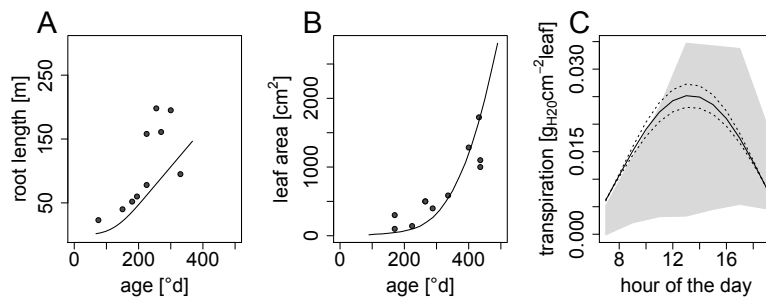


Figure 9.4: Comparison between experimental and simulated data. **A.** Comparison between experimental (circles) and simulated (line) root length values. **B.** Comparison between experimental (circles) and simulated (line) shoot area values. **C.** Comparison between experimental (grey area) and simulated (lines) transpiration values. Plain line represents the mean simulated transpiration value while the dashed lines represent the standard deviation range due to day to day variations .

9.2 Results and discussions

9.2.1 Root system size and hydraulic regulations

Water uptake by plants can be considered in economical term, the shoot and the root defining respectively a potential demand and a supply capacity. In the plant-soil system, the evaporative demand is mainly defined by the leaf area, the stomatal conductance (g_s) and the VPD. On the other hand, the supply capacity is set by the root system architecture, its hydraulic properties and the local soil water potential (Draye et al., 2010). When the demand exceeds the supply capacity, the system is put under strain as long as the demand decreases or the supply increases.

In order to test the effect of the root-to-shoot surface ratio (RSSR) on the hydraulic status of the plant, simulations with different initial numbers of seminal roots (between 0 and 6) and with the same root growth rate and shoot system development were performed. The carbon module was disabled to avoid feedbacks between transpiration, growth and C allocation.

In a first set of simulations, the hydraulic regulation and soil water depletion were disabled to isolate the effect of the root system size (tab. 9.1.I). These were enabled in a second set of simulations, through the use of modifier functions (tab. 9.1.II).

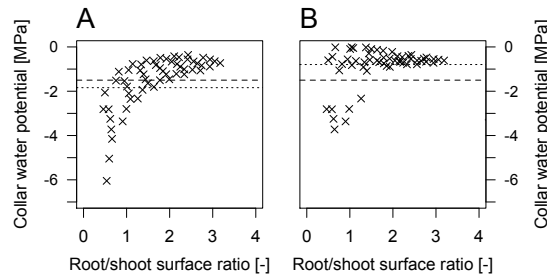


Figure 9.5: Relationship between the Root-to-shoot surface ratio and the collar water potential. **A.** Without hydraulic regulation. **B.** With hydraulic regulation. Dashed lines represent the permanent wilting point (-1.5 MPa). Dotted lines represent the 75th percentile. Each point represent the collar water potential at noon at different days.

Figure 9.5.A summarizes the relationship between RSSR and the plant water potential (computed at the collar level). Considering a permanent wilting point at -1.5 MPa, the simulations suggests that a minimum RSSR value of 2.0 is needed for a theoretical plant that would not regulate its root, leaf and axial conductances. Allowing the plant to regulate these hydraulic properties widens the range of viable RSSR values (fig. 9.5.B).

These simulation results show that a shoot:root allometry is beneficial for the maintenance of water potential values above the permanent wilting point (-1.5 MPa). They also indicate that the regulation of hydraulic properties contributes to stabilize the plant water potential but does not completely overcome the effect of structural allometry. As such, the simulations reproduce many experimental results that showed that an undersized root system leads to greater tension in the xylem (Hacke et al., 2000; Sperry et al., 1998). The simulation also suggest that the range of viable root-to-shoot ratios is rather large and influenced by the hydraulic regulation strategy used by plants.

9.2.2 Hydraulic signal alone is not sufficient to reproduce effect of different irrigation practices

Four watering scenario were simulated in order to compare the response of plants to different water management practices (tab. 9.1.III): well-watered (WW), water deficit (WD), partial root zone drying (PRD) and re-watering (RW). In the WW treatment, the soil water potential was maintained at a constant value (field capacity) during the whole simulation while in the WD treatment, the absorbed water was depleted from the containing soil voxels and a basic horizontal redistribution of water in the soil was enabled. In the PRD treatment, the soil domain was split vertically in two compartments simulated respectively as WW and WD. Finally, in the RW simulation, the soil was treated as in the WD treatment, except that re-watering events were simulated every 100 hours by resetting the initial soil water potential in all voxels (fig. 9.6.A). All treatments were applied from the beginning of the simulations.

Compared to WW, all treatments led to a clear reduction of the soil water potential. The PRD was able to maintain the soil water potential at a lower but stable value until 250 hours, thereby avoiding the abrupt transitions that occur in the RW treatment (fig. 9.6.A).

9. MODELING WATER FLOW AND ITS REGULATIONS.

Not surprisingly, reducing the water availability for the plant had a direct effect on the transpiration (fig. 9.6.B). Consistently with the soil water potential evolution, WD plants presented the lowest transpiration, while the PRD and RW scenario generated intermediate transpiration. The reduction of transpiration, in turn, led to a reduction of plant growth, although relatively small (fig. 9.6.C).

Throughout the simulation, the leaf water potential displayed a regular decline in all treatments, which should be attributed to a decrease in the RSSR (fig. 9.6.D). Interestingly, until 250 hours, the leaf water potential difference between the different treatments and WW were similar to the soil water potential difference.

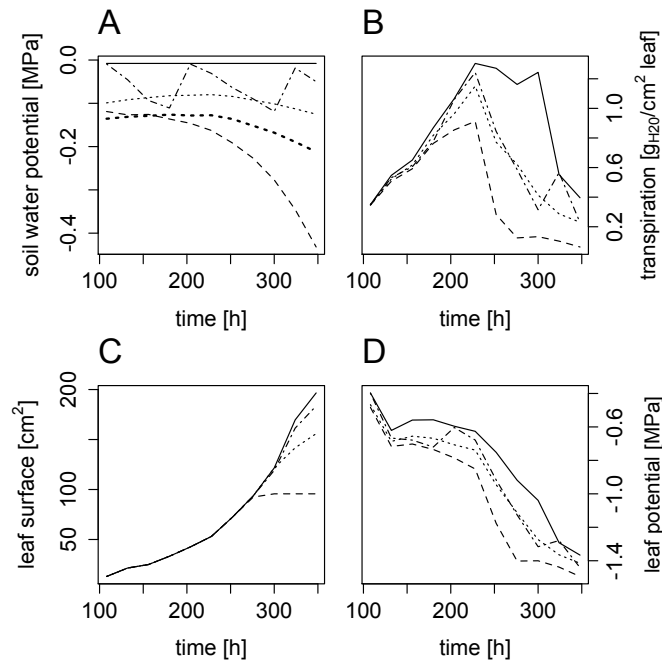


Figure 9.6: Effect of the irrigation technique on the plant water status. **A.** Average soil water content at the vicinity of the roots. **B.** Transpiration rate. **C.** Total leaf surface. **D.** Leaf water potential. Plain lines: WW. Dashed lines: WS. Dotted lines: PRD (all). Bold dotted line: PRD (dry compartment). Dashed-dotted lines: RW. Values were taken at 12:00 on the last day of the simulation.

Figure 9.7 describes the influence of the irrigation technique on the root water status. WD plants have smaller root systems, lower root water potential and conductivities and also a reduced uptake compared to the WW plant. It is difficult to assess if the latter result from the smaller uptake capacity (root surface) and/or the smaller demand (leaf size and leaf conductance). As for the previous results, the PRD and RW scenarios exhibit intermediate values.

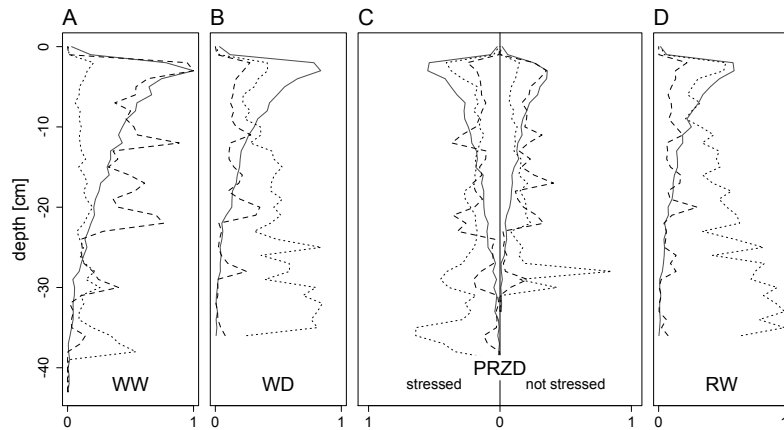


Figure 9.7: Effect of the irrigation technique on the roots: **A.** well watered, **B.** water deficit, **C.** partial root zone drying (left panel: water stress; right panel: well watered) and **D.** re-watering. Plain grey lines represent the root surface (sum per depth), dashed lines represent the water uptake (sum per depth) and dotted lines represent the root water potential (unsigned average per depth). All values are normalized to the maximal value of each variable across all scenarios.

One should notice that the water uptake profiles did not strictly correspond to the root surface profiles, particularly for the WD plant. The phenomenon, known as the compensation mechanism (Couvreur et al., 2012; Draye et al., 2010) arises when regions of the root system are surrounded by a soil layer that has a lower conductivity than the soil in the vicinity of the rest of the root system, or when the integrated conductance between roots and the collar differ among roots. When this occurs, the water uptake by roots with low soil/root conductances will be lowered and compensated by a larger water uptake by the other roots. This occurs typically in the WD, in the non-irrigated part of

the PRD and in the RW treatments, where the lower root water potential increases water uptake at depth. In other words, uptake sites are not only defined by the root placement in the soil. They depend on the integration of the root system architecture, the root hydraulic properties and the water availability in the surrounding soil. (Draye et al., 2010; Lobet et al., 2012).

PlaNet-Maize effectively reproduces the effect of different irrigation practices that is generally observed experimentally. As a general rule, decreasing the amount of available water for plant reduces the plant transpiration and, above a certain threshold, decreasing plant growth as well (fig. 9.6).

However, PlaNet-Maize could not capture experimental difference classically observed between PRD and RW treatment. Indeed, a growing body of evidence indicate that PRD has a beneficial influence on the plant water consumption and yield compared to RW (as an example, see the works of Dodd (2007) and Kang et al. (2000)). In these experiments, no major differences in leaf water potential were observed (as in our simulations, fig. 9.6.C), but significant differences in final yield were recorded between the treatments. Evidently, the transpiration – assimilation feedback that is used in PlaNet-Maize is not able to simulate this response. For this to work, the instantaneous WUE coefficient should be adjusted as a function of the soil water potential sensed by the plant.

The yield response to PRD is generally explained by differences in abscissic acid (ABA) production in the roots. It seems plausible from our simulations that a root signal informing leaves about the soil water potential might be sufficient to adjust stomatal conductance and restore a leaf water potential equivalent to the WW. This would reduce assimilation on the short term but would save water for future use. Including ABA signalling in PlaNet-Maize might thus help to reproduce the typical yield response to PRD treatment. This would lead ultimately to an apparent adjustment of the instantaneous WUE coefficient as a function of the soil water potential.

Based on the response of the leaf water potential (ψ_{leaf}) to decrease in soil water potential (ψ_{soil}), plant can exhibit either an isohydric (ψ_{leaf} remains constant under decreasing ψ_{soil}) or anisohydric (ψ_{leaf} decreases under decreasing ψ_{soil}) behaviour. In our model, ψ_{leaf} tends to decrease with a decreasing ψ_{soil} , which suggest an anisohy-

dric behaviour (fig. 9.8). However, experimental data have shown the opposite in the fields, hence labelling maize as an isohydric plant (Ben Haj Salah, Tardieu, 1997; Tardieu et al., 1992). Such isohydric behaviour has been characterised by an interplay between g_s , ψ_{leaf} and the concentration of ABA in the xylem sap (Tardieu, Simonneau, 1998). Implementing ABA in PlaNet-Maize should help enabling an isohydric behaviour in our simulations.

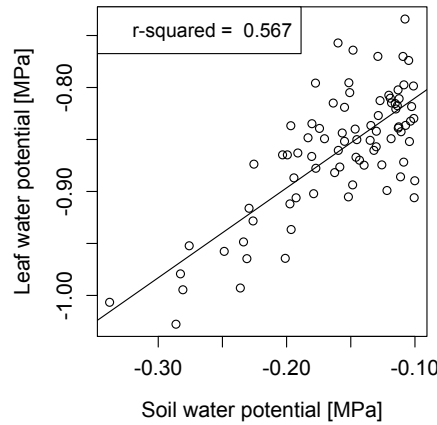


Figure 9.8: Response of leaf water potential to soil drying in PlaNet-Maize .

9.2.3 Regulation sensibility

Finally, sensitivity analysis was performed to assess the effect of the regulation g_s , K_r and K_x implemented through the use of modifiers (tab. 9.1.IV). For each conductance, the modifier function was shifted towards lower and higher water potential values, leading, respectively to delayed and faster responses to changes in water potential (fig. 9.9). This analysis revealed contrasting differences between the relative effects of the three regulation processes.

The results of the analysis on g_s are given in figures 9.10.1A-1C and 9.11.1A-1C. Increasing the sensibility of g_s to the water potential leads to early stomatal closure which causes the reduction of transpiration and the maintenance of a high water potential. This does not

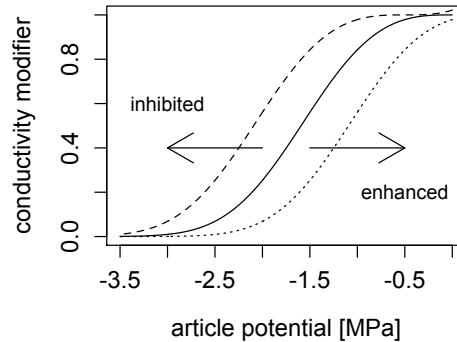


Figure 9.9: Regulation sensibility. Plain line represents the control regulation curve. Dashed line represent the delayed response. Dotted line represent the faster response.

affect root conductances but has a dramatic impact on plant growth and leaf area. Fortunately, the saved water is available later and allows plants to transpire for a longer period (fig. 9.10.1C, arrow). On the opposite, decreasing the sensibility of g_s to the water potential leads to stomata being more open, a higher transpiration and a rapid decrease of the plant water potential, which expected decrease of the root radial conductance and increase of xylem cavitation.

The changes in the sensibility of K_r (figs. 9.10.2A-2C and 9.11.2A-2C) and K_x (figs. 9.10.3A-3C and 9.11.3A-3C) have smaller effect on the plant water status compared to g_s . The largest effects are seen under faster K_r response, where a rapid reduction of the root radial conductivity occurs, leads to a sensible reduction of the plant water potential, stomatal opening and transpiration. Interestingly, this effect was obtained without any consequences on growth and leaf area and appears thus as plausible way to achieve conservative water use. Neither delayed K_r nor altered K_x responses have important consequences on the plant water dynamics.

Contrasting transpiration dynamics were thus observed between plants with modified g_s and K_r responses. On the one side, the delayed g_s response allows the plant to sustain the evaporative demand at the cost of a quick drying of the soil, and is therefore valuable in conditions where water supply is non limiting. On the other side, the faster

g_s and K_r responses lead to a conservative use of water that allows transpiration maintenance later in the season. Recent experimental data suggest that such water saving strategy during the vegetative growth is correlated with terminal drought resistance (Kholová et al., 2010; Tardieu, 2011; Zaman-Allah et al., 2011a; Zaman-Allah et al., 2011b). Some of our simulations differed from these results by the strong reduction in plant size which was not observed in field conditions. It has to be noted, however, that the drought susceptible and resistant genotypes used in these experiments did not differ necessarily by the same mechanisms as the ones considered in our simulations.

Beyond their effect on the plant water dynamics, the modifier functions also change the spatial patterns of water extraction by roots in slightly different ways. These modifications rely mostly on the changes of radial vs axial root conductivities, as a large K_r/K_x ratio tends to concentrate water uptake in the upper layers, while a lower ratio tends to distribute the uptake vertically (Draye et al., 2010). This is most noticeable in the K_r sensitivity analysis where the K_r/K_x ratio increases under a delayed response of K_r and decreases under a faster response (fig. 9.11). It follows that the uptake pattern is decreased by a constant value under the faster K_r response while it is more increased in upper layers under the delayed K_r response.

These sensitivity analyses emphasize the interplay between the regulation of g_s , K_r and K_x . Obviously, making these regulations all dependent on the local water potential is largely responsible for this interplay, but this only reflects the structural integration of these regulations which all contribute to the same water flow. It follows that the classical experimental methodology consisting in the manipulation of a single regulating mechanism should be complemented with at least some characterisation of how this manipulation could affect the other mechanisms. PlaNet-Maize provides the required framework to integrate many different factors influencing the water dynamics.

9. MODELING WATER FLOW AND ITS REGULATIONS.

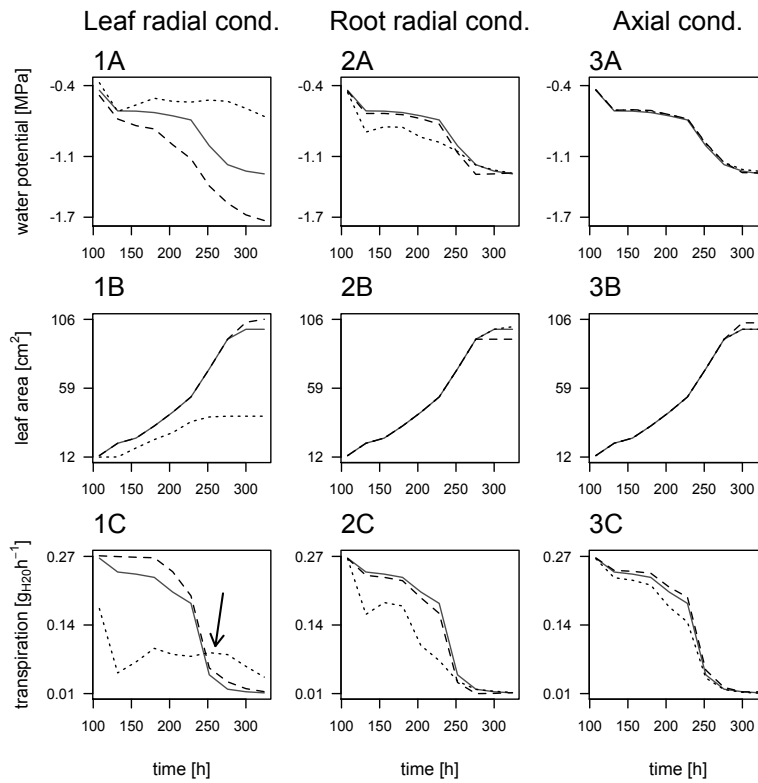


Figure 9.10: Effect of the regulation processes on the plant water status. **1-**: changed regulation of leaf radial conductivity; **2-**: changed regulation of root radial conductivity; **3-**: changed regulation of axial conductance; **-A:** evolution of the collar water potential; **-B:** evolution of shoot surface; **-C:** evolution of the relative transpiration (to the leaf area). Plain lines represent the controls, with no modification of the regulation processes, dashed lines represents the inhibited regulation processes and dotted lines represent the enhanced regulation processes.

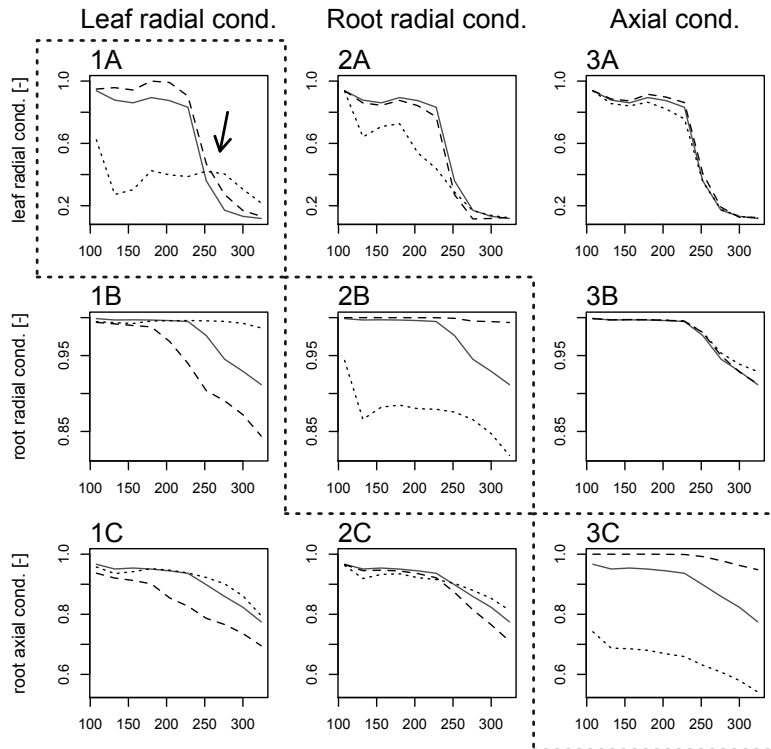


Figure 9.11: Effect of the regulation processes on the plant water status. **1-**: changed regulation of leaf radial conductivity; **2-**: changed regulation of root radial conductivity; **3-**: changed regulation of axial conductance; **-A**: evolution of the leaf radial conductivity; **-B**: evolution of the root radial conductivity; **-C**: evolution of the root axial conductance. Plain lines represent the controls, with no modification of the regulation processes, dashed lines represents the inhibited regulation processes and dotted lines represent the enhanced regulation processes. Framed plots highlight the differences in regulation sensibility for each scenario.

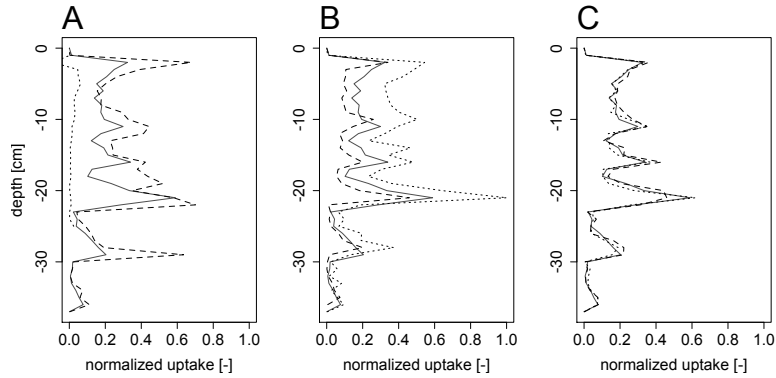


Figure 9.12: Effect of the regulation processes on the root water uptake profiles. **A:** modified leaf radial conductivity; **B:** modified root radial conductivity; **C:** modified axial conductance. Plain grey lines represent the controls, with no modification of the regulation processes, dashed lines represents the inhibited regulation processes and dotted lines represent the enhanced regulation processes. All values are normalized.

9.3 Conclusions and perspectives

9.3.1 *Functional-structural modeling as a useful tool to decrypt plant water relations*

PlaNet-Maize was successfully used to simulate water flows in the entire soil-plant-atmosphere continuum with a resolution down to the plant element level. This first version of the model was able to reproduce the effect of root architecture and hydraulic properties on the water relations in the plant as previously shown in former models (Draye et al., 2010; Janott et al., 2011). In addition, by implementing simple regulatory processes acting on the local values of K_r and K_x , we found that the virtual plant was able to tightly control its water status.

Divergences were observed between experimental and modeling results for contrasted water management practices. PlaNet-Maize was not able to reproduce the beneficial effect of PRD over RW treatment. This difference appeared supposedly because a finer signaling of local soil conditions (via the production and translocation of ABA) was not implemented in the model.

Finally, PlaNet-Maize was used to show the effect of modified sensibilities for the different regulation sites. Enhanced sensibilities enable the plant to react more quickly to environmental constrain and therefore to have conservative water use behaviors. Results show that changing the sensibilities at the root system level (either K_x and/or K_r) can have a non-negligible effect on the plant water status by increasing its overall water use efficiency.

9.3.2 Envisaged model development

A first envisaged development path for PlaNet-Maize would be the improvement of its water-related modules. Firstly, in order to model more realistic condition and test the influence of different soil environment, integration of a more realistic soil module, such as Hydrus or R-SWMS (Javaux et al., 2008), are required. Moreover, as discussed previously, the implementation of a long distance signal between the root and the shoot, such as ABA, should be implemented to enable a finer sensing of the local variations in the soil water content.

A second direction for the development of the model would be to link it which lower scale models, down to the cell level (Band et al., 2012). Indeed, the modular nature of the PlaNet based models allows an easy and straightforward integration with other models.

Finally, a third direction would be to extend the model from vegetative to reproductive stages, in order to assess the effect of terminal drought stress on grain formation and, ultimately, yield. Again, the modular structure of PlaNet-Maize easily allows the creation of new article types needed to simulate flowering and grain filling.

9.3.3 Future experimental needs

Functional-structural plant model rely on quantitative data to be accurate and representative of the reality. Unfortunately, in some area, notably regarding plant hydraulics, this quantitative knowledge is missing. As functional-structural models are now recognized as useful tools for the plant science community (Tardieu, 2010), more and more modeling project arise and therefore there is an increasing need for more quantitative biological data.

A FIRST STEP TOWARD AN EXPLICIT MODELING OF ABA PRODUCTION AND TRANSLOCATION ON THE WATER UPTAKE DYNAMICS IN THE SPAC



ABSCISIC ACID (ABA) is a plant hormone involved in a variety of physiological processes comprising leaf abscission (Taiz, Zeiger, 1998), leaf elongation (Tardieu, 2010) and modulation of tissue hydraulic conductivity (Parent et al., 2009). Regarding water flow control, ABA produced in the leaves acts as an endogenous signal triggering stomatal closure. It is also thought to act as a long distance signal that is produced by roots experiencing water deficit and translocated to the leaves in the xylem stream (Davies, Zhang, 1991; de Smet et al., 2006). However, the contribution of ABA as a long distance signal, compared with leaf-supplied ABA and with hydraulic signals manifested by the xylem water potential, is still a matter of controversy (Christmann et al., 2007; Holbrook et al., 2002).

In the previous chapter (see chap. 9), we have shown that the sole hydraulic signal was not sufficient to reproduce uptake patterns in response to heterogenous soil drying conditions. This chapter presents a first attempt to explicitly model the ABA production, degradation, translocation and their effect on the transpiration flow.

10.1 Model description

PlaNet-Maize is a functional structural plant model which simulates the growth and development of a complete maize plant. The model also simulates water flows in the soil-plant-atmosphere continuum (including regulation in the shoot and the roots, see chapter 9 for more details about the model).

Different aspects of ABA signaling were implemented in PlaNet-Maize in order to investigate its contribution as a root-to-shoot stress signal and in a feed-back process. The ABA module of PlaNet-Maize comprises ABA production, degradation and transport, as well as a response of the leaf radial (stomatal) conductance to ABA.

10.1.1 ABA production

Local abscisic acid production was implemented as a function of the article endogenous water potential based on experimental data from Dodd et al. (2008). ABA is produced in the leaf and root articles. It has to be noted that these experimental data were obtained with sunflower (*Helianthus annuus*).

$$[ABA]_{prod} = a.e^{b.\psi_x} \quad (10.1)$$

where $[ABA]_{prod}$ is the production of ABA [nM], a and b are parameters which depend on the article type (tab. 10.1) and ψ_x is the article endogenous water potential [MPa] (fig. 10.1).

Table 10.1: Parameters for the ABA production functions in PlaNet-Maize

article	a	b
root	9.5635	-5.224
leaf	4.7818	-5.224

10.1.2 ABA degradation

ABA degradation was computed as an exponential decay function based on its half-life in the different tissues:

$$dABA = qABA.(1 - 2^{-\Delta t/t_{1/2}}) \quad (10.2)$$

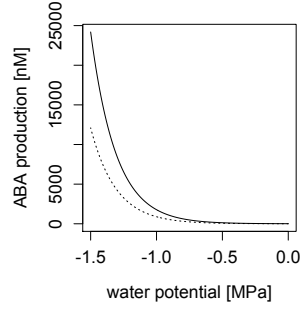


Figure 10.1: ABA production as a function of plant water potential. Plain line: production in the roots. Dashed line: production in the leaves.

were $dABA$ is the degradation of ABA [$\text{mol}\cdot\text{h}^{-1}$], $qABA$ is the initial quantity of ABA [mol], Δt is the time step [h] and $t_{1/2}$ is the half-life of ABA degradation [h] (tab. 10.2).

Table 10.2: Half lives of ABA in the different plant articles.

article	$t_{1/2}$ [h]	source
root	0.7	Jia et al., 1996
leaf	0.96	Ren et al., 2007
stem	0.7	Jia et al., 1996

10.1.3 ABA transport

For the transport function, ABA was considered as moving with the xylem sap. An implicit matrix resolution was used to solve the ABA redistribution in the plant based on the water fluxes resolution:

$$Q_i^t = Q_i^{t+1} - \sum J_{in}^t \cdot C_{source}^t \cdot \Delta t + \sum J_{out}^t \cdot C_i^t \cdot \Delta t \quad (10.3)$$

where Q_i^t is the quantity of ABA in the article at the time step t , Q_i^{t+1} is the quantity of ABA in the article at the time step $t + 1$, J_{in}^t is the water flux coming from the article neighbors, C_{source}^t is the ABA concentration in the neighbors, J_{out}^t is the water flux from the article to the neighbors and C_i^t is the ABA concentration in the article.

10. MODELING ABA FLUXES AND THEIR EFFECTS.

This equation is computed at the plant level by using a linear matrix system that encompasses all the plant elements. The resolution of the system returns a new ABA concentration in every article.

10.1.4 Stomatal conductance g_s

The regulation of stomatal conductance was implemented such that stomata are closed during the night and are opened as a function of water potential and ABA concentration during the day.

Although abscisic acid has been shown to have numerous effects on the plant physiology, only its effect on the leaf radial conductance was implemented in PlaNet-Maize . A modified version of the model of Tardieu, Davies (1993) was used to compute the cumulative effects of the ABA concentration and the endogenous water potential on the leaf conductance:

$$ABA_{modifier} = \frac{g_{smin} + (g_{smax} - g_{smin})e^a}{g_{smax}} \quad (10.4)$$

where g_{smin} is the minimal leaf radial conductance, g_{smax} is the maximal leaf radial conductance and a is defined as:

$$a = [ABA] - 4,2510^{-3}e^{2,78\psi} \quad (10.5)$$

where $[ABA]$ is the local abscisic acid concentration [nM], and ψ is the article water potential [MPa]. The result of equation 10.4 is used as a modifier for the leaf radial conductivity (fig. 10.2).

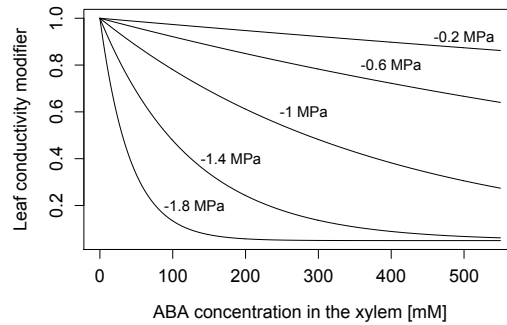


Figure 10.2: Leaf conductivity modifier as a function of xylem water potential and ABA concentration. Adapted from Tardieu, Davies (1993)

10.1.5 Conditions for simulations

In order to evaluate the ABA module in PlaNet-Maize , four scenarios were run (tab. 10.3). The first scenario aimed at testing the influence of ABA in non limiting conditions (soil water potential was therefore kept constant). The second scenario investigated the response of the ABA module to decreasing soil water content. The last simulation tested the individual influence of the different ABA production processes by shutting off ABA production in leaves or in roots.

In these simulations, the carbon module and the regulation of hydraulic, presented in the chapter 9, were disabled. Similarly, soil drying was not implemented as a function of root water uptake but was assumed to be homogeneous over the soil domain (not related to the root water uptake) and to decrease linearly as a function of time after 150 hours of simulation (from -0.2 MPa to -1.3 MPa). These different simplifications were made to isolate the effect of the ABA module.

Table 10.3: Conditions for the ABA simulations.

Simulation	Soil drying	ABA_{leaf}	ABA_{root}	ABA transport
I	no	yes	yes	yes
II	yes	yes	yes	yes
III	yes	yes	no	yes
IV	yes	no	yes	yes

10.2 Preliminary results

Figure 10.4, 10.5 and 10.6 shows, respectively, the evolution of the plant articles water potential, the evolution of ABA production and the evolution of transpiration for the first two scenarios (tab. 10.3.I and II).

As expected, daily variations could be observed reflecting the daily variations in the environmental demand. Generally, following stomatal opening in the morning, the transpiration demand increased and the xylem water potential decreased (fig. 10.4.A and B), triggering the production of ABA (fig. 10.5.A-C). Finally, the presence of ABA in the leaves induced a closure of the stomata and regulation of the overall water flow in the SPAC (fig. 10.6.A and B).

In situations of soil drying, the same effects were observed with a greater intensity. Indeed, the simultaneous increase of transpiration and decrease of soil water potential were responsible for the onset of a greater tension in the xylem (fig. 10.4.A and B, green lines), a more important ABA production (fig. 10.5.A-C, green lines) and a greater decrease of transpiration (fig. 10.6.A and B).

In the previous chapter, we postulated that the isohydric behavior of the maize plant, that was not observed in our simulations, could be achieved by adding long distance ABA signalling in the model (chap 9). Indeed, ABA is thought to be a supplemental layer in the regulation process, enabling a better sensing of the local variations in soil water content (Tardieu et al., 1992). However, despite the implementation of the ABA module, the simulated plant still displayed an anisohydric behavior (fig. 10.3).

Although, at first, the model seemed to simulate fairly well the effect of ABA in the water uptake dynamics, it appeared that some behaviors were not correctly reproduced.

In order to investigate the possible causes of the divergence between the simulated results and the reality, two additional scenarios were run (tab. 10.3.III and IV). For these simulations, the ABA production was shut off in roots or in leaves. In both cases, ABA transport and response functions were maintained. The aim of these simulations was to evaluate if the core of experimental evidence used for these simulations were supporting a long distance signaling role for ABA .

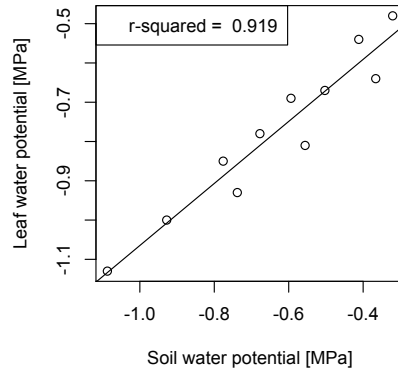


Figure 10.3: Response of leaf water potential to soil drying in PlaNet-Maize ABA.

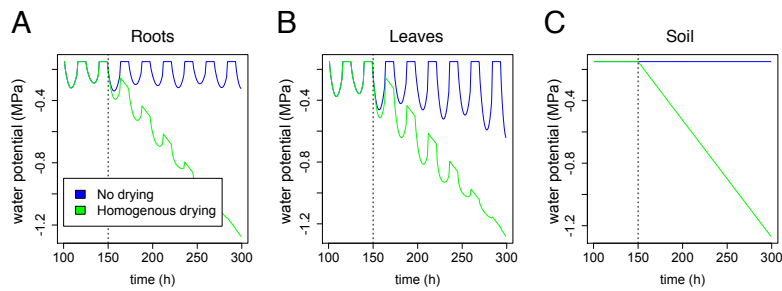


Figure 10.4: Evolution of the average water potential of the different plant organs for two scenarios: no soil drying and homogenous soil drying. **A.** Roots. **B.** Leaves. **C.** Soil. Blue lines: no soil drying. Green lines: homogenous soil drying. The vertical dotted line indicates the beginning of the soil drying.

Figure 10.7 shows the evolution of the ABA concentration when the production is shut off in the leaves or the roots. Not surprisingly, disabling the ABA production in the roots has a direct effect on its presence in the roots (fig. 10.7.A, green line). However, no effects were observed at the shoot level, where the quantity of ABA in leaves remains the same as the standard situation (fig. 10.7.B, green line).

10. MODELING ABA FLUXES AND THEIR EFFECTS.

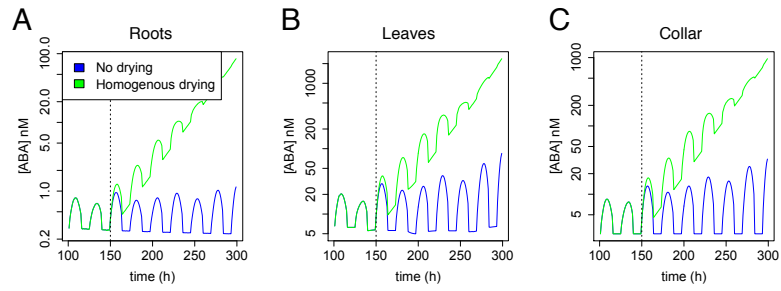


Figure 10.5: Evolution of the average ABA concentration in the different plant organs for two scenarios. Blue lines = no soil drying. Green lines = homogenous soil drying. **A.** Roots. **B.** Leaves. **C.** Collar. The vertical dotted line indicates the beginning of the soil drying.

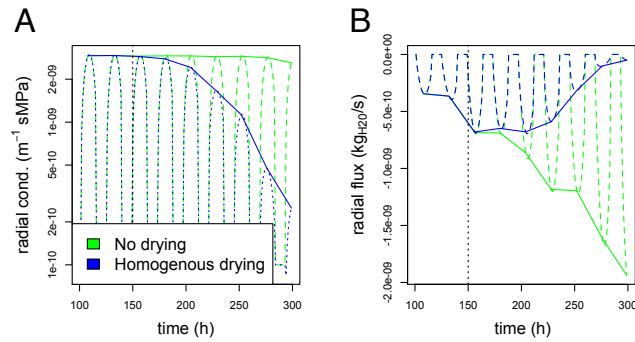


Figure 10.6: Evolution of the average leaf radial conductance (**A**) and of the transpiration for two scenarios (**B**). Blue lines = no soil drying. Green lines = homogenous soil drying. Vertical dotted line indicate the beginning of the soil drying.

However, shutting down the production of ABA in the leaves had the opposite effect. No changes in ABA content were observed in the roots (fig. 10.7.A, red line) while a strong decrease was observed in the leaves (fig. 10.7.B, red line). The fact that some level of ABA was still present in the leaves confirmed the fact that the transport implementation was working correctly.

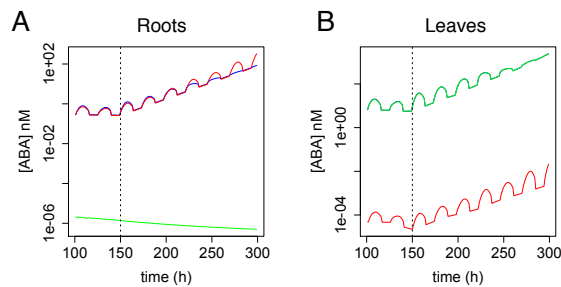


Figure 10.7: Evolution of the average ABA concentration in the different plant organs. **A.** Roots. **B.** Leaves. Blue lines: normal scenario. Green lines: no ABA production in the root. Red lines: no ABA production in the leaves. The vertical dotted line indicates the beginning of the soil drying.

Suppressing the ABA production in the roots had almost no effect at the leaf level (fig. 10.8.A and B, blue lines). Indeed, on all graphs, the curves of the control and the simulation with ABA in the root were superimposed. On the contrary, shutting off the ABA production in the leaves led to an absence of regulation at the leaf level, the quantity of ABA coming from the root system being too small to trigger any kind of response.

10.3 Discussions

The results presented previously suggest that the core of knowledge used to design the ABA module in PlaNet-Maize does not support the role of ABA as a long-distance signal. This observation is in disagreement with previous work that have observed strong correlations between the concentration of ABA in the xylem and the regulation of the stomata (Tardieu, Davies, 1993; Tardieu, Simonneau, 1998; Tardieu et al., 1992).

10. MODELING ABA FLUXES AND THEIR EFFECTS.

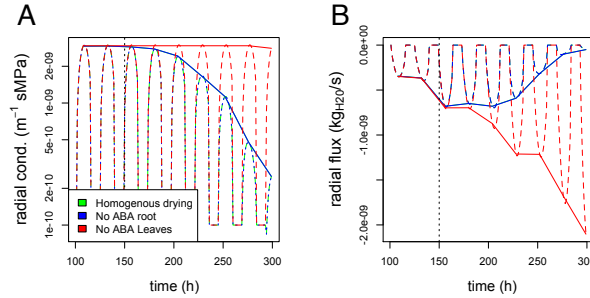


Figure 10.8: Evolution of the average leaf radial conductance (**A**) and of the transpiration for two scenarios (**B**). Green lines: normal scenario. Blue lines: no ABA production in the root. Red lines: no ABA production in the leaves. The vertical dotted line indicates the beginning of the soil drying.

It appears therefore that the simple implementation of ABA production and transport in PlaNet-Maize was not able to reproduce experimental observations. Different elements could be identified in the implementation that might have caused the observed divergence between the model and the experiments.

ABA production

In order to implement the production of ABA in the different plant segments as a function of the segment water potential, quantitative relations were required. However, few quantitative data were available in the literature and none on maize. The data used in the model comes from an experiment with sunflower (*Helianthus annuus*, Dodd et al. (2008)), which is known to have an anisohydric behavior (Tardieu, Simonneau, 1998). Increasing the production of ABA in the roots or changing the sites of ABA production might modify its contribution to signaling.

ABA degradation

When it is conjugated with glucose, ABA forms a much more stable molecule (ABA-GE) that is thought to play a major role as a long distance signal (Jiang, Hartung, 2008; Lee et al., 2006; Schroeder, Nambara, 2006). In this version of the model, only one form of ABA was considered. Decreasing the degradation kinetics of ABA in the different plant organs could be a way to simulate the higher stability

of ABA-GE in the xylem and modify the predicted contribution of ABA as a long-distance signal.

Using global relations for local functions

More generally, most of the functions implemented in the model derive from relations established at the plant level. For the implementation of the ABA module in PlaNet-Maize , because local functions were not found in the literature, it was assumed that global functions could be used locally.

10.4 Conclusions

In this chapter, we presented a first step toward the explicit modeling at the article level of ABA production, degradation, transport and effect on the water flow in situations of soil water deficit.

At this stage of development, the model seems to be unable to simulate the role of ABA as a long distance signal. Indeed, when ABA production was blocked in the roots, no (or very small) differences were observed at the leaf level. The only signal that seems to be acting efficiently was the variation in water potential.

Different elements were identified in the implementation of the module that could explain our results. These elements were related either to a lack of quantitative data at a local level and the over-simplification of the ABA dynamics in the model.

The next step in the improvement of the model should be a sensitivity analysis on the production and degradation rates of ABA in the different plant articles. Such analysis might provide helpful insight on further model improvements, which is a prerequisite to using PlaNet-Maize as a comparative tool to evaluate different scenarios (climate x genotype x management).

PART VI

DISCUSSION AND
PERSPECTIVES

In this final section, we will discuss the principal advances, limitations and perspectives linked to each objective of the thesis.



What we call the beginning is often the end. And to make an end is to make a beginning. The end is where we start from.

T. S. ELIOT

GENERAL DISCUSSION



THE OBJECTIVE OF THIS THESIS was to develop new tools and methods **(1)** to analyse the flows of water in the soil-root domain and **(2)** to quantify the contribution of plant regulatory processes acting on these flows. Since the latter operate at molecular, tissue and organ scales, different strategies have been considered to develop a global and precise view of the whole system.

To address this general objective, three methodological objectives were defined, relating to the development of new tools and methods (fig. 11.1). Three «proof-of-concept» objectives were also defined to illustrate the utility of these new tools to understanding the role of plant regulatory processes in the water dynamics of the soil-root domain. In this section, we will discuss the progress achieved, the identified limitations and some perspectives for each objective.

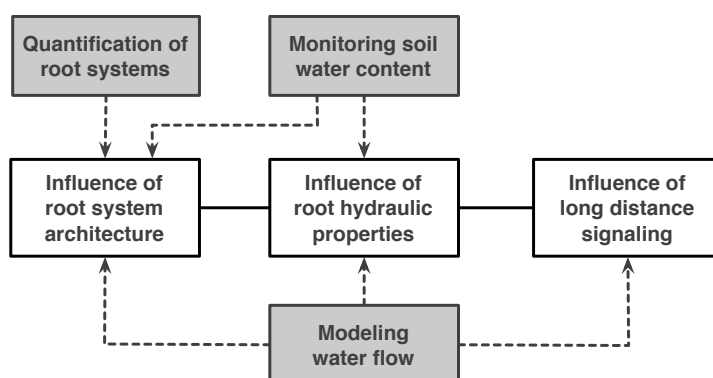


Figure 11.1: Specific objectives of the thesis. Grey boxes represent methodological objectives. White boxes represent research objectives.

11.1 Quantification of complex root architectures

In order to enable the quantitative description of complex root architectures, we have developed a new image analysis toolbox. SmartRoot is a semi-automated root tracing software that allows the analysis of a wide range of root images.

Advances

In this thesis, SmartRoot was successfully used to fully characterise root systems of maize plants grown in rhizotrons. The datasets generated from the root images were used to (1) compute a wide range of root system descriptions (see §6) and (2) create root system input files for the model R-SWMS (see §7)

Nowadays, SmartRoot is the only available software that can provide a detailed dataset containing morphological, topological and geographical informations about the root system. We believe such dataset, in addition to classical root morphological parameters, enables elaborated architectural analysis (Barthelemy, Caraglio, 2007). For example, Fitter's architectural indexes can be computed from topological information (Fitter, 1987) or dynamic traits such as the growth rates of first and second order roots can be inferred from static topological and morphological traits (Lecompte et al., 2001).

Table 11.1: Projects using SmartRoot in their image analysis workflow

Plant	Growing device	Institution
<i>Solanum tuberosum</i>	Rhizotron	UCL
<i>Zea mays</i>	Rhizotron	UCL
<i>Oriza sp.</i>	Rhizotron	UCL
<i>Musa sp.</i>	Rhizotron	UCL
<i>Zea mays</i>	Aeroponic	INRA (LEPSE)
<i>Triticum aestivum</i>	Gel chambers	University of Queensland
<i>Hordeum vulgare</i>	Aeroponic	UCL
<i>Hordeum vulgare</i>	Pouches	ETH Zurich
<i>Brassica rapa</i>	Rhizotron	James Hutton Institute
<i>Hordeum vulgare</i>	Rhizotron	Forschungszentrum Julich

11.1. Quantification of complex root architectures

After the publication of SmartRoot in the scientific literature (Lobet et al., 2011), the software was released in the public domain. Since then, SmartRoot has been downloaded more than 1400 times according to the website statistics. The average download rate is about 20 downloads/week¹. Table 11.1 presents a selection of research projects using (or that used) SmartRoot. These statistics confirm the interest of SmartRoot for the root research community.

During the development of SmartRoot, we became aware that a large number of root image analysis software were developed by other research groups. However, the information concerning these tools was scattered around the web, usually on lab webpages and it was difficult to have a global view of all available software. In order to help root researchers to find the right tool for their research, a web repository was created to list the existing software (<http://www.root-image-analysis.org>). Since it was launched online in June 2011, the site has more than 14.000 page-views from all around the world (fig. 11.2) which confirms the need for a comparison of root image analysis tools.

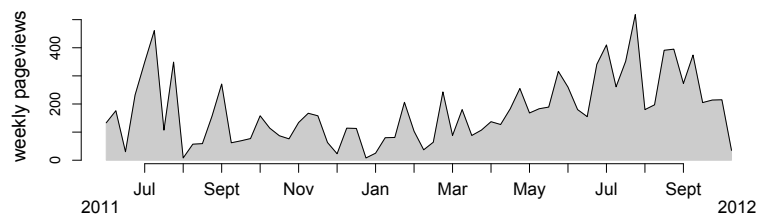


Figure 11.2: Weekly visits on the website <http://www.root-image-analysis.org>.
Source: Google Analytics

¹<http://sourceforge.net/projects/smartroot/files/stats>

Limitations

The principal limitation of SmartRoot is its inability to automatically analyse root images. Although it was designed to be free from user interaction, the semi-automated nature of SmartRoot forbid its use for large scale studies and high-throughput workflows.

A second limitation of the software is that, at this stage, SmartRoot is a two-person project, which threatens its development on the long term. Once publicly available, the life of the software depends on its maintenance, update and compatibility with new operating systems, which can hardly be done by a single person not fully dedicated to the task.

Perspectives

Software development

The development of SmartRoot is still in progress. We are constantly improving the software based on user's feedbacks and on our own needs. Different features are currently in development.

Firstly, following a recent image analysis meeting², it was decided to create a common data structure for different root image analysis tools dealing with root architecture. Having a common data structure would allow the use of complementary software in the same workflow. Currently, this project groups people from Cornell University, the University of Nottingham and the Université catholique de Louvain.

Secondly, despite the fact that SmartRoot was built as a semi-automated tool, we believe that some degree of automation could be achieved. We are currently thinking of ways to streamline the tracing process so that, for simple images, the user input would be minimal. Fully automated tools are already available (Armengaud et al., 2009; Clark et al., 2012; Galkovskyi et al., 2012) but generally lack efficient tracing correction and provide fewer measurements than SmartRoot.

²International Workshop on Image Analysis Methods for Plant Science, Nottingham, 2012

Thirdly, in order to ensure that SmartRoot keeps evolving in the future, we are considering the possibility to make it open source. This would widen the developer base and enrich SmartRoot development with new concepts and ideas.

Applications

Moving from the development of the software to its future applications, we believe SmartRoot opens the way to new types of analysis and experiments.

As a first example, the use of the complete dataset generated with the software could improve future genetic analysis of root system growth en development (de Dorlodot et al., 2007). In addition to simple traits (total weight, length of the longest root,..), more complex or dynamics traits could be acquired (lateral growth rate (Lecompte et al., 2001), gravitropism (Ge et al., 2000; Trachsel et al., 2013), topological index (Fitter, 1987)) in genetic analysis.

A second example would be to use these experimental data with existing models to help untangle soil-root interactions. As shown in chapter 7, the information contained in the SmartRoot dataset can be used to generate digital versions of complex root systems that can serve as input variables in functional structural soil-plant models. While such coupling as been done for the analysis of water flow in the framework of this thesis, we believe it could be use to investigate a variety of soil-root interaction (e.g. effect of the soil density (Nagel et al., 2012) or local nutrient supply).

11.2 Monitoring soil water content in the soil-plant domain

The observation of water flow in the soil-root domain is challenging and usually requires heavy equipments and infrastructure (Esser et al., 2010; Lambot et al., 2008; Mooney et al., 2011; Oswald et al., 2008). Moreover, the concurrent observation of root system architecture is not always straightforward and restricts the downstream analysis of the results. Amongst existing techniques, the light transmission imaging technique (LTI) stands as an easy way to rapidly acquire 2D soil water content distribution and root architectural information. However, the technique was never used with more than six plants at the same time (Garrigues et al., 2006).

Advances

We scaled up the LTI experimental setup to monitor 20 plants in parallel. Our new system uses smaller rhizotrons, with a fully automated watering system and a mobile dark room to capture the light transmission images directly in the greenhouse. As a result, a complete imaging session of the 20 plants could be performed in 30 minutes by a single person, allowing us to monitor the evolution of the soil water content of a larger number of rhizotrons (see §6)

The downstream image processing required to transform raw images in soil water content dataset was fully automated. Although it takes some computing time to process all the images of one experiment, it removes the burden of manual processing and the potential error bounded to eye-based analysis.

In this thesis, the LTI technique was used with two different studies. On the one hand, we used the technique to monitor changes in soil water content for a large number of plants. The acquired images were used to link root architectural features with contrasted evolutions of soil water depletion in different soil layers. On the other hand, we also used the technique to perform a more detailed analysis of water flow in the soil-root domain. The LTI datasets have been used as inputs of the model R-SWMS and, in return, the model gave access to variables that were not accessible experimentally such as the distribution of water potential values in the root system xylem or the distribution of water uptake sites.

Limitations

The first limitation of the LTI technique is the nature of the substrate. The substrate has to be completely white to allow an efficient transmission of light and, at the same time, must have a reasonably good water retention curve. The better compromise, according to Garrigues et al. (2006), is a mixture of 98.5% of white sand and 1.5% of white clay. It provides a satisfactory relationship between transmitted light and soil water content, but has a very steep water retention curve that makes it very different from most European soils.

A second limitation lies in the intrinsic soil heterogeneity observed in the rhizotrons. Although the filling process was optimized to ensure a uniform compaction, small compaction variations were observed in the rhizotrons at the end of the experiment. Such heterogeneity precludes the use of water content distribution analysis at small scales (e.g. sub-centimeter scale).

A third limitation results from the need of detailed root system architecture characterization. The split-and-combine method (§4) was designed for this analysis. However, the time required to scan and trace the different root systems is substantial and is a limitation for larger throughput.

Finally, the technique gives access to the distribution of water content in the soil, but not to water fluxes *per se* (see §7). This limitation can be overcome by using a soil-root water flow models during the analysis, but comes at an heavy computational cost that severely limits the number of plants that can be analyzed.

Perspectives

Given its different drawbacks, we envision two desirable evolutions for the LTI technique: (1) a greater degree of automation would enable its use for genetic studies and (2) a better coupling with water flow models would make it suitable for in-depth water uptake dynamic studies.

11. GENERAL DISCUSSION

Genetic studies

Genetic studies focusing on drought resistance traits often use either global measurements of soil water content (Henry et al., 2012; Schopach, Sadok, 2012; Tuberosa, 2012) or 1D water content profile (Hund et al., 2009; Vandoorne et al., 2012) to determine the level of water shortage experienced by the plant. However, these methods are likely to neglect the effect of local soil water depletion on the plant physiology (Dodd et al., 2010; Sobeih et al., 2004). The LTI technique ensures the rapid acquisition of 2D soil water content profiles and therefore enables a better characterisation of the stress perceived by the plants. As such, we believe it could be used in genetic studies focussed on drought resistance.

In this regard, the main perspective concerning the light transmission imaging techniques concerns the level of automation of the image acquisition process. In this project, we scaled up the LTI experiment from 6 to 20 plants. Moving further, it should be possible to automate the data acquisition steps by building a robot, similar to the one presented by Nagel et al. (2012). This would allow the monitoring of a greater number of plants with enhanced temporal resolution.

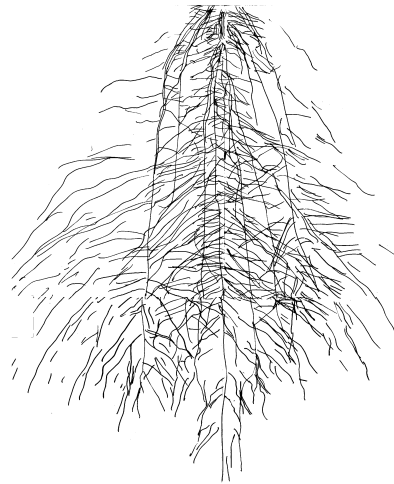


Figure 11.3: Manual root drawing

As discussed above, root system architectures were characterized using a time-consuming technique. We believe the level of details obtained with this method was not necessarily required for the type of analysis performed here. In order to streamline the root architecture acquisition step, we propose to use the data contained in root drawings made during the experiment (fig. 11.3). The analysis of such drawings could be fully automated using either in-house ImageJ macro or any other available software such as GiARoots (Galkovskyi et al., 2012).

In-depth studies of water uptake dynamics

The high resolution of the 2D soil water content profiles makes LTI suitable for in-depth analysis of water uptake dynamics and soil-root interactions. However, as discussed earlier, the main drawback to such analysis is that it does not enable the observation of water flow *per se*, but rather the distribution of water content in the soil.

In this regard, the main perspective would be to integrate the model-based analysis in the analysis workflow to be able to infer differences in water uptake dynamics from the observed soil water content variations. This integration would require a greater computational capacity or a faster water flux resolution algorithm such as the one proposed by Couvreur et al. (2012). In addition to the improvement of the model, more experimental measurements are needed for its calibration. In this respect, the water potential at the plant collar would be a valuable information.

11.3 Modeling water flow in the Soil-Plant-Atmosphere Continuum

Plant models are becoming more popular in plant science (Tardieu, 2010). They have the potential to help untangle complex mechanisms and explore new breeding strategies (Hammer et al., 2010).

Advances

We developed a new model, PlaNet-Maize, that simulates the growth and development of an entire maize plant as well as water fluxes in the soil-plant-atmosphere continuum. This model was the first attempt, to our knowledge, to simulate explicitly the flow of water and its regulation in the entire plant down to the segment level.

In this thesis, PlaNet-Maize was used to investigate the quantitative contribution of different plant features in the uptake process. More precisely, the model was used to evaluate the influence of the root system size (relative to the shoot) and the regulation of hydraulic properties (in the shoot and the roots) on the water uptake dynamics.

Limitations

The main limitation encountered during the model construction was the lack of quantitative data available in the literature. While most of the processes implemented in the model have been extensively studied, the majority of these studies did not contain usable quantitative data. As a result, most of the biological relationships used in the model might not be accurate. As an example, the effect of cavitation was implemented at the article (sub-organ) level. However, this level of resolution was rarely obtained experimentally, forcing us to use sensitivity curves obtained at the plant level in the model implementation. Such down-scaling might be the cause of errors.

At several occasions, the model failed to reproduce experimental results. Firstly, the isohydric behavior observed in maize plant was not observed in our simulations (the leaf and root water potentials followed closely the one of the soil). Moreover, the model failed to reproduce the effect of partial root zone drying on the plant transpiration and growth. Finally, the implementation of ABA production and transport as a long distance signal did not produce the expected results.

Perspectives

Model development

At the current stage of development of the model, the principal perspective in the de model development lies in the validation of its different processes. As stated earlier, the majority of the relations used in the different modules were observed at the plant level but implemented at the local level. As a consequence, a more robust validation of the model, and more precisely of its water module is required.

Secondly, the lack of experimental data at the organ scale highlights the need for additional experimental characterisation of the plant response to its environment. Although we are aware that such quantification might be technically challenging, highly time-consuming and might lack the interest of more qualitative research, it would prove to be highly valuable for the model-assisted understanding of the most prominent aspects of water flow regulation and the design of water-saving genotypes for a range of environmental scenarios.

Regarding the implementation of the abscisic acid module (production, transport and effects), our first simulation results indicated that the implemented production and degradation rates did not support a root-to-shoot signaling based on ABA. A sensitivity analysis on these rates would clarify whether these results are due to inadequate production and degradation rates or derive from other aspects of the model conception.

Finally, the current carbon implementation is based on global production and distribution rules and does not take advantage of the object-oriented structure of PlaNet-Maize. An explicit implementation of the carbohydrates fluxes, similarly as in previous models (Drouet, Pagès, 2003, 2007), would enable a more realistic carbon allocation and, if required, the addition of phloem-based, shoot-to-root signaling processes (e.g. auxins).

Model applications

As pointed out by Tardieu (2010), although plant and crop models are now commonly used to evaluate global process (transpiration, production, etc) at the field level, their use in plant biology is still in its infancy.

We believe PlaNet-Maize is a useful tool that can address a wide range of biological questions. The use of the model enables the simultaneous observation of all plant variables and states. As a direct consequence, the interplay between different plant regulation mechanisms, that is challenging to record experimentally, can be easily observed using the model. Moreover, given a robust validation, the model could be used to investigate new research paths at a minimal cost and provide insights on future experimental needs (Postma, Lynch, 2011a,b).

Finally, the comprehensive interface provided by CrossTalk makes PlaNet-Maize a potential educational tool for plant biology students. By changing the set of available variables in the CrossTalk interface, one can design the model to fit specific teaching purposes and provide additional tools to the students. Moreover, the different relations implemented in the model can be presented and serve as basis for more quantitative physiological discussions.

11.4 Quantification of the influence of root architecture

Root system architecture plays a central role in the acquisition of water. It is often thought as setting an upper limit to the amount of water that can be extracted because it delineates the volume of soil explored by the plant (King et al., 2003; Lobet et al., 2012).

Advances

In this thesis, we used the light transmission imaging technique (LTI) to link changes in soil water content explicitly with various root architectural features, ranging from the root system size to the distribution of roots in different soil layers. The effect of root system size was also addressed using the model PlaNet-Maize.

Our results highlighted the fact that the changes in water content in the top soil layers (2/3 of the rhizotrons) were not (or only slightly) influenced by the different root architectural features. This seems consistent with the fact that, for all the plants used in the analysis, the quantity of roots in the top soil layers was sufficient to extract all the needed water. According to Passioura (1983) 1 cm of root length is sufficient to extract all the water contained in 1 cm³ of soil, a density that was reached by most plants in the top soil layers.

However, large differences were observed in the bottom layer of the rhizotrons. The presence and the proportion of roots at depth was positively correlated with the decrease in water content in this soil layer. More interestingly, our results showed that the soil water content decrease associated with deep-rooted plants was more evenly distributed vertically. It was hypothesized that, as a consequence, water depletion in the rhizosphere would be delayed, allowing a better water redistribution in the soil. More than just permitting the access to water in the bottom soil layers (Hammer et al., 2009; Henry et al., 2012; Kashiwagi et al., 2006; Shen et al., 2001; Steele et al., 2007), deep root systems enable a better distribution of the decrease in SWC and secure the hydraulic conductivity of the vulnerable rhizospheric compartment (Carminati et al., 2012, 2009).

The contribution of root system size was also tested using PlaNet-Maize. Simulation results highlighted the necessity to maintain some size allometry between the root and the shoot. More precisely, the root-to-shoot surface ratio has been shown to influence the water potential balance in the plant. If the root system is undersized compared to the shoot, the transpiration demand set by the leaves might not be satisfied and the tension in the xylem is likely to increase, making it more susceptible to cavitation. These results are consistent with previous experimental observations (Hacke et al., 2000; Sperry, Saliendra, 1994).

Limitations

Although the plants used in our study presented a large variability in the different root traits, it would have been interesting to use genotypes having known contrasted root architectures. Additionally, the use of architectural mutants would have brought more contrasted variations. It has to be noted that lateral-rootless mutants (lrt1, Hochholdinger, Feix (1998)) were tested in our experimental setup but failed to grow successfully .

A second limitation in this study was the lack of data about the hydraulic properties of the different plants. As we have discussed in the chapter 1, root radial conductance and axial conductivity are likely to have an influence on the water uptake patterns (Draye et al., 2010; Wasson et al., 2012). Having conductivity values of root segments, or at the root system level would have brought useful additional informations in the analysis.

11.5 Quantification of the influence of root hydraulic properties

Root hydraulic properties are thought to play an important role in the distribution of water uptake along the root system (Draye et al., 2010; Wasson et al., 2012). Unfortunately, evaluating their quantitative importance is difficult because they are thought to be highly variable in space (from one root segment to another, Hachez et al. (2006); Pockman, Sperry (2000)) and in time (maturation of root segment, regulation, Hachez et al. (2012); Sperry et al. (1988b)).

Advances

In this thesis, the contribution of root hydraulic properties in the water uptake process was approached using the models R-SWMS and PlaNet-Maize.

Using R-SWMS

Firstly, we used the model R-SWMS to reproduce soil water content patterns observed experimentally. In this regard, different hypotheses were tested, including varying root radial and axial hydraulic properties. These changes triggered noticeable modifications in the water potential distribution in the root system. Decreasing the root radial conductance increased significantly the tension inside the xylem, while the onset of cavitation had the opposite effect. These data confirm previously observed results (Doussan et al., 1998; Doussan et al., 2006; Draye et al., 2010).

However, despite these changes, only small differences were observed between the different soil water content profiles and root uptake patterns. Because the soil used in the experiment had a very steep conductivity curve, it is likely that the limiting step to the water flow in the soil-root system was the low soil conductivity. In that case, changes in the root hydraulic properties would not affect the overall system. As a result, the validation of the different simulations was not possible based only on the soil water content distribution.

Using Planet-Maize

Secondly, we attempted to quantify the importance of the different regulatory processes affecting the local hydraulic conductivities of the plant. Using PlaNet-Maize, we could simultaneously observe and compare the changes in root radial conductance, xylem axial conductivity and leaf conductance.

Not surprisingly, the regulation of the leaf conductance had the largest effect on the plant water status. By controlling the quantity of water lost in the atmosphere, the stomata remains the master control of the water flow in the soil-plant-atmosphere continuum. However, the other regulations sites had a non negligible influence on the system. The reduction in root radial conductance or xylem conductivity led to decreases in the xylem water potential that triggered the closure of the stomata. Increasing the sensibility of either regulation sites (faster response under decreasing water potential) triggered faster decreases of xylem potential, faster transpiration reductions and a more conservative use of the water resources.

These results suggest that modifying root hydraulic properties can have an effect on the plant water management strategies. However, the influence of soil conductivity and stomata regulation should not be forgotten since, in many situations, they might have a much larger influence on the global flow. As a result, our simulations suggest that the regulation of root hydraulic conductivities should not be regarded as a way to control the flow in the SPAC (although it does in some circumstances) but rather as a way to adjust the sites of water uptake as a function of the environment.

Limitations

The different functions implemented to simulate the hydraulic regulation of the plant, either in R-SWMS or PlaNet-Maize, were kept very simple. While these simplifications ensured a fast computation and an easier interpretation of the different results, they might have produced inaccurate results.

Additionally, the lack of quantitative data found in the literature concerning the distribution and variations of root hydraulic properties in the root system forced us to use many a priori parameter values in the model water flux implementation.

11.6 Quantification of the influence of long distance signaling

Long distance root-shoot signaling processes are essential for the plant water management since they inform the shoot organs from potential soil water shortage. Among the existing signals, differences in xylem water potential and abscissic acid are thought to be predominant players (Tardieu, Davies, 1993).

Advances

The quantitative role of ABA as a long distance signal between the root and the shoot was assessed using the model PlaNet-Maize.

Several functions of ABA production, degradation, transport and effect are available in the literature. We implemented these functions in the PlaNet-Maize architecture and used model simulations to evaluate if this core of functions and available data supports a long distance contribution of ABA to the regulation of water flow. Although the ABA module seemed to correctly influence water flow dynamics in the plant, further investigations revealed that the amount of root-supplied ABA reaching the leaves would be negligible compared to the leaf-supplied ABA.

Limitations

The ABA dynamics in the plant is far more complex than its current implementation in PlaNet-Maize. As an example, recent work have highlighted the role of other forms of ABA, such as the ABA-GE (Jiang, Hartung, 2008; Lee et al., 2006; Schroeder, Nambara, 2006), in the transmission of the signal from the shoot to the leaves. In PlaNet-Maize, the absence of such alternative form of ABA transport and the short half-life of ABA molecules in the xylem might be the reason for the lack of long-distance signaling. In this case, the existence of ABA-GE in the xylem might be simulated by changing the ABA degradation kinetics.

CONCLUSIONS

12

In conclusion, the creation of new tools and methods opened new avenues for the observation and analysis of water flow in the soil-plant-atmosphere continuum.

Firstly, the creation of SmartRoot, coupled with a new experimental setup (based on the light transmission imaging technique) allowed the parallel monitoring of root system architecture and soil water content. Secondly, the coupling of the soil-root model R-SWMS and a new functional structural plant model, PlaNet-Maize , enabled the quantification of yet unexplored aspects of water uptake from experimental results.

From an experimental point of view, the use of the different techniques highlighted the importance of different root features as regulatory elements of the water flow in the system. More precisely, the root system architecture and the root hydraulic properties were shown to be able to finely influence the uptake process in response to changes in the soil environment.

More generally, this thesis highlighted the need for integrated approaches for the analysis of water flow in the soil-plant-atmosphere continuum. An explicit consideration of all plant and soil parameters is required if one aims at tailoring the water uptake dynamics of a given plant/environment association.

GENERAL BIBLIOGRAPHY

1. Abramoff, M. D., Magalhães, P. J., Ram, S. J. (2004). Image processing with ImageJ. *Biophotonics international*, 11, 36–42 (cit. on p. 55).
2. Alexandersson, E, Fraysse, L, Sjøvall-Larsen, S, Gustavsson, S, Fellert, M, Karlsson, M, Johanson, U, Kjellbom, P (2005). Whole gene family expression and drought stress regulation of aquaporins. *Plant Molecular Biology*, 59, 469–484 (cit. on p. 30).
3. Allen, L. H., Jr., Kakani, V. G., Vu, J. C. V., Boote, K. J. (2011). Elevated CO₂ increases water use efficiency by sustaining photosynthesis of water-limited maize and sorghum. *Journal of Plant Physiology*, 168, 1909–1918 (cit. on p. 145).
4. Aravena, J. E., Berli, M., Ghezzehei, T. A., Tyler, S. W. (2011). Effects of Root-Induced Compaction on Rhizosphere Hydraulic Properties - X-ray Microtomography Imaging and Numerical Simulations. *Environmental Science & Technology*, 45, 425–431 (cit. on p. 26).
5. Armengaud, P, Zambaux, P, Hills, A, Sulpice, R, Pattison, R. J., Blatt, M. R., Amtmann, A (2009). EZ-Rhizo: integrated software for the fast and accurate measurement of root system architecture. *The Plant Journal*, 57, 945–956 (cit. on pp. 52, 53, 186).
6. Aroca, R, Porcel, R, Ruiz-Lozano, J. M. (2011). Regulation of root water uptake under abiotic stress conditions. *Journal of Experimental Botany*, 63, 43–57 (cit. on p. 21).
7. Aroca, R, Ferrante, A, Vernieri, P, Chrispeels, M. J. (2006). Drought, Abscisic Acid and Transpiration Rate Effects on the Regulation of PIP Aquaporin Gene Expression and Abundance in *Phaseolus vulgaris* Plants. *Annals of Botany*, 98, 1301–1310 (cit. on p. 31).
8. Arsenault, J.-L., Poulcur, S, Messier, C, Guay, R (1995). Win-RHIZO, a Root-measuring System with a Unique Overlap Correction Method. *HortScience*, 30, 906 (cit. on pp. 10, 52, 53, 76).

GENERAL BIBLIOGRAPHY

9. Arya, L., Farrell, D., Blake, G. (1975). Field Study of Soil-Water Depletion Patterns in Presence of Growing Soybean Roots .1. Determination of Hydraulic Properties of Soil. *Soil Science Society of America Journal*, 39, 424–430 (cit. on pp. 27, 39).
10. Band, L. R., Fozard, J. A., Godin, C, Jensen, O. E., Pridmore, T, Bennett, M. J., King, J. R. (2012). Multiscale Systems Analysis of Root Growth and Development: Modeling Beyond the Network and Cellular Scales. *The Plant Cell* (cit. on p. 165).
11. Barthelemy, D, Caraglio, Y (2007). Plant Architecture: A Dynamic, Multilevel and Comprehensive Approach to Plant Form, Structure and Ontogeny. *Annals of Botany*, 99, 375–407 (cit. on p. 184).
12. Basu, P., Pal, A. (2012). A new tool for analysis of root growth in the spatio-temporal continuum. *New Phytologist* (cit. on p. 53).
13. Basu, P., Pal, A., Lynch, J. P., Brown, K. M. (2007). A Novel Image-Analysis Technique for Kinematic Study of Growth and Curvature. *Plant Physiology*, 145, 305 (cit. on p. 53).
14. Ben Haj Salah, H, Tardieu, F (1997). Control of Leaf Expansion Rate of Droughted Maize Plants under Fluctuating Evaporative Demand. *Plant Physiology*, 893–900 (cit. on p. 159).
15. Bernier, J., Serraj, R., Kumar, A., Venuprasad, R., Impa, S., RP, V. G., Oane, R., Spaner, D., Atlin, G. (2009). The large-effect drought-resistance QTL qtl12.1 increases water uptake in upland rice. *Field Crops Research*, 110, 139–146 (cit. on pp. 38, 39, 44, 96, 132).
16. Berntson, G. M., Woodward, F. I. (1992). The Root System Architecture and Development of *Senecio vulgaris* in Elevated CO₂ and Drought. *Functionnal Ecology*, 6, 324–333 (cit. on p. 100).
17. Bibikova, T., Gilroy, S. (2003). Root Hair Development. *Journal of Plant Growth Regulation*, 21, 383–415 (cit. on p. 27).
18. Bidel, L, Pagès, L, Riviere, L, Pelloux, G, Lorendeau, J (2000). MassFlowDyn I: A Carbon Transport and Partitioning Model for Root System Architecture. *Annals of Botany*, 85, 869–886 (cit. on pp. 11, 140).

19. Blum, A (2005). Drought resistance, water-use efficiency, and yield potential—are they compatible, dissonant, or mutually exclusive? *Australian Journal of Agricultural Research*, *56*, 1159–1168 (cit. on p. 5).
20. Bohrer, G, Mourad, H, Laursen, T. A., Drewry, D, Avissar, R, Poggi, D, R, O., Katul, G. G. (2005). Finite element tree crown hydrodynamics model (FETCH) using porous media flow within branching elements: a new representation of tree hydrodynamics. *Water Resources Research*, *41*, 1–17 (cit. on p. 150).
21. Borisjuk, L, Rolletschek, H, Neuberger, T. (2012). Surveying the plant's world by magnetic resonance imaging. *The Plant Journal*, *70*, 129–146 (cit. on p. 41).
22. Boursiac, Y., Boudet, J., Postaire, O., Luu, D.-T., Tournaire-Roux, C., Maurel, C. (2008). Stimulus-induced downregulation of root water transport involves reactive oxygen species-activated cell signalling and plasma membrane intrinsic protein internalization. *The Plant Journal*, *56*, 207–218 (cit. on p. 31).
23. Boyer, J. S. *Measuring the water status of plants and soils*; Academic Press, 1995 (cit. on p. 37).
24. Bramley, H., Turner, N., Turner, D., Tyerman, S. D. (2009). Roles of Morphology, Anatomy, and Aquaporins in Determining Contrasting Hydraulic Behavior of Roots. *Plant Physiology*, *150*, 348–364 (cit. on pp. 28, 30, 96, 150).
25. Burton, A. L., Williams, M, Lynch, J. P., Brown, K. M. (2012). RootScan: Software for high-throughput analysis of root anatomical traits. *Plant and Soil* (cit. on p. 53).
26. Busch, J, Mendelssohn, I. A., Lorenzen, B, Brix, H, Miao, S (2006). A rhizotron to study root growth under flooded conditions tested with two wetland Cyperaceae. *Flora*, *201*, 429–439 (cit. on pp. 67, 100).
27. Carminati, A, Vetterlein, D, Koebernick, N, Blaser, S, Weller, U, Vogel, H.-J. (2012). Do roots mind the gap? *Plant and Soil* (cit. on pp. 127, 195).
28. Carminati, A, Moradi, A. B., Vetterlein, D, Vontobel, P, Lehmann, E. H., Weller, U, Vogel, H, Oswald, S. E. (2010). Dynamics of soil water content in the rhizosphere. *Plant and Soil*, *332*, 163–176 (cit. on pp. 10, 41, 116).

GENERAL BIBLIOGRAPHY

29. Carminati, A, Schneider, C. L., Moradi, A. B., Zarebanadkouki, M., Vetterlein, D., Vogel, H., Hildebrandt, A., Weller, U., Schueler, L., Oswald, S. E. (2011). How the Rhizosphere May Favor Water Availability to Roots. *Vadose Zone Journal*, 10, 988–998 (cit. on p. 26).
30. Carminati, A, Vetterlein, D., Weller, U., Vogel, H.-J., Oswald, S. E. (2009). When Roots Lose Contact. *Vadose Zone Journal*, 8, 805–809 (cit. on pp. 27, 51, 127, 195).
31. Cassiani, G, Bruno, V, Villa, A, Fusi, N (2006). A saline trace test monitored via time-lapse surface electrical resistivity tomography. *Journal of Applied Geophysics*, 59, 244–259 (cit. on p. 99).
32. Chaumont, F, Moshelion, M (2005). Regulation of plant aquaporin activity. *Biology of the Cell*, 97, 749–764 (cit. on pp. 22, 30, 31, 127).
33. Cheng, W, Coleman, D. C., Box, J. E. (1991). Measuring root turnover using the minirhizotron technique. *Agriculture, Ecosystems & Environment*, 34, 261–267 (cit. on pp. 67, 100).
34. Christman, M. A., Sperry, J. S., Smith, D. D. (2012). Rare pits, large vessels and extreme vulnerability to cavitation in a ring-porous tree species. *New Phytologist*, 193, 713–720 (cit. on p. 34).
35. Christmann, A, Weiler, E. W., Steudle, E, Grill, E. (2007). A hydraulic signal in root-to-shoot signalling of water shortage. *The Plant Journal*, 52, 167–174 (cit. on p. 167).
36. Clark, R, MacCurdy, R, Jung, J, Shaff, J, McCouch, S. R., Aneshansley, D, Kochian, L (2011). 3-Dimensional Root Phenotyping with a Novel Imaging and Software Platform. *Plant Physiology* (cit. on p. 52).
37. Clark, R. T., Famoso, A. N., Zhao, K., Shaff, J. E., Craft, E. J., Bustamante, C. D., McCouch, S. R., Aneshansley, D. J., Kochian, L. V. (2012). High-throughput 2D root system phenotyping platform facilitates genetic analysis of root growth and development. *Plant, Cell and Environment*, no–no (cit. on pp. 52, 53, 186).
38. Clearwater, M. J., Goldstein, G. In *Vascular Transport in Plants*; Holbrook, N. M., Zwieniecki, M. A., Eds.; Elsevier Academic Press: London, 2005, pp 375–399 (cit. on p. 35).

39. Cochard, H (2002). Xylem embolism and drought-induced stomatal closure in maize. *Planta*, *215*, 466–471 (cit. on pp. 33, 150).
40. Cochard, H, Casella, E, Mencuccini, M (2007). Xylem vulnerability to cavitation varies among poplar and willow clones and correlates with yield. *Tree Physiology*, *27*, 1761–1767 (cit. on p. 33).
41. Cochard, H, Venisse, J.-S., Barigah, T. S., Brunel, N., Herbette, S., Guilliot, A., TYREE, M. T., Sakr, S. (2007). Putative role of aquaporins in variable hydraulic conductance of leaves in response to light. *Plant Physiology*, *143*, 122–133 (cit. on p. 29).
42. Couvreur, V, Vandenberg, J, Javaux, M (2012). A simple three-dimensional macroscopic root water uptake. *Hydrology and Earth System Sciences*, 1–39 (cit. on pp. 87, 117, 120, 157, 191).
43. Czarnes, S., Hallett, P. D., Bengough, A. G., Young, I. M. (2000). Root- and microbial-derived mucilages affect soil structure and water transport. *European Journal of Soil Science*, *51*, 435–443 (cit. on p. 26).
44. Damour, G., Simonneau, T, Cochard, H, Urban, L. (2010). An overview of models of stomatal conductance at the leaf level. *Plant, Cell and Environment*, *33*, 1419–1438 (cit. on p. 139).
45. Darrah, P. R. (1993). The rhizosphere and plant nutrition: a quantitative approach. *Plant and Soil*, *155-156*, 1–20 (cit. on p. 26).
46. Davies, W. J., Zhang, J (1991). Root Signals and the Regulation of Growth and Development of Plants in Drying Soil. *Annual Review of Plant Physiology and Plant Molecular Biology*, *42*, 55–76 (cit. on p. 167).
47. de Dordodot, S, Forster, B, Pagès, L, Price, A, Tuberosa, R, Draye, X. (2007). Root system architecture: opportunities and constraints for genetic improvement of crops. *TRENDS in Plant Science*, *12*, 474–481 (cit. on pp. 39, 44, 51, 52, 187).
48. de Smet, I, Zhang, H, Inzé, D, Beeckman, T (2006). A novel role for abscisic acid emerges from underground. *TRENDS in Plant Science*, *11*, 434–439 (cit. on pp. 51, 167).
49. Delzon, S, Douthe, C, Sala, A, Cochard, H (2010). Mechanism of water-stress induced cavitation in conifers: bordered pit structure and function support the hypothesis of seal capillary-seeding. *Plant, Cell and Environment*, *33*, 2101–2111 (cit. on p. 34).

GENERAL BIBLIOGRAPHY

50. Devienne-Baret, F, Richard-Molard, C, Chelle, M, Maury, O, Ney, B (2006). Ara-rhizotron: An effective culture system to study simultaneously root and shoot development of Arabidopsis. *Plant and Soil*, 280, 253–266 (cit. on p. 100).
51. Dexter, A. (1987). Compression of Soil Around Roots. *Plant and Soil*, 97, 401–406 (cit. on p. 26).
52. Diggle, A. J. (1988). ROOTMAP—a model in three-dimensional coordinates of the growth and structure of fibrous root systems. *Plant and Soil*, 105, 169–178 (cit. on pp. 11, 140).
53. Dodd, I. C. (2005). Root-To-Shoot Signalling: Assessing The Roles of ‘Up’ In the Up and Down World of Long-Distance Signalling In Planta. *Plant and Soil*, 274, 251–270 (cit. on p. 13).
54. Dodd, I. C. (2007). Soil moisture heterogeneity during deficit irrigation alters root-to-shoot signalling of abscisic acid. *Functional Plant Biology*, 34, 439–448 (cit. on p. 158).
55. Dodd, I. C., Egea, G, Davies, W. J. (2008). Abscisic acid signalling when soil moisture is heterogeneous: decreased photoperiod sap flow from drying roots limits abscisic acid export to the shoots. *Plant, Cell and Environment*, 31, 1263–1274 (cit. on pp. 168, 176).
56. Dodd, I. C., Egea, G, Watts, C. W., Whalley, W. R. (2010). Root water potential integrates discrete soil physical properties to influence ABA signalling during partial rootzone drying. *Journal of Experimental Botany*, 61, 3543–3551 (cit. on pp. 42, 190).
57. Doussan, C, Pagès, L, Vercambre, G (1998). Modelling of the hydraulic architecture of root systems: An integrated approach to water absorption - Model description. *Annals of Botany*, 81, 213–223 (cit. on pp. 23, 38, 96, 197).
58. Doussan, C, Vercambre, G, Pagès, L (1998). Modelling of the hydraulic architecture of root systems: and integrated approach to water absorption - Distribution of axial and radial conductances in maize. *Annals of Botany*, 81, 225–232 (cit. on pp. 6, 37, 41, 120, 148).
59. Doussan, C, Pierret, A, Garrigues, E, Pagès, L (2006). Water Uptake by Plant Roots: II – Modelling of Water Transfer in the Soil Root-system with Explicit Account of Flow within the Root System – Comparison with Experiments. *Plant and Soil*, 283, 99–117 (cit. on pp. 38, 41, 147, 148, 197).

60. Downie, H, Holden, N, Otten, W, Spiers, A. J., Valentine, T. A., Dupuy, L (2012). Transparent Soil for Imaging the Rhizosphere. *PLoS ONE*, 7 (cit. on p. 51).
61. Draye, X., Pagès, L (2006). CrossTalk: a simulation platform for the linking of existing soil, plant and atmosphere models. *IEEE-Conference Proceeding Service, PM06*, 95–100 (cit. on p. 142).
62. Draye, X., Kim, Y., Lobet, G., Javaux, M. (2010). Model-assisted integration of physiological and environmental constraints affecting the dynamic and spatial patterns of root water uptake from soils. *Journal of Experimental Botany*, 61, 2145–2155 (cit. on pp. 12, 21, 27, 38, 40, 42, 43, 51, 85, 96, 133, 140, 154, 157, 158, 161, 164, 196, 197).
63. Drouet, J.-L., Pagès, L (2003). GRAAL: a model of GRowth, Architecture and carbon ALlocation during the vegetative phase of the whole maize plant. Model description and parametrisation. *Ecological Modelling*, 165, 143–173 (cit. on pp. 11, 140, 144–147, 193).
64. Drouet, J.-L., Pagès, L (2007). GRAAL-CN: A model of GRowth, Architecture and ALlocation for Carbon and Nitrogen dynamics within whole plants formalised at the organ level. *Ecological Modelling*, 206, 231–249 (cit. on pp. 146, 193).
65. Duan, H, Schuler, M. A. (2005). Differential expression and evolution of the Arabidopsis CYP86A subfamily. *Plant Physiology*, 137, 1067–1081 (cit. on p. 32).
66. Dupriez, M Effet combiné de la croissance racinaire et de la prise d'eau: comparaison entre modélisation avec le logiciel RSWMS et observation sur rhizotrons. MA thesis, Université catholique de Louvain, 2009 (cit. on p. 237).
67. Efetova, M., Zeier, J., Riederer, M., Lee, C.-W., Stingl, N., Mueller, M., Hartung, W., Hedrich, R., Deeken, R. (2007). A Central Role of Abscisic Acid in Drought Stress Protection of Agrobacterium-Induced Tumors on Arabidopsis. *Plant Physiology*, 145, 853–862 (cit. on p. 32).
68. Ehlert, C., Maurel, C., Tardieu, F, Simonneau, T (2009). Aquaporin-Mediated Reduction in Maize Root Hydraulic Conductivity Impacts Cell Turgor and Leaf Elongation Even without Changing Transpiration. *Plant Physiology*, 150, 1093–1104 (cit. on p. 127).

69. Enstone, D. E., Peterson, C. A. (2005). Suberin lamella development in maize seedling roots grown in aerated and stagnant conditions. *Plant, Cell and Environment*, *28*, 444–455 (cit. on p. 29).
70. Enstone, D. E., Peterson, C. A., Ma, F. (2003). Root Endodermis and Exodermis: Structure, Function, and Responses to the Environment. *Journal of Plant Growth Regulation*, *21*, 335–351 (cit. on pp. 22, 29, 96, 139).
71. Esau, K *Plant Anatomy*, Second Edition; John Wiley & Sons: New York, 1965 (cit. on p. 26).
72. Eshel, A, Waisel, Y. In *Plant Roots: The Hidden Half*; Waisel, Y, Eshel, A, Kafkafi, U, Eds.; Marcel Dekker, Inc, 1996 (cit. on pp. 37, 74).
73. Esser, H. G., Carminati, A, Vontobel, P, Lehmann, E. H., Oswald, S. E. (2010). Neutron radiography and tomography of water distribution in the root zone. *Journal of Plant Nutrition and Soil Science*, *173*, 757–764 (cit. on pp. 41, 99, 188).
74. Fan, M., Bai, R., Zhao, X., Zhang, J (2007). Aerenchyma Formed Under Phosphorus Deficiency Contributes to the Reduced Root Hydraulic Conductivity in Maize Roots. *Journal of Integrative Plant Biology*, *49*, 598–604 (cit. on p. 28).
75. Fitter, A. H. (1987). An Architectural Approach to the Comparative Ecology of Plant Root Systems. *New Phytologist*, *106*, 61–77 (cit. on pp. 184, 187).
76. Fournier, C, Andrieu, B (1998). A 3D Architectural and Process-based Model of Maize Development. *Annals of Botany*, *81*, 233–250 (cit. on p. 140).
77. French, A. P., Ubeda-Tomas, S., Holman, T., Bennett, M., Pridmore, T. (2009). High-Throughput Quantification of Root Growth Using a Novel Image-Analysis Tool. *Plant Physiology*, *150*, 1784–1795 (cit. on pp. 52, 53).
78. French, A. P., Wilson, M. H., Kenobi, K., Dietrich, D., Voss, U., Ubeda-Tomas, S., Pridmore, T. P., Wells, D. M. (2012). Identifying biological landmarks using a novel cell measuring image analysis tool: Cell-o-Tape. *Plant Methods*, *8*, 7 (cit. on p. 53).
79. Frensch, J, Steudle, E (2007). Axial and radial hydraulic resistance to roots of maize. *Plant Physiology*, *91*, 719–726 (cit. on p. 12).

80. Galkovskyi, T., Mileyko, Y., Bucksch, A., Moore, B., Symonova, O., Price, C. A., Topp, C. N., Iyer-Pascuzzi, A. S., Zurek, P. R., Fang, S., Harer, J., Benfey, P. N., Weitz, J. S. (2012). GiA Roots: software for the high throughput analysis of plant root system architecture. *BMC Plant Biology*, *12*, 116 (cit. on pp. 53, 82, 83, 186, 191).
81. Gardner, W. R. (1965). Dynamic Aspects of Soil-Water Availability to Plants. *Annual Review of Plant Physiology*, *16*, 323–342 (cit. on pp. 25, 85).
82. Gardner, W., Ehlig, C. (1962). Some Observations on Movement of Water to Plant Roots. *Agronomy Journal*, *54*, 453–456 (cit. on pp. 27, 39).
83. Garrigues, E (2002). Prélèvements hydriques par une architecture racinaire; imagerie quantitative et modelisation des transferts d'eau dans le système sol-Plante. *INRA*, 143 (cit. on pp. 103, 120).
84. Garrigues, E, Doussan, C, Pierret, A (2006). Water uptake by plant roots: I - Formation and propagation of a water extraction front in mature root systems as evidenced by 2D light transmission imaging. *Plant and Soil*, *283*, 83–98 (cit. on pp. 10, 12, 41, 79, 80, 85, 90, 99, 102, 103, 107, 116, 118, 121, 188, 189).
85. Ge, Z, Rubio, G., Lynch, J. P. (2000). The importance of root gravitropism for inter-root competition and phosphorus acquisition efficiency: results from a geometric simulation model. *Plant and Soil*, *218*, 159–171 (cit. on pp. 11, 51, 52, 85, 140, 187).
86. Gilroy, S., Jones, D. L. (2000). Through form to function: root hair development and nutrient uptake. *TRENDS in Plant Science*, *5*, 56–60 (cit. on p. 27).
87. Godin, C, Sinoquet, H (2005). Functional-structural plant modelling. *New Phytologist*, *166*, 705–708 (cit. on pp. 11, 46).
88. Gregory, P. J., Ingram, J. S. I., Brklacich, M (2005). Climate change and food security. *Philosophical Transactions of the Royal Society B: Biological Sciences*, *360*, 2139–2148 (cit. on p. 5).
89. Guidi, G., Poggio, G., Petruzzelli, G. (1985). The Porosity of Soil Aggregates from Bulk Soil and from Soil Adhering to Roots. *Plant and Soil*, *87*, 311–314 (cit. on p. 26).

GENERAL BIBLIOGRAPHY

90. Hachez, C, Moshelion, M, Zelazny, E, Cavez, D, Chaumont, F (2006). Localization and quantification of plasma membrane aquaporin expression in maize primary root: a clue to understanding their role as cellular plumbers. *Plant Molecular Biology*, 62, 305–323 (cit. on pp. 29, 30, 32, 37, 197).
91. Hachez, C, Veselov, D., Ye, Q, Reinhardt, H., Knipfer, T, Fricke, W, Chaumont, F (2012). Short-term control of maize cell and root water permeability through plasma membrane aquaporin isoforms. *Plant, Cell and Environment*, 35, 185–198 (cit. on pp. 29–32, 197).
92. Hacke, U. G., Jansen, S (2009). Embolism resistance of three boreal conifer species varies with pit structure. *New Phytologist*, 182, 675–686 (cit. on p. 34).
93. Hacke, U. G., Sauter, J. J. (1996). Drought-Induced Xylem Dysfunction in Petioles, Branches, and Roots of *Populus balsamifera* L. and *Alnus glutinosa* (L.) Gaertn. *Plant Physiology*, 111, 413–417 (cit. on p. 34).
94. Hacke, U. G., Sperry, J. S. (2003). Limits to xylem refilling under negative pressure in *Laurus nobilis* and *Acer negundo*. *Plant, Cell and Environment*, 26, 303–311 (cit. on p. 35).
95. Hacke, U. G., Sperry, J. S., Pittermann, J. J. (2000). Drought experience and cavitation resistance in six shrubs from the Great Basin, Utah. *Basic and Applied Ecology*, 1 (cit. on pp. 34, 95, 155, 196).
96. Hacke, U. G., Stiller, V, Sperry, J. S., Pittermann, J. J., McCulloh, K. A. (2001). Cavitation fatigue. Embolism and refilling cycles can weaken the cavitation resistance of xylem. *Plant Physiology*, 125, 779–786 (cit. on p. 34).
97. Hacke, U. G., Sperry, J. S., Ewers, B. E., Ellsworth, D. S., Schäfer, K. V. R., RR, O. (2000). Influence of soil porosity on water use in *Pinus taeda*. *Oecologia*, 124, 495–505 (cit. on pp. 34, 151).
98. Hackett, C, Rose, D. A. (1972). A model of the Extension and Branching of a Seminal Root of Barley, and Its Use in Studying Relations Between Root Dimensions. I. The Model. *Australian Journal of Biological Sciences*, 25, 681–690 (cit. on p. 68).

99. Hallett, P. D., Gordon, D. C, Bengough, A. G. (2003). Plant influence on rhizosphere hydraulic properties: direct measurements using a miniaturized infiltrometer. *New Phytologist*, *157*, 597–603 (cit. on p. 26).
100. Hammer, G., Dong, Z., Mclean, G., Doherty, A., Messina, C., Schussler, J., Zinselmeier, C., Paszkiewicz, S., Cooper, M. (2009). Can Changes in Canopy and/or Root System Architecture Explain Historical Maize Yield Trends in the U.S. Corn Belt? *Crop Science*, *49*, 299–312 (cit. on pp. 12, 38, 51, 195).
101. Hammer, G. L., van Oosterom, E., Mclean, G., Chapman, S. C., Broad, I., Harland, P., Muchow, R. C. (2010). Adapting APSIM to model the physiology and genetics of complex adaptive traits in field crops. *Journal of Experimental Botany*, *61*, 2185–2202 (cit. on p. 192).
102. Hedfalk, K, Törnroth-Horsefield, S, Nyblom, M, Johanson, U, Kjellbom, P, Neutze, R (2006). Aquaporin gating. *Current Opinion in Structural Biology*, *16*, 447–456 (cit. on p. 127).
103. Henry, A., Cal, A. J., Batoto, T. C., Torres, R. O., Serraj, R. (2012). Root attributes affecting water uptake of rice (*Oryza sativa*) under drought. *Journal of Experimental Botany* (cit. on pp. 96, 190, 195).
104. Henry, A., Gowda, V. R. P., Torres, R. O., McNally, K. L., Serraj, R. (2011). Variation in root system architecture and drought response in rice (*Oryza sativa*): Phenotyping of the OryzaSNP panel in rainfed lowland fields. *Field Crops Research*, *120*, 205–214 (cit. on pp. 38, 96).
105. Herbette, S, Cochard, H (2010). Calcium Is a Major Determinant of Xylem Vulnerability to Cavitation. *Plant Physiology*, *153*, 1932–1939 (cit. on p. 34).
106. Hinsinger, P., Gobran, G. R., Gregory, P. J., Wenzel, W. W. (2005). Rhizosphere geometry and heterogeneity arising from root-mediated physical and chemical processes. *New Phytologist*, *168*, 293–303 (cit. on p. 26).
107. Hochholdinger, F, Feix, G (1998). Early post-embryonic root formation is specifically affected in the maize mutant lrt1. *The Plant Journal*, *16*, 247–255 (cit. on p. 196).
108. Hochholdinger, F, Park, W. J., Sauer, M, Woll, K (2004). From weeds to crops: genetic analysis of root development in cereals. *TRENDS in Plant Science*, *9*, 42–48 (cit. on pp. 68, 70, 144).

GENERAL BIBLIOGRAPHY

109. Hodge, A, Berta, G, Doussan, C, Merchan, F, Crespi, M (2009). Plant root growth, architecture and function. *Plant and Soil*, 321, 153–187 (cit. on p. 51).
110. Hodge, A. (2004). The plastic plant: root responses to heterogeneous supplies of nutrients. *New Phytologist*, 162, 9–24 (cit. on p. 37).
111. Holbrook, N. M., Zwieniecki, M. (1999). Embolism Repair and Xylem Tension: Do We Need a Miracle? *Plant Physiology*, 120, 7–10 (cit. on pp. 35, 139).
112. Holbrook, N. M., Shashidhar, V, James, R., Munns, R. (2002). Stomatal control in tomato with ABA-deficient roots: response of grafted plants to soil drying. *Journal of Experimental Botany*, 53, 1503 (cit. on p. 167).
113. Hose, E, Clarkson, D, Steudle, E, Schreiber, L, Hartung, W (2001). The exodermis: a variable apoplastic barrier. *Journal of Experimental Botany*, 52, 2245–2264 (cit. on p. 29).
114. Hose, E., Steudle, E, Hartung, W (2000). Abscisic acid and hydraulic conductivity of maize roots: a study using cell- and root-pressure probes. *Planta*, 211, 874–882 (cit. on p. 31).
115. Hund, A, Ruta, N, Liedgens, M (2009). Rooting depth and water use efficiency of tropical maize inbred lines, differing in drought tolerance. *Plant and Soil*, 318, 311–325 (cit. on p. 190).
116. Hund, A, Trachsel, S, Stamp, P (2009). Growth of axile and lateral roots of maize: I development of a phenotyping platform. *Plant and Soil*, 325, 335–349 (cit. on pp. 52, 96).
117. Iyer-Pascuzzi, A., Symonova, O., Mileyko, Y., Hao, Y., Belcher, H., Harer, J., Weitz, J., Benfey, P. N. (2010). Imaging and Analysis Platform for Automatic Phenotyping and Trait Ranking of Plant Root Systems. *Plant Physiology*, 152, 1148–1157 (cit. on p. 52).
118. Jackson, R. B., Sperry, J. S., Dawson, T. E. (2000). Root water uptake and transport: using physiological processes in global predictions. *TRENDS in Plant Science*, 5, 482–488 (cit. on p. 21).

119. Jahnke, S., Menzel, M. I., van Dusschoten, D., Roeb, G. W., Bühler, J., Minwuyet, S., Blümmer, P., Temperton, V. M., Hombach, T., Streun, M., Beer, S., Khodaverdi, M., Ziemons, K., Coenen, H. H., Schurr, U. (2009). Combined MRI-PET dissects dynamic changes in plant structures and functions. *The Plant Journal*, *59*, 634–644 (cit. on pp. 41, 51, 99).
120. Jang, J. Y., Kim, D. G., Kim, Y. O., Kim, J. S., Kang, H (2004). An expression analysis of a gene family encoding plasma membrane aquaporins in response to abiotic stresses in *Arabidopsis thaliana*. *Plant Molecular Biology*, *54*, 713–725 (cit. on p. 30).
121. Janott, M., Gayler, S., Gessler, A., Javaux, M., Klier, C., Priesack, E. (2011). A one-dimensional model of water flow in soil-plant systems based on plant architecture. *Plant and Soil*, *341*, 233–256 (cit. on pp. 140, 150, 164).
122. Jarbeau, J. A., Ewers, F. W., Davis, S. D. (1995). The mechanism of water-stress-induced embolism in two species of chaparral shrubs. *Plant, Cell and Environment*, *18*, 189–196 (cit. on p. 34).
123. Jarvis, N. (2010). Comment on “Macroscopic Root Water Uptake Distribution Using a Matric Flux Potential Approach”. *Vadose Zone Journal*, *9*, 499 (cit. on p. 43).
124. Jarvis, P. G. (1976). The Interpretation of the Variations in Leaf Water Potential and Stomatal Conductance Found in Canopies in the Field. *Philosophical Transactions of the Royal Society B: Biological Sciences*, *273*, 593–610 (cit. on p. 149).
125. Javaux, M., Schroeder, T., Vanderborght, J, Vereecken, H (2008). Use of a three-dimensional detailed modeling approach for predicting root water uptake. *Vadose Zone Journal*, *7*, 1079–1088 (cit. on pp. 12, 38, 41, 87, 117, 120, 140, 147, 148, 165).
126. Javot, H, Maurel, C (2002). The role of aquaporins in root water uptake. *Annals of Botany*, *90*, 301–313 (cit. on pp. 19, 21, 22, 127, 139, 150).
127. Javot, H, Lauvergeat, V, Santoni, V, Martin-Laurent, F, Guclu, J, Vinh, J, Heyes, J, Franck, K. I., Schaffner, A. R., Bouchez, D, Maurel, C (2003). Role of a Single Aquaporin Isoform in Root Water Uptake. *Plant Cell*, *15*, 509–522. (Cit. on pp. 29, 30).

GENERAL BIBLIOGRAPHY

128. Jia, W., Zhang, J., Zhang, D.-P. (1996). Metabolism of xylem-delivered ABA in relation to ABA flux and concentration in leaves of maize and *Commelina communis*. *Journal of Experimental Botany*, *47*, 1085–1091 (cit. on p. 169).
129. Jiang, F., Hartung, W (2008). Long-distance signalling of abscisic acid (ABA): the factors regulating the intensity of the ABA signal. *Journal of Experimental Botany*, *59*, 37 (cit. on pp. 176, 199).
130. Johnson, D. M., McCulloh, K. A., Woodruff, D. R., Meinzer, F. C. (2012). Evidence for xylem embolism as a primary factor in dehydration-induced declines in leaf hydraulic conductance. *Plant, Cell and Environment*, *35*, 760–769 (cit. on p. 33).
131. Johnson, W., Jackson, L., Ochoa, O (2000). Lettuce, a shallow-rooted crop, and *Lactuca serriola*, its wild progenitor, differ at QTL determining root architecture and deep soil water exploitation. *TAG Theoretical and Applied Genetics*, *101*, 1066–1073 (cit. on pp. 38, 39).
132. Kaldenhoff, R, Grote, K, Zhu, J. J., Zimmermann, U (1998). Significance of plasmalemma aquaporins for water-transport in *Arabidopsis thaliana*. *Plant Journal*, *14*, 121–128 (cit. on p. 30).
133. Kang, S, Liang, Z, Pan, Y, Shi, P (2000). Alternate furrow irrigation for maize production in an arid area. *Agricultural water management*, *45*, 267–274 (cit. on p. 158).
134. Karahara, I, Ikeda, A, Kondo, T, Uetake, Y (2004). Development of the Casparian strip in primary roots of maize under salt stress. *Planta*, *219*, 41–47 (cit. on p. 29).
135. Kashiwagi, J., Krishnamurthy, L., Crouch, J. H., Serraj, R. (2006). Variability of root length density and its contributions to seed yield in chickpea (*Cicer arietinum* L.) under terminal drought stress. *Field Crops Research*, *95*, 171–181 (cit. on pp. 38, 195).
136. Kemna, A., Kulesa, B., Vereecken, H (2002). Imaging and characterisation of subsurface solute transport using electrical resistivity tomography (ERT) and equivalent transport models. *Journal of Hydrology*, *267*, 125–146 (cit. on p. 99).

137. Kholová, J., Hash, C. T., Kakkera, A., Kocová, M., Vadez, V (2010). Constitutive water-conserving mechanisms are correlated with the terminal drought tolerance of pearl millet [*Penisetum glaucum* (L.) R. Br.]. *Journal of Experimental Botany*, *61*, 369–377 (cit. on pp. 95, 161).
138. King, J., Gay, A., Sylvester-Bradley, R., Bingham, I., Foulkes, J., Gregory, P, Robinson, D (2003). Modelling Cereal Root Systems for Water and Nitrogen Capture: Towards an Economic Optimum. *Annals of Botany*, *91*, 383–390 (cit. on pp. 38, 46, 132, 195).
139. Knipfer, T, Fricke, W (2010). Root pressure and a solute reflection coefficient close to unity exclude a purely apoplastic pathway of radial water transport in barley (*Hordeum vulgare*). *New Phytologist*, *187*, 159–170 (cit. on p. 28).
140. Knipfer, T, Besse, M., Verdeil, J.-L., Fricke, W (2011). Aquaporin-facilitated water uptake in barley (*Hordeum vulgare* L.) roots. *Journal of Experimental Botany*, *62*, 4115–4126. (Cit. on p. 28).
141. Kutschera, L, Sobotik, M, Lichtenegger, E. *Wurzeln : Bewurzelung von Pflanzen in verschiedenen Lebensräumen*; Land Oberösterreich. OÖ. Landesmuseum, 1997 (cit. on p. 8).
142. Lambot, S, Slob, E. C., van den Bosch, I, Stockbroeckx, B, Scheers, B, Vanclooster, M (2004). Estimating soil electric properties from monostatic ground-penetrating radar signal inversion in the frequency domain. *Water Resources Research*, *40*, 1–12 (cit. on p. 99).
143. Lambot, S, Slob, E. C., vandenBosch, I, Strockbroeckx, B, Vanclooster, M (2004). Modeling of Ground-Penetrating Radar for accurate characterization of subsurface electric properties. *IEEE Transactions on Geoscience and Remote Sensing*, *42*, 2555–2567 (cit. on p. 99).
144. Lambot, S., Binley, A., Slob, E., Hubbard, S. (2008). Ground Penetrating Radar in Hydrogeophysics. *Vadose Zone Journal*, *7*, 137 (cit. on pp. 99, 188).
145. Landsberg, J, Fowkes, N (1978). Water movement through plant roots. *Annals of Botany*, *42*, 493–508 (cit. on pp. 38, 147).
146. Le Bot, J, Serra, V, Fabre, J, Draye, X., Adamowicz, S, Pagès, L (2010). DART: a software to analyse root system architecture and development from captured images. *Plant and Soil*, *326*, 261–273 (cit. on pp. 10, 52, 53, 87).

147. Lecompte, F, Ozier-Lafontaine, H, Pagès, L (2001). The relationships between static and dynamic variables in the description of root growth. Consequences for field interpretation of rooting variability. *Plant and Soil*, 236, 19–31 (cit. on pp. 37, 64, 68, 184, 187).
148. Lee, K. H., Piao, H. L., Kim, H.-Y., Choi, S. M., Jiang, F., Hartung, W., Hwang, I., Kwak, J. M., Lee, I.-J., Hwang, I. (2006). Activation of Glucosidase via Stress-Induced Polymerization Rapidly Increases Active Pools of Abscisic Acid. *Cell*, 126, 1109–1120 (cit. on pp. 176, 199).
149. Li, X, Wang, X, Yang, Y, Li, R, He, Q, Fang, X, Luu, D. T., Maurel, C, Lin, J (2011). Single-Molecule Analysis of PIP2;1 Dynamics and Partitioning Reveals Multiple Modes of Arabidopsis Plasma Membrane Aquaporin Regulation. *Plant Cell*, 23, 3780–3797 (cit. on p. 31).
150. Li, Y, Sperry, J. S., Shao, M (2009). Hydraulic conductance and vulnerability to cavitation in corn (*Zea mays* L.) hybrids of differing drought resistance. *Environmental and Experimental Botany*, 66, 341–346 (cit. on pp. 12, 33, 41, 44, 126, 127, 149, 151).
151. Lloret, P. G., Casero, P. J. In *Plant Root. The Hidden Half*; Waisel, Y, Eshel, A, Kafkafi, U, Eds.; Plant Roots. The Hidden Half, 2002, pp 127–155 (cit. on p. 68).
152. Lobet, G. Observation de la dynamique de prélèvement de l'eau chez le maïs à l'aide d'imagerie par transmission lumineuse. MA thesis, Université catholique de Louvain, 2008 (cit. on p. 116).
153. Lobet, G., Draye, X. (2012). Rhizotrons blueprints. *figshare* (cit. on pp. 87, 100).
154. Lobet, G., Pagès, L, Draye, X. In *IEEE Plant Growth Modeling and Applications*, 2012, pp 1–5 (cit. on p. 12).
155. Lobet, G., Pagès, L, Draye, X. (2011). A Novel Image Analysis Toolbox Enabling Quantitative Analysis of Root System Architecture. *Plant Physiology*, 157, 29–39 (cit. on pp. 53, 89, 185).
156. Lobet, G., Hachez, C, Chaumont, F, Javaux, M, Draye, X. In *Plant Roots: The Hidden Half*; Eshel, A, Beeckman, T, Eds.; Taylor and Francis, 2012 (cit. on pp. 51, 85, 96, 158, 195).

157. Lopez, F, Bousser, A, Sissoëff, I, Gaspar, M, Lachaise, B, Hoarau, J, Mahè, A (2003). Diurnal Regulation of Water Transport and Aquaporin Gene Expression in Maize Roots: Contribution of PIP2 Proteins. *Plant and Cell Physiology*, 44, 1384–1395 (cit. on p. 29).
158. Luu, D. T., Martiniere, A, Sorieul, M, Runions, J, Maurel, C (2011). Fluorescence recovery after photobleaching reveals high cycling dynamics of plasma membrane aquaporins in Arabidopsis roots under salt stress. *Plant Journal*, 69, 894–905 (cit. on p. 31).
159. Lynch, J. P. (1995). Root Architecture and Plant Productivity. *Plant Physiology*, 109, 7 (cit. on pp. 10, 51).
160. Lynch, J. P. (2007). Roots of the second green revolution. *Australian Journal of Botany*, 55, 493–512 (cit. on p. 44).
161. Lynch, J. P., Brown, K. M. (2012). New roots for agriculture: exploiting the root phenome. *Philosophical Transactions of the Royal Society B: Biological Sciences*, 367, 1598–1604 (cit. on p. 38).
162. Lynch, J. P., Nielsen, K. L., Davis, R. D., Jabllokow, A. G. (1997). SimRoot: Modelling and visualization of root systems. *Plant and Soil*, 188, 139–151 (cit. on pp. 11, 140).
163. Maathuis, F. J. et al. (2003). Transcriptome analysis of root transporters reveals participation of multiple gene families in the response to cation stress. *Plant Journal*, 35, 675–692 (cit. on p. 30).
164. Mahdieh, M., Mostajeran, A. (2009). Abscisic acid regulates root hydraulic conductance via aquaporin expression modulation in *Nicotiana tabacum*. *Journal of Plant Physiology*, 166, 1993–2003 (cit. on p. 31).
165. Mairhofer, S., Zappala, S., Tracy, S. R., Sturrock, C., Bennett, M., Mooney, S. J., Pridomore, T. (2012). RooTrak: Automated Recovery of Three-Dimensional Plant Root Architecture in Soil from X-Ray Microcomputed Tomography Images Using Visual Tracking. *Plant Physiology*, 158, 561–569 (cit. on pp. 41, 53).
166. Mallants, D., Mohanty, B. P., Vervoort, A., Feyen, J. (1997). Spatial analysis of saturated hydraulic conductivity in a soil with macropores. *Soil Technology*, 10, 115–131 (cit. on p. 25).

167. Marcum, K. B., Morton, S., Engelke, M., White, R. (1995). Rooting characteristics and associated drought resistance of zoysiagrasses. *Agronomy Journal*, *87*, 534–538 (cit. on p. 38).
168. Martinez-Ballesta, M. C., Aparicio, F., Pallas, V., Martinez, V., Carvajal, M (2003). Influence of saline stress on root hydraulic conductance and PIP expression in Arabidopsis. *Journal of Plant Physiology*, *160*, 689–697 (cit. on p. 31).
169. Martre, P, Morillon, R, Barrieu, F, North, G. B., Nobel, P. S., Chrispeels, M (2002). Plasma membrane aquaporins play a significant role during recovery from water deficit. *Plant Physiology*, *130*, 2101–2110 (cit. on pp. 29, 30).
170. Maurel, C, Chrispeels, M. J. (2001). Aquaporins. A Molecular Entry into Plant Water Relations. *Plant Physiology*, *125*, 135–138. (Cit. on p. 29).
171. Maurel, C, Simonneau, T, Sutka, M (2010). The significance of roots as hydraulic rheostats. *Journal of Experimental Botany*, *61*, 3191–3198 (cit. on pp. 21, 30, 31).
172. Maurel, C, Verdoucq, L, Luu, D, Santoni, V (2008). Plant aquaporins: membrane channels with multiple integrated functions. *Annual Review of Plant Biology*, *59*, 595–624 (cit. on pp. 29, 96, 127, 139, 150).
173. Maurel, C, Reizer, J, Schroeder, J, Chrispeels, M (1993). The vacuolar membrane protein gamma-TIP creates water specific channels in *Xenopus* oocytes. *EMBO Journal*, *12*, 2241–2247 (cit. on p. 22).
174. McCully, M. E., Boyer, J. S. (1997). The expansion of maize root-cap mucilage during hydration .3. Changes in water potential and water content. *Physiologia Plantarum*, *99*, 169–177 (cit. on p. 26).
175. McCully, M. E., Huang, C. X., Ling, L. E. C. (1998). Daily embolism and refilling of xylem vessels in the roots of field-grown maize. *New Phytologist*, *138*, 327–342 (cit. on pp. 35, 139).
176. McCully, M. (1999). Root Xylem Embolisms and Refilling. Relation to Water Potentials of Soil, Roots, and Leaves, and Osmotic Potentials of Root Xylem Sap. *Plant Physiology*, *199*, 1001–1008 (cit. on p. 35).

-
177. Meijering, E, Jacob, M, Sarria, J. C. F., Steiner, P, Hirling, H, Unser, M (2004). Design and validation of a tool for neurite tracing and analysis in fluorescence microscopy images. *Cytometry*, 58A, 167–176 (cit. on p. 76).
178. Mollier, A., Pellerin, S (1999). Maize root system growth and development as influenced by phosphorus deficiency. *Journal of Experimental Botany*, 50, 487–497 (cit. on p. 145).
179. Molz, F., Remson, I (1970). Extraction term models of soil moisture use by transpiring plants. *Water Resources Research*, 6, 1346 (cit. on p. 46).
180. Mooney, S. J., Pridmore, T. P., Helliwell, J., Bennett, M. J. (2011). Developing X-ray Computed Tomography to non-invasively image 3-D root systems architecture in soil. *Plant and Soil*, 352, 1–22 (cit. on pp. 51, 99, 188).
181. Moradi, A. B., Carminati, A., Lamparter, A., Woche, S. K., Bachmann, J., Vetterlein, D., Vogel, H.-J., Oswald, S. E. (2012). Is the Rhizosphere Temporarily Water Repellent? *Vadose Zone Journal* (cit. on p. 26).
182. Moshelion, M, Becker, D, Biela, A, Uehlein, N, Hedrich, R, Otto, B, Levi, H, Moran, N, Kaldenhoff, R (2002). Plasma membrane aquaporins in the motor cells of *Samanea saman*: diurnal and circadian regulation. *Plant Cell*, 14, 727–739. (Cit. on p. 29).
183. Nagarajah, S, Ratnasuriya, G. B. (1981). Clonal variability in root growth and drought resistance in tea (*Camellia sinensis*). *Plant and Soil*, 60, 153–155 (cit. on p. 38).
184. Nagel, K. A. et al. (2012). GROWSCREEN-Rhizo is a novel phenotyping robot enabling simultaneous measurements of root and shoot growth for plants grown in soil-filled rhizotrons. *Functional Plant Biology* (cit. on pp. 187, 190).
185. Nagel, O. W., Konings, H., Lambers, H. (1994). Growth rate, plant development and water relations of the ABAdeficient tomato mutant sitiens. *Physiologia Plantarum*, 92, 102–108 (cit. on p. 31).
186. Neumann, G, George, T. S., Plassard, C (2009). Strategies and methods for studying the rhizosphere - the plant science toolbox. *Plant and Soil*, 321, 431–456 (cit. on p. 79).

GENERAL BIBLIOGRAPHY

187. Newman, E. I. (1969). Resistance to Water Flow in Soil and Plant. I. Soil Resistance in Relation to Amounts of Root - Theoretical Estimates. *Journal of Applied Ecology*, 6, 1–12 (cit. on p. 27).
188. Newman, E. (1969). Resistance to Water Flow in Soil and Plant. II. a Review of Experimental Evidence on Rhizosphere Resistance. *Journal of Applied Ecology*, 6, 261–272 (cit. on p. 40).
189. Nielsen, K., Bouma, T., Lynch, J., Eissenstat, D. M. (1998). Effects of phosphorus availability and vesicular-arbuscular mycorrhizas on the carbon budget of common bean (*Phaseolus vulgaris*). *New Phytologist*, 139, 647–656 (cit. on p. 39).
190. Oswald, S. E., Menon, M., Carminati, A, Vontobel, P, Lehmann, E. H., Schulin, R. (2008). Quantitative Imaging of Infiltration, Root Growth, and Root Water Uptake via Neutron Radiography. *Vadose Zone Journal*, 7, 1035 (cit. on p. 188).
191. Pagès, L, Jordan, M. O., Picard, D (1989). A simulation model of the three-dimensional architecture of the maize root system. *Plant and Soil*, 119, 147–154 (cit. on p. 140).
192. Pagès, L, Serra, V., Draye, X., Doussan, C, Pierret, A (2010). Estimating root elongation rates from morphological measurements of the root tip. *Plant and Soil*, 328, 35–44 (cit. on p. 64).
193. Pagès, L, Vercambre, G, Drouet, J.-L., Lecompte, F, Collet, C, LeBot, J (2004). RootTyp: a generic model to depict and analyse the root system architecture. *Plant and Soil*, 258, 103–119 (cit. on pp. 68, 144).
194. Palta, J. A., Chen, X., Milroy, S. P., Rebetzke, G. J., Dreccer, M. F., Watt, M (2011). Large root systems: are they useful in adapting wheat to dry environments? *Functional Plant Biology*, 38, 347 (cit. on p. 95).
195. Parent, B, Hachez, C, Redondo, E, Simonneau, T, Chaumont, F, Tardieu, F (2009). Drought and Abscisic Acid Effects on Aquaporin Content Translate into Changes in Hydraulic Conductivity and Leaf Growth Rate: A Trans-Scale Approach. *Plant Physiology*, 149, 2000–2012 (cit. on pp. 31, 101, 167).
196. Passioura, J. B. (1983). Roots and drought resistance. *Agricultural water management*, 7, 265–280 (cit. on pp. 96, 114, 195).
197. Passioura, J. B. (1980). The Transport of Water from Soil to Shoot in Wheat Seedlings. *Journal of Experimental Botany*, 31, 333–345 (cit. on pp. 27, 40).

198. Peirce, G. J. (1936). The State of Water in Ducts and Tracheids. *Plant Physiology*, *11*, 623–628 (cit. on pp. 23, 33, 151).
199. Péret, B, de Rybel, B, Casimiro, I, Benkova, E, Swarup, R, Laplaze, L, Beekman, T, Bennett, M. (2009). Arabidopsis lateral root development: an emerging story. *TRENDS in Plant Science*, *14*, 399–408 (cit. on pp. 37, 51).
200. Perumalla, C. J., Peterson, C. A. (1986). Deposition of Casparian bands and suberin lamellae in the exodermis and endodermis of young corn and onion roots. *Canadian Journal of Botany*, 1872–1878 (cit. on pp. 28, 29).
201. Peterson, C. A., Murrmann, M., Steudle, E (1993). Location of the major barriers to water and ion movement in young roots of *Zea mays* L. *Planta*, *190*, 127–136 (cit. on p. 29).
202. Pierret, A, Doussan, C, Capowicz, Y, Bastardie, F, Pagès, L (2007). Root functional architecture: a framework for modelling the intreplay between roots and soil. *Vadose Zone Journal*, *6*, 269–281 (cit. on p. 26).
203. Pinheiro, H. A., DaMatta, F., Chaves, A. R. M., Loureiro, M. E., Ducatti, C (2005). Drought Tolerance is Associated with Rooting Depth and Stomatal Control of Water Use in Clones of *Coffea canephora*. *Annals of Botany*, *96*, 101–108 (cit. on p. 38).
204. Pockman, W. T., Sperry, J. S. (2000). Vulnerability to xylem cavitation and the distribution of Sonoran Desert vegetation. *American Journal of Botany*, *87*, 1287–1299 (cit. on pp. 33, 197).
205. Postma, J. A., Lynch, J. P. (2011). Root Cortical Aerenchyma Enhances the Growth of Maize on Soils with Suboptimal Availability of Nitrogen, Phosphorus, and Potassium. *Plant Physiology*, *156*, 1190–1201 (cit. on p. 194).
206. Postma, J. A., Lynch, J. P. (2011). Theoretical evidence for the functional benefit of root cortical aerenchyma in soils with low phosphorus availability. *Annals of Botany*, *107*, 829–841 (cit. on pp. 11, 146, 194).
207. Pregitzer, K. S., Hendrick, R. L., Fogel, R. (1993). The demography of fine roots in response to patches of water and nitrogen. *New Phytologist*, *125*, 575–580 (cit. on p. 37).
208. Purnell, H. M. (1960). Studies of the family Proteaceae. I. Anatomy and morphology of the roots of some Victorian species. *Australian Journal of Botany*, *8*, 38–50 (cit. on p. 70).

GENERAL BIBLIOGRAPHY

209. Qi, X, Qi, J, Wu, Y (2007). RootLM: a simple color image analysis program for length measurement of primary roots in Arabidopsis. *Plant Root*, 1, 10–16 (cit. on p. 53).
210. Ranathunge, K., Schreiber, L., Franke, R. (2011). Suberin research in the genomics era—New interest for an old polymer. *Plant Science*, 180, 399–413 (cit. on p. 22).
211. Rasband, W. *ImageJ* (cit. on p. 55).
212. Read, D. B., Gregory, P. J., Bell, A. E. (1999). Physical properties of axenic maize root mucilage. *Plant and Soil*, 211, 87–91 (cit. on p. 26).
213. Read, D. B., Bengough, A. G., Gregory, P. J., Crawford, J. W., Robinson, D, Scrimgeour, C. M., Young, I. M., Zhang, K., Zhang, X (2003). Plant roots release phospholipid surfactants that modify the physical and chemical properties of soil. *New Phytologist*, 157, 315–326 (cit. on p. 26).
214. Ren, H, Wei, K, Jia, W, Davies, W. J., Zhang, J (2007). Modulation of Root Signals in Relation to Stomatal Sensitivity to Root-sourced Abscisic Acid in Drought-affected Plants. *Journal of Integrative Plant Biology*, 49, 1410–1420 (cit. on p. 169).
215. Rewald, B, Ephrath, J. (2011). A root is a root is a root? Water uptake rates of Citrus root orders. *Plant, Cell and Environment*, 34, 33–42 (cit. on p. 37).
216. Reynolds, M, Dreccer, F, Trethowan, R (2006). Drought-adaptive traits derived from wheat wild relatives and landraces. *Journal of Experimental Botany*, 58, 177–186 (cit. on pp. 38, 39).
217. Richards, L. A (1931). Capillary conduction of liquids through porous mediums. *Physics-a Journal of General and Applied Physics*, 1, 318–333 (cit. on p. 25).
218. Robinson, D. A., Jones, S. B., Wraith, J. M., Or, D, Friedman, S. P. (2003). A Review of Advances in Dielectric and Electrical Conductivity Measurement in Soils Using Time Domain Reflectometry. *Vadose Zone Journal*, 2, 444–475 (cit. on p. 99).
219. Ruiz-Lozano, J. M., Alguacii, M. d. M., Barzana, G, Vemieri, P, Aroca, R (2009). Exogenous ABA accentuates the differences in root hydraulic properties between mycorrhizal and non mycorrhizal maize plants through regulation of PIP aquaporins. *Plant Molecular Biology*, 70, 565–579 (cit. on p. 31).

-
220. Schoppach, R., Sadok, W. (2012). Differential sensitivities of transpiration to evaporative demand and soil water deficit among wheat elite cultivars indicate different strategies for drought tolerance. *Environmental and Experimental Botany*, *84*, 1–10 (cit. on p. 190).
221. Schreiber, L, Hartmann, K, Skrabs, M, Zeier, J (1999). Apoplastic barriers in roots: chemical composition of endodermal and hypodermal cell walls. *Journal of Experimental Botany*, *50*, 1267–1280 (cit. on p. 28).
222. Schröder, N., Javaux, M., Vanderborght, J, Steffen, B., Vereecken, H (2012). Effect of Root Water and Solute Uptake on Apparent Soil Dispersivity: A Simulation Study. *Vadose Zone Journal* (cit. on p. 117).
223. Schröder, T, Tang, L, Javaux, M, Vanderborght, J, Körfgen, B, Vereecken, H (2009). A grid refinement approach for a three-dimensional soil-root water transfer model. *Water Resour. Res.* *45*, W10412 (cit. on pp. 25, 87, 117).
224. Schroeder, J. I., Nambara, E. (2006). A Quick Release Mechanism for Abscisic Acid. *Cell*, *126*, 1023–1025 (cit. on pp. 176, 199).
225. Secchi, F, Gilbert, M. E., Zwieniecki, M. A. (2011). Transcriptome Response to Embolism Formation in Stems of *Populus trichocarpa* Provides Insight into Signaling and the Biology of Refilling. *Plant Physiology*, *157*, 1419–1429 (cit. on p. 35).
226. Secchi, F, Zwieniecki, M. A. (2010). Patterns of PIP gene expression in *Populus trichocarpa* during recovery from xylem embolism suggest a major role for the PIP1 aquaporin subfamily as moderators of refilling process. *Plant, Cell and Environment*, *33*, 1285–1297 (cit. on p. 35).
227. Secchi, F, Zwieniecki, M. A. (2011). Sensing embolism in xylem vessels: the role of sucrose as a trigger for refilling. *Plant, Cell and Environment*, *34*, 514–524 (cit. on p. 35).
228. Segal, E., Kushnir, T., Mualem, Y., Shani, U. (2008). Water Uptake and Hydraulics of the Root Hair Rhizosphere. *Vadose Zone Journal*, *7*, 1027 (cit. on p. 27).
229. Shane, M. W., Lambers, H (2005). Cluster Roots: A Curiosity in Context. *Plant and Soil*, *274*, 101–125 (cit. on p. 70).

230. Shen, L, Courtois, B, McNally, K. L., Robin, S, Li, Z (2001). Evaluation of near-isogenic lines of rice introgressed with QTLs for root depth through marker-aided selection. *TAG Theoretical and Applied Genetics*, 103, 75–83 (cit. on pp. 38, 39, 195).
231. Shroeder, T., Javaux, M., Vanderborght, J, Koerfgen, B., Vereecken, H (2008). Effect of local soil hydraulic conductivity drop using a three-dimensional root water uptake model. *Vadose Zone Journal*, 7, 1089–1098 (cit. on p. 117).
232. Siefritz, F, Tyree, M. T., Lovisolo, C, Schubert, A (2002). PIP1 Plasma Membrane Aquaporins in Tobacco. *The Plant Cell Online*, 14, 869–876 (cit. on pp. 29, 30).
233. Skene, K. R. (2000). Pattern Formation in Cluster Roots: Some Developmental and Evolutionary Considerations. *Annals of Botany*, 85, 901–908 (cit. on p. 70).
234. Smit, A. L., Bengough, A. G., Engels, C, Noordwijk, M. v., Pellerin, S, vandeGeijn, S. C. (2000). Root Methods. A handbook. *Springer Edition*, 1–588 (cit. on p. 67).
235. Sobeih, W. Y., Dodd, I. C., Bacon, M. A., Grierson, D, Davies, W. J. (2004). Long-distance signals regulating stomatal conductance and leaf growth in tomato (*Lycopersicon esculentum*) plants subjected to partial root-zone drying. *Journal of Experimental Botany*, 55, 2353 (cit. on p. 190).
236. Somma, F, Hopmans, J., Clausnitzer, V (1998). Transient three-dimensional modeling of soil water and solute transport with simultaneous growth, root water and nutrient uptake. *Plant and Soil*, 202, 281–293 (cit. on pp. 140, 145, 146).
237. Sperry, J. S., Donnelly, J. R., Tyree, M. T. (1988). A method for measuring hydraulic conductivity and embolism in xylem. *Plant, Cell and Environment*, 11, 35–40 (cit. on p. 34).
238. Sperry, J. S., Donnelly, J. R., Tyree, M. T. (1988). Seasonal Occurrence of Xylem Embolism in Sugar Maple (*Acer saccharum*). *American Journal of Botany*, 75, 1212–1218 (cit. on pp. 33, 34, 151, 197).
239. Sperry, J. S., Ikeda, T (1997). Xylem cavitation in roots and stems of Douglas-fir and white fir. *Tree Physiology*, 17, 275–280 (cit. on pp. 33, 34).
240. Sperry, J. S., Saliendra, N. Z. (1994). Intra- and inter-plant variation in xylem cavitation in *Betula occidentalis*. *Plant, Cell and Environment*, 17, 1233–1241 (cit. on pp. 34, 196).

241. Sperry, J. S., Stiller, V, Hacke, U. G. In *Plant Roots: the Hidden Half*; Waisel, Y, Eshel, A, Kafkafi, U, Eds.; Marcel Dekker, Inc: New York, 2002, pp 663–681 (cit. on pp. 23, 34, 95, 96).
242. Sperry, J. S., Adler, F. R., Campbell, G. S., Comstock, J. P. (1998). Limitation of plant water use by rhizosphere and xylem conductance: results from a model. *Plant, Cell and Environment*, 21, 347–359 (cit. on pp. 34, 95, 126, 139, 155).
243. Sperry, J. S., Saliendra, N. Z., Pockman, W. T., Cochard, H, Cruiziat, P, Davis, S. D., Ewers, F. W., Tyree, M. T. (1996). New evidence for large negative xylem pressures and their measurement by the pressure chamber method. *Plant, Cell and Environment*, 19, 427–436 (cit. on p. 126).
244. Sperry, J. S., Holbrook, N. M., Zimmermann, M. H., Tyree, M. T. (1987). Spring Filling of Xylem Vessels in Wild Grapevine. *Plant Physiology*, 83, 414–417 (cit. on p. 34).
245. Steele, K., Virk, D., Kumar, R, Prasad, S., Witcombe, J. (2007). Field evaluation of upland rice lines selected for QTLs controlling root traits. *Field Crops Research*, 101, 180–186 (cit. on pp. 38, 39, 96, 195).
246. Steudle, E (2001). The cohesion-tension mechanism and the acquisition of water by plant roots. *Annual Review of Plant Physiology and Plant Molecular Biology*, 53, 847–875 (cit. on p. 139).
247. Steudle, E (2000). Water uptake by plant roots: an integration of views. *Plant and Soil*, 226, 45–56 (cit. on pp. 22, 133).
248. Steudle, E, Frensch, J. (1989). Osmotic responses of maize roots. *Planta*, 177, 281–295 (cit. on p. 37).
249. Steudle, E, Peterson, C. A. (1998). How does water get through roots? *Journal of Experimental Botany*, 49, 775–788 (cit. on pp. 5, 22, 28, 33, 133, 139).
250. Stiller, V, Sperry, J. S. (2002). Cavitation fatigue and its reversal in sunflower (*Helianthus annuus* L.) *Journal of Experimental Botany*, 53, 1155–1161 (cit. on p. 34).
251. Sutka, M, Li, G, Boudet, J, Boursiac, Y, Doumas, P, Maurel, C (2011). Natural variation of root hydraulics in *Arabidopsis* grown in normal and salt-stressed conditions. *Plant Physiology*, 155, 1264–1276 (cit. on pp. 28, 30, 32).
252. Taiz, L, Zeiger, E *Plant Physiology*; Sinauer Associates, 1998 (cit. on p. 167).

GENERAL BIBLIOGRAPHY

253. Tardieu, F (2011). Any trait or trait-related allele can confer drought tolerance: just design the right drought scenario. *Journal of Experimental Botany*, 63, 25–31 (cit. on p. 161).
254. Tardieu, F (2010). Why work and discuss the basic principles of plant modelling 50 years after the first plant models? *Journal of Experimental Botany*, 61, 2039–2041 (cit. on pp. 11, 165, 167, 192, 194).
255. Tardieu, F, Davies, W. J. (1993). Integration of hydraulic and chemical signalling in the control of stomatal conductance and water status of droughted plants. *Plant, Cell and Environment*, 16, 341–349 (cit. on pp. 13, 170, 175, 199).
256. Tardieu, F, Simonneau, T (1998). Variability among species of stomatal control under fluctuating soil water status and evaporative demand: modelling isohydric and anisohydric behaviours. *Journal of Experimental Botany*, 49, 419–432 (cit. on pp. 34, 159, 175, 176).
257. Tardieu, F, Zhang, J, Katerji, N, Bethenod, O, Palmer, S, Davies, W. J. (1992). Xylem ABA controls the stomatal conductance of field-grown maize subjected to soil compaction or soil drying. *Plant, Cell and Environment*, 15, 193–197 (cit. on pp. 159, 172, 175).
258. Team, R. C. *R: A Language and Environment for Statistical Computing*; Vienna, Austria (cit. on pp. 84, 104).
259. Thévenaz, P., Ruttimann, U. E., Unser, M (1998). A pyramid approach to subpixel registration based on intensity. *IEEE Transn Image Process*, 7, 27–41 (cit. on pp. 65, 238).
260. Thomas, R., Fang, X., Ranathunge, K., Anderson, T. R., Peterson, C. A., Bernards, M. A. (2007). Soybean Root Suberin: Anatomical Distribution, Chemical Composition, and Relationship to Partial Resistance to *Phytophthora sojae*. *Plant Physiology*, 144, 299–311 (cit. on p. 29).
261. Thompson, A., Andrews, J., Mulholland, B., Mckee, J., Hilton, H., Horridge, J., Farquhar, G., Smeeton, R., Smillie, I., Black, C., Taylor, I. (2007). Overproduction of Abscisic Acid in Tomato Increases Transpiration Efficiency and Root Hydraulic Conductivity and Influences Leaf Expansion. *Plant Physiology*, 143, 1905 (cit. on p. 31).

-
262. Tidwell, V. C., Glass, R. J. (1994). X ray and visible light transmission for laboratory measurement of two-dimensional saturation fields in thin-slab systems. *Water Resources Research*, *30*, 2873–2882 (cit. on pp. 90, 102).
263. Törnroth-Horsefield, S, Wang, Y, Hedfalk, K, Johanson, U, Karlsson, M, Tajkhorshid, E, Neutze, R, Kjellbom, P (2006). Structural mechanism of plant aquaporin gating. *Nature*, *439*, 689–694 (cit. on p. 31).
264. Tournaire-Roux, C., Sutka, M., Javot, H, Gout, E., Gerbeau, P., Luu, D.-T., Bligny, R., Maurel, C. (2003). Cytosolic pH regulates root water transport during anoxic stress through gating of aquaporins. *Nature*, *425*, 393–397 (cit. on pp. 29, 31).
265. Trachsel, S, Kaeppler, S. M., Brown, K. M., Lynch, J. P. (2013). Maize root growth angles become steeper under low N conditions. *Field Crops Research*, *140*, 18–31 (cit. on p. 187).
266. Tuberosa, R. (2012). Phenotyping for drought tolerance of crops in the genomics era. *Frontiers in Physiology*, *3*, 1–26 (cit. on pp. 10, 12, 95, 190).
267. Tyerman, S. D., Bohnert, H. J., Maurel, C, Steudle, E, Smith, J. A. C. (1999). Plant aquaporins: their molecular biology, biophysics and significance for plant water relations. *Journal of Experimental Botany*, *50*, 1055–1071 (cit. on p. 30).
268. Tyree, M. T., Sperry, J. S. (1989). Vulnerability of Xylem to Cavitation and Embolism. *Annual Review of Plant Physiology and Plant Molecular Biology*, *40*, 19–36 (cit. on pp. 23, 33, 34, 151).
269. Uehlein, N, Otto, B, Hanson, D. T., Fischer, M, McDowell, N, Kaldenhoff, R (2008). Function of *Nicotiana tabacum* aquaporins as chloroplast gas pores challenges the concept of membrane CO₂ permeability. *The Plant Cell*, *20*, 648–657 (cit. on p. 29).
270. van Genuchten, M. (1980). A closed-form equation for predicting the hydraulic conductivity of unsaturated soils. *Soil Science Society of America Journal*, *44*, 891–898 (cit. on p. 148).
271. van den Honert, T. H. (1948). Water transport in plants as a catenary process. *Discussions of the Faraday Society*, *3*, 146–153 (cit. on p. 21).

272. van der Weele, C., Jiang, H., Palaniappan, K., Ivanov, V., Palaniappan, K., Baskin, T. (2003). A New Algorithm for Computational Image Analysis of Deformable Motion at High Spatial and Temporal Resolution Applied to Root Growth. Roughly Uniform Elongation in the Meristem and Also, after an Abrupt Acceleration, in the Elongation Zone. *Plant Physiology*, *132*, 1138 (cit. on p. 53).
273. Vandeleur, R. K., Mayo, G, Shelden, M. C., Gilliam, M, Kaiser, B. N., Tyerman, S. D. (2009). The role of plasma membrane intrinsic protein aquaporins in water transport through roots: diurnal and drought stress responses reveal different strategies between isohydric and anisohydric cultivars of grapevine. *Plant Physiology*, *149*, 445–460 (cit. on pp. 29–32).
274. Vanderborght, J, Kemna, A., Hardelauf, H. (2005). Potential of electrical resistivity tomography to infer aquifer transport characteristics from tracer studies: A synthetic case study. *Water Resources Research*, *41* (cit. on p. 99).
275. Vandoorne, B, Beff, L, Lutts, S, Javaux, M (2012). Root Water Uptake Dynamics of *Cichorium intybus* var. *sativum* Under Water-Limited Conditions. *Vadoze Zone Journal* (cit. on p. 190).
276. Veen, B. W., Van Noordwijk, M., De Willigen, P., Boone, F., Kooistra, M. (1992). Root-Soil Contact of Maize, as Measured by a Thin-Section Technique. *Plant and Soil*, *139*, 131–138 (cit. on p. 27).
277. Walker, J. P., Willgoose, G. R., Kalma, J. D. (2004). In situ measurement of soil moisture: a comparison of techniques. *Journal of Hydrology*, *293*, 85–99 (cit. on p. 99).
278. Wasson, A. P., Richards, R. A., Chatrath, R, Misra, S. C., Prasad, S. V. S., Rebetzke, G. J., Kirkegaard, J. A., Christopher, J. T., Watt, M (2012). Traits and selection strategies to improve root systems and water uptake in water-limited wheat crops. *Journal of Experimental Botany*, *63*, 3485–3498 (cit. on pp. 12, 38, 96, 132, 196, 197).
279. Watt, M, Evans, J. (1999). Proteoid Roots. Physiology and Development. *Plant Physiology*, *121*, 317–323 (cit. on p. 70).
280. Watt, M, McCully, M., Canny, M. (1994). Formation and Stabilization of Rhizosheaths of *Zea-Mays* L. *Plant Physiology*, *106*, 179–186 (cit. on p. 26).

-
281. Whalley, W. R., Riseley, B., LeedsHarrison, P. B, Bird, N. R. A, Leech, P. K, Adderley, W. P (2004). Structural differences between bulk and rhizosphere soil. *European Journal of Soil Science*, *56*, 353–360 (cit. on p. 26).
282. Yang, S, Tyree, M. T. (1992). A theoretical model of hydraulic conductivity recovery from embolism with comparison to experimental data on *Acer saccharum*. *Plant, Cell and Environment*, *15*, 633–643 (cit. on p. 34).
283. Yang, X, Li, Y, Ren, B, Ding, L, Gao, C, Shen, Q, Guo, S (2012). Drought-Induced Root Aerenchyma Formation Restricts Water Uptake in Rice Seedlings Supplied with Nitrate. *Plant and Cell Physiology*, *53*, 495–504 (cit. on p. 28).
284. Yazdanbakhsh, N, Fisahn, J (2009). High throughput phenotyping of root growth dynamics, lateral root formation, root architecture and root hair development enabled by PlaRoM. *Functional Plant Biology*, *36*, 938–946 (cit. on p. 52).
285. Ye, Q, Steudle, E (2006). Oxidative gating of water channels (aquaporins) in corn roots. *Plant, Cell and Environment*, *29*, 459–470 (cit. on p. 30).
286. Zaman-Allah, M, Jenkinson, D. M., Vadez, V (2011). A conservative pattern of water use, rather than deep or profuse rooting, is critical for the terminal drought tolerance of chickpea. *Journal of Experimental Botany*, *62*, 4239–4252 (cit. on pp. 95, 161).
287. Zaman-Allah, M., Jenkinson, D. M., Vadez, V (2011). Chickpea genotypes contrasting for seed yield under terminal drought stress in the field differ for traits related to the control of water use. *Functional Plant Biology*, *38*, 270 (cit. on p. 161).
288. Zelazny, E., Borst, J. W., Muylaert, M., Batoko, H., Hemminga, M. A., Chaumont, F (2007). FRET imaging in living maize cells reveals that plasma membrane aquaporins interact to regulate their subcellular localization. *Proceedings of the National Academy of Sciences of the United States of America*, *104*, 12359–12364 (cit. on p. 31).
289. Zhang, J, Zhang, X (1995). Exudation rate and hydraulic conductivity of maize roots are enhanced by soil drying and abscisic acid treatment. *New Phytologist*, *131*, 329–336 (cit. on p. 31).
290. Zhu, J., Brown, K. M., Lynch, J. P. (2010). Root cortical aerenchyma improves the drought tolerance of maize (*Zea mays* L.) *Plant, Cell and Environment*, *33*, 740–749 (cit. on p. 39).

GENERAL BIBLIOGRAPHY

291. Zhu, J., Kaeppeler, S. M., Lynch, J. P. (2005). Mapping of QTLs for lateral root branching and length in maize (*Zea mays* L.) under differential phosphorus supply. *TAG Theoretical and Applied Genetics*, *111*, 688–695 (cit. on p. 37).
292. Zimmermann, H. M., Hartmann, K, Schreiber, L, Steudle, E (2000). Chemical composition of apoplastic transport barriers in relation to radial hydraulic conductivity of corn roots (*Zea mays* L.) *Planta*, *210*, 302–11. (Cit. on p. 29).
293. Zufferey, V, Cochard, H, Améglio, T, Spring, J. L., Viret, O (2011). Diurnal cycles of embolism formation and repair in petioles of grapevine (*Vitis vinifera* cv. Chasselas). *Journal of Experimental Botany*, *62*, 3885–3894 (cit. on pp. 33, 35).
294. Zwieniecki, M. A., Holbrook, N. M. (2009). Confronting Maxwell's demon: biophysics of xylem embolism repair. *TRENDS in Plant Science*, *14*, 530–534 (cit. on pp. 35, 36, 139).

PART VII

ANNEXES

HOAGLAND SOLUTION



1. Make up stock solutions and store in separate bottles with appropriate label.
2. Add each component to 800mL deionized water then fill to 1L and adjust the pH to 5.0 (with either HCl or NaOH).
3. After the solution is mixed, it is ready to water plants.

Component	Stock Solution	mL/1L
2M KNO ₃	202g/L	2.5
2M Ca(NO ₃) ₂ x 4H ₂ O	236g/0.5L	2.5
FeEDTA	15g/L	1.5 x 2 = 3
2M MgSO ₄ x 7H ₂ O	493g/L	1
1M NH ₄ NO ₃	80g/L	1
Minors:		1
	H ₃ BO ₃	2.86g/L
	MnCl ₂ x 4H ₂ O	1.81g/L
	ZnSO ₄ x 7H ₂ O	0.22g/L
	CuSO ₄	0.051g/L
	H ₃ MoO ₄ x H ₂ O or	0.09g/L
	Na ₂ MoO ₄ x 2H ₂ O	0.12g/L
1M KH ₂ PO ₄ (pH 6.0 w/ 3M KOH)	136g/L	0.5
	KOH 3M	168,3g/L

IMAGE ACQUISITION AND TREATMENT FOR LIGHT TRANSMISSION IMAGING EXPERIMENTS

B

B.1 Image acquisition

Rhizotrons were placed in a small black chamber, between a light source (10 light tubes, 36W, Sylvania Standard F36W/33-640-T8) and a regular CCD camera (Canon EOS 450D with a lens Canon EF 50mm 1:1.8) (fig. B.1). The camera was placed at approximately 2 m from the rhizotron, its sensibility set to 200 ISO, the aperture speed to 1/60 [sec] and the aperture to 5.6. A colored Plexiglass sample was fixed next to the rhizotrons for light recalibration.

For every measurement, rhizotrons were placed in the device and five successive pictures were taken to minimize the effect of light occlusion. Additionally, at the beginning of the experiment, pictures of every rhizotron, saturated with nutrient solution, were taken.

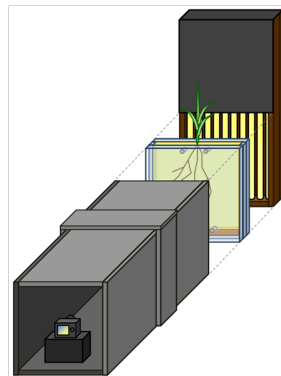


Figure B.1: Setup used for the acquisition of light transmission images. Illustration from Dupriez (2009).

B.2 Image processing

The general principle of the image processing procedure was to transform images captured with the light transmission imaging technique into time-series (stack) of 2D maps of soil water content. The following transformations were applied to the images:

1. Stacking of images
2. Registration of images for each time step
3. Averaging of the 5 images for each time step
4. Color registration
5. Registration of averaged images for each time-series
6. Saturated Intensity Ratio image creation
7. Humidity image creation
8. Size reduction and text file creation

Steps 1 to 6 were performed using ImageJ macro. Step 7 and 8 using R scripts.

B.2.1 Change image type

Color images were changed to 8-bit greyscale images. Moreover, since pixel values in 8-bit images are restricted to integer between 0 and 255, the image type was changed from 8-bit the 32-bit. This transformation substantially increases the file size, but enable to storage of real numbers (in this case, humidity values) in every pixels.

B.2.2 Geographic registration

Although no movement of camera was supposed to happen between every image repetition, a geographic registration was performed to align the images prior to the averaging step. Registration was done using the ImageJ plugin StackReg (Thévenaz et al., 1998).

B.2.3 Average of the image repetitions

Averages of the image repetitions were performed using the ImageJ built-in function `Images > Stacks > Z Project...`

B.2.4 Color registration

Using the color samples placed next to the rhizotrons, a color registration was performed between every image of the time-series and the image of the corresponding saturated rhizotron. This step corrected the images for light transmission variations due to ambient light differences at the time of image captures.

B.2.5 Geographic registration

A second geographic registration is performed to align the different images of the same time-series. Again this step is done using the plugin StackReg.

B.2.6 SIR images creation

As stated previously, the quantity of light crossing the substrate depend in the soil water content, but also on the soil compaction. Unfortunately, despite a careful filling of the rhizotrons, compaction could not be assumed to be homogenous inside and across the different rhizotrons. To overcome this heterogeneity, every image was transformed in a Saturated Intensity Ratio (SIR) image following the equation:

$$I_{SIR} = \frac{I_{sat} - I_i}{I_{sat}} \quad (\text{B.1})$$

where I_{SIR} is the SIR image, I_{sat} is the saturated image and I_i is an image of the time-series. Dividing every time-series image by its corresponding saturated image removed the local compaction differences.

B.2.7 Humidity image creation

The transformation from pixel to humidity values was done using an exponential relation:

$$hum = a.e^{(b \cdot x)} \quad (\text{B.2})$$

where a and b are shape parameters and

$$x = \ln(1 - SIR) \quad (\text{B.3})$$

where SIR is the value of the pixels in the SIR image. Based on experimental calibration, a and b were initially set to 0.3 and 4.251 respectively (fig. B.2). To account for substrate compaction differences, a correction of the calibration equation was performed for every

B. LIGHT TRANSMISSION IMAGING

rhizotrons by minimizing the differences between their measured and computed water content.

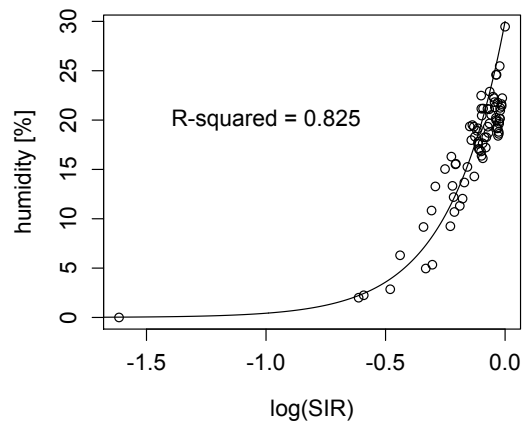


Figure B.2: Light transmission imaging calibration.